Self-Assembled Thin Films with Tunable Release Kinetics for Biomedical Applications

by

Bryan B. Hsu

B.S. Chemical Engineering
B.S. Materials Science and Engineering
University of California-Berkeley, 2007

M.S. Chemistry
Massachusetts Institute of Technology, 2011

Submitted to the Department of Chemistry
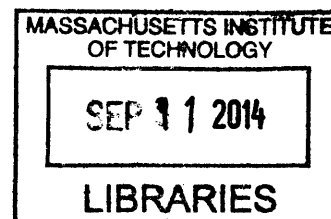in Partial Fulfillment of the Requirements of the Degree of

Doctor of Philosophy in Biological Chemistry

at the

MASSACHUSETTS INSTITUTE OF TECHNOLOGY

September 2014

Signature redacted

Signature of Author...
Department of Chemistry
August 8, 2014

Signature redacted

Certified by..
Paula T. Hammond
David H. Koch (1962) Professor in Engineering
Thesis Supervisor

Signature redacted

Accepted by...
Robert W. Field
Chairman, Departmental Committee on Graduate Students

This doctoral thesis has been examined by a committee of professors from the Departments of Chemistry, Chemical Engineering, and Biology as follows:

Signature redacted

....

Alice Y. Ting
Ellen Swallow Richards Associate Professor of Chemistry
Thesis Committee Chair

Signature redacted

....

Paula T. Hammond
David H. Koch (1962) Professor of Chemical Engineering
Thesis Supervisor

Signature redacted

....

Catherine L. Drennan
HHMI Professor and Investigator of Chemistry and Biology
Thesis Committee Member

Signature redacted

....

Jianzhu Chen
Cottrell Professor of Immunology and Biology
Thesis Committee Member

Signature redacted

....
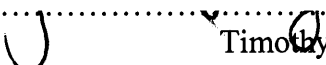
Timothy Swager
John D. MacArthur Professor of Chemistry
Thesis Committee Member

Self-Assembled Thin Films with Tunable Release Kinetics for Biomedical Applications

By

Bryan B. Hsu

Submitted to the Department of Chemistry on August 8, 2014, in partial fulfillment of the requirements for the degree of Doctor of Philosophy

Abstract

The appropriate drug delivery approach is critical to therapeutic success without causing serious harm. Systemic delivery is a common method for delivering drugs but high dosages are needed to maintain elevated plasma levels, which can increase the risk of adverse drug reactions. Locally delivering these drugs offers an interesting alternative by significantly reducing the necessary dosages for therapeutic effect. Unfortunately, controlled delivery strategies can be limited with regards to the types of drugs as well as their release kinetics, especially if more than one drug is involved. Furthermore, for implantable devices biocompatibility and biodegradability are important considerations for minimizing undesirable side effects.

This thesis utilizes the layer-by-layer (LbL) approach for the construction of biodegradable thin films that are capable of controlling the kinetics of localized drug delivery. Typically, controlling the release profiles of more than one drug is difficult, especially from a single film or device. To treat especially recalcitrant diseases, it is sometimes necessary to utilize complex or multimodal drug release behavior for positive therapeutic outcome. We first examined the use a naturally-derived, hydrolytically-degradable polyanion, poly(β-L-malic acid) (PMLA), for use in LbL films to control the rate of film erosion and hence protein elution which was tuned from minutes to weeks depending on the film's architecture. We further adapted the film architecture with subtle chemical modifications for sequential protein release without significant overlap and staged release where a rapid hemostat release coincided with sustained antibiotic release for more than 24 hours. We also examined a biodegradable thin film formulation capable of long-term (14+ months) elution of an active small molecule drug. For rapid hemostasis, it is sometimes difficult to achieve without use of sensitive biologics that require constant refrigeration and so we utilized films composed of self-assembling peptide nanofibers, which we found to be extremely robust and rapidly capable of forming nanofiber based clots despite prolonged incubation in elevated temperatures (2 months at 60°C). Overall this work expands on the controlled release repertoire by investigating fundamental aspects as well as translational applications.

Thesis Supervisor: Paula T. Hammond
Title: David H. Koch (1962) Professor in Engineering

Acknowledgements

To Professor Paula Hammond—I could write an entire thesis chapter thanking her. Without the opportunity to join her lab there is no way I would have been able to succeed in science. She took a chance on me when no one else did, and her support, encouraging attitude and guidance were critical to helping me through the rough patches in my research. For all of the things she has done in revitalizing my interest in science, I will forever be grateful.

To all of the undergraduates that I've had the opportunity to work with (Samantha, Kelsey, Will, Jovana, Nick, Monica)—thank you for all of your work, positive attitudes, and willingness to go the distance.

To my past mentors in research—there's no way I could properly thank you for the way you've shaped me as a scientist. I first got excited about research from Rob, the graduate student that mentored me while I was still an undergraduate at UC Berkeley. Without him, I would never have gotten interested in doing research to start with. Working in Professor Gabor Somorjai's lab was a formative experience, and he was the first person to give the opportunity to work semi-independently. The chance to test out my own theories sparked my scientific curiosity. My incredible luck continued in Mohsen Yeganeh's research lab at ExxonMobil Research and Engineering, which gave me the chance to see how things were done in industry and instilled my interest in interdisciplinary research. At MIT, I will always be thankful to Professor Alex Klibanov during my formative first years in graduate school for his critical eye and attention to detail, which showed me how to truly be objective and scientific in my research.

To my scientific collaborators—no amount of my gratitude would be enough. Professors Eggehard Holler and Julia Ljubimova at Cedar Sinai Medical Center were critical contributors to the research involving their degradable polyanion and I was incredibly lucky for their generosity and input. Shuguang Zhang gave me invaluable guidance and I am privileged to have been able to work with such a prominent pioneer in the field of self-assembling peptides.

To my thesis committee—during some really tough times in graduate school, your support was what helped me stay the course. Professor Alice Ting always had great career advice and was willing to step up to the plate for me if needed. Professor Cathy Drennan helped get me through one of the toughest experiences of my life and I will forever be grateful. Professor Jianzhu Chen stuck with me through my whole time here even through the rough times. Professor Tim Swager gave me deceptively simple but profound advice early in on in graduate school that has been an important factor in guiding my career.

To the support staff at the ISN—so many parts of my work would not have been possible without their direct and indirect help. Bill and Steve were the backbone of the ISN and kept the ship afloat, Amy and Donna made sure all of the necessary materials for research were readily stocked, John and Kurt were always ready to help when I needed it, Josh and Maureen made sure I had the finances to get my research done, and Marlisha was just a wonderful person in general.

To the non-academia people in my life—I don't know what I would have done without you. Without Roberta, the love of my life, there's no way I would have made it through the last couple of years intact. My happiness and perspective on life changed for the better after I met her and no amount of words could describe how lucky I am. Knowing I had the support of my family made the difficult things a bit easier. It took graduate school to get me to know Johnnie, Jack, and Jim but I know they'll be lifelong friends. For the friends I made both in the Hammond lab and in the chemistry department, I couldn't imagine having such a unique experience without you.

Table of Contents

6

List of Figures

8

9

List of Tables

Chapter 1
Introduction

1.1   Drug Delivery

Drugs have transformed lives worldwide, becoming ubiquitous to society with an almost unconscious presence. For an open wound one can apply antibiotic ointment to prevent infection; for a headache or pain one can take non-steroidal anti-inflammatory (NSAID) tablets; for quitting cigarettes one can apply a nicotine patch. Each of these applications represents a delivery approach that makes the application of the drug convenient and simplified without the need of medical expertise. Unfortunately, some drugs cannot be delivered through these routes nor are these formulations able to effectively recapitulate the complex dosage regimens that are sometimes needed to treat especially recalcitrant diseases. With the development of new drugs and an expanding biological understanding of how to use them more effectively, there is a great need for achieving better control over the rates and sequences of drug elution.
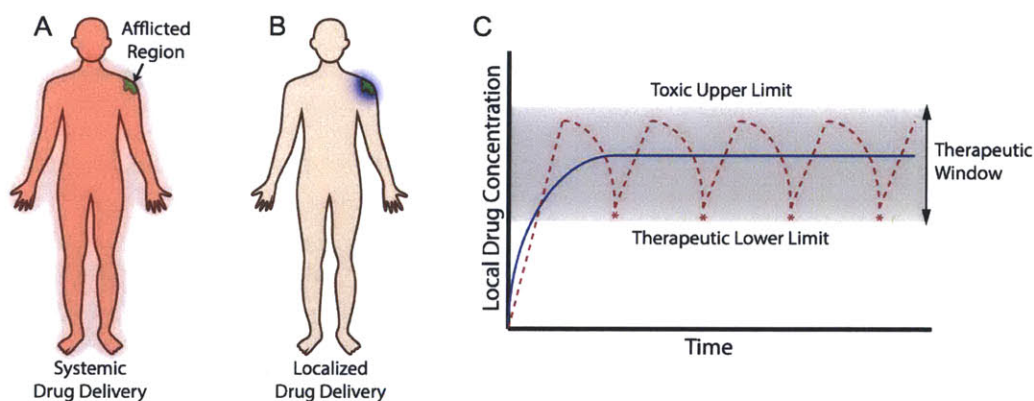
Figure 1-1. Idealized drug delivery pharmacokinetics. Common treatment of an afflicted region of the body (*green*) entails a drug (*red*) to be distributed throughout the body (A) while alternatively the same affliction (*green*) may be treated with drug (*blue*) locally (B). Systemic administration aims to maintain blood concentrations above a threshold level but below a toxic upper limit (*red dashed line*) and usually requires multiple doses (*red asterisks*) because of elimination while a controlled delivery device can maintain a sustained drug release (blue solid line).

In drug treatments, therapeutics are frequently delivered systemically where they are circulated in the bloodstream at elevated concentrations to treat diseases (Figure 1-1A), and this usually requires relatively large dosages to raise plasma concentrations into the drug's therapeutic window (i.e, above sub-therapeutic levels but below toxic levels). In contrast, locally delivering the drug can elevate the concentrations in a selected region, and once diffusing away becomes considerably diluted when reaching the bloodstream (Figure 1-1B). This minimizes the incidences of adverse drug reactions that can be associated with prolonged exposure to high concentrations of drug, as can be the case with systemic delivery(1).

Interest in more efficient drug delivery and reducing the unwanted side effects has fueled the development of localized delivery strategies. While topical application is one of the most convenient ways for local delivery and has been successful in some cases, it is frequently difficult unless treating open wounds (e.g., from military conflict, disasters, accidents, or diseases) because the skin and underlying tissue can occlude access to the more deeply afflicted regions. Parenteral delivery has become more attractive with the advances in surgical technique, especially the development of minimally invasive surgery(2), and thus the use of small biodegradable drug delivery devices implanted in the body are becoming more practical and possible approaches as treatment.

In addition to the route by which a drug is delivered whether systemic or locally, one must consider its frequency and duration. For beneficial effect, drug concentrations often times need to be within a therapeutic window for extended periods of time, but maintaining these elevated plasma concentrations can be difficult due to rapid excretion and metabolism. Bolus means of drug delivery (e.g., injection) can spike the plasma concentration for a short period of time, but to maintain these levels requires multiple dosages resulting in fluctuating plasma

concentrations that can sometimes vary wildly if dosing regimens are not followed correctly (Figure 1-1C). Using an external means to control the drug levels, such as with an intravenous drip, can arrest these issues, but is tremendously inconvenient and the systemic exposure over prolonged times frequently generates unwanted adverse drug reactions(1). Combining the features of localized delivery with controlled drug release can not only stabilize the plasma concentrations by maintaining a steady state between drug elution and bioelimination (Figure 1-1C), but also minimize adverse drug reactions and increase patient compliance to improve therapeutic outcome(3).

In localized controlled delivery systems, the mechanism for drug elution can be fundamentally described through diffusion-controlled, swelling-controlled, and degradation-controlled mechanisms(4). The last approach is desirable because it has biodegradability built into the drug release mechanism where degradation of the device corresponds with drug release. In a common formulation, a hydrolytically degradable polymer containing ester groups along the backbone is used as a bulk material with drug impregnated throughout so that cleavage of these ester groups facilitates erosion to liberate the entrapped drug. In such materials, tuning the polymer degradation behavior significantly influences the kinetics of drug elution with two primary modes of degradation: bulk erosion and surface erosion. If the polymer matrix is sufficiently hydrophobic to repel swelling with water then polymer hydrolysis is restricted to the solid-liquid interface leading to a surface erosion mechanism where degradation gradually eats its way through the matrix from the outside-in. In contrast, if the influx of water occurs on a similar time scale as polymer hydrolysis, the presence of water throughout the material can facilitate bulk erosion throughout the matrix. In realistic conditions, the drug release profile may exhibit a mixture of these two effects, including contributions from drug diffusion or an initial

burst release caused by non-uniform distribution during fabrication(5). There are a number of controlled release devices based on this premise in clinical use including poly(ε-caprolactone), poly(lactic acid), poly(glycolic acid) and poly(lactic-*co*-glycolic acid)(1).

Despite the success of these materials based on hydrophobic polyester matrices for controlled drug release, there remain limitations that preclude its more broad use. For example, to cast the polymer requires organic solvent, which may denature sensitive biologics and non-uniformly distribute the drug. Also, physically entrapping drug in these materials requires significant amounts of polyester materials, which can produce considerable acid during hydrolysis and have deleterious effects on release kinetics. Cracking of material has also been observed, which can lead to additional deregulation of drug elution(5). Although they have been shown to be successful in a number of cases, an alternative approach could yield improved and more versatile delivery kinetics to more closely recapitulate complex drug dosing regimens that are sometimes necessary for treatment of multi-drug resistant or difficult to treat diseases.

1.2   Layer-by-Layer Film Assembly

The Layer-by-Layer (LbL) approach to film assembly is a unique way for generating multifunctional thin films. Since its initial description more than two decades ago(6), it has been adapted to a broad range of applications ranging from sensors and batteries to biomedical devices and targeted drug treatments(7). What makes this technique stand apart from others is the way these films are constructed; they can be assembled from aqueous solutions on a lab bench at room temperature without the need of extraneous equipment, organic solvents, or extreme conditions. As an instructive example at this process (Figure 1-2A), a substrate (e.g., with negative surface charge) is incubated in an aqueous solution of polycation that allows the

15

polymer to bind to the surface through electrostatics. This not only neutralizes the substrate's anionic surface charge, but also reverses it through overcompensation by the polycation. After rinsing away the non-specifically bound material, the substrate is then immersed into a solution of polyanion for its deposition by complexation at the surface, which again reverses the surface functionality. After rinsing again, this constitutes a single cycle and repeating this cycle generates a polyelectrolyte multilayer of (polycation/polyanion)$_n$ film architecture with n-bilayers deposited (Figure 1-2B). Because of the multitude of electrostatic crosslinks, these films resist dissolution in water unless a significant fraction of these bonds are broken, such as from high ionic strengths of solution or significant changes in pH. Other types of intermolecular interactions can also be exploited in a similar fashion for LbL assembly including hydrogen(8) or covalent(9) linkages, which increases the versatility of this approach for incorporating a diversity of materials.
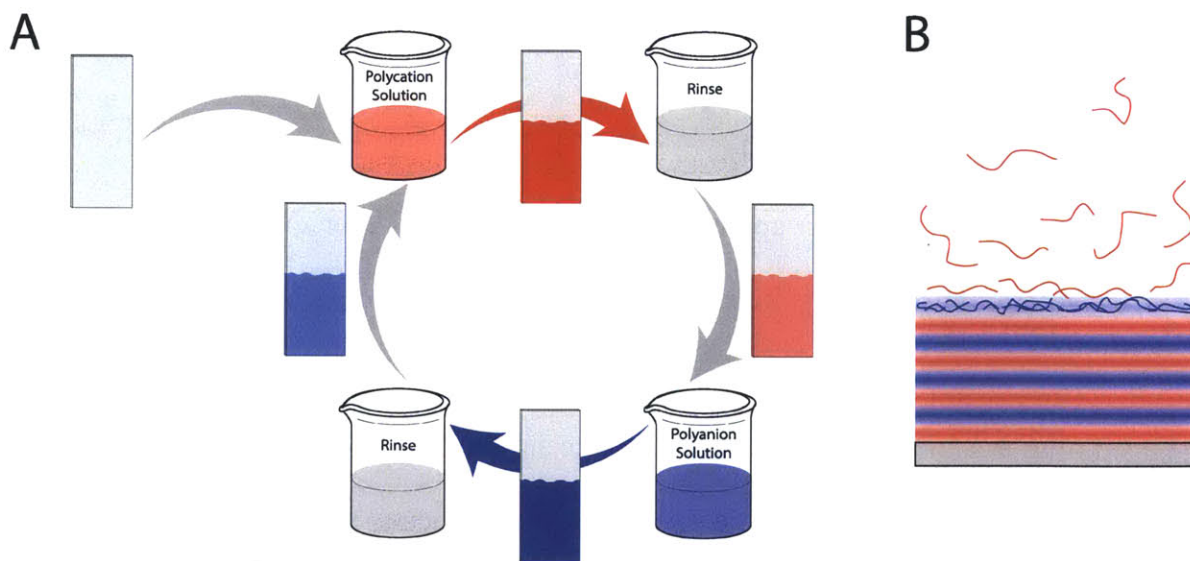
Figure 1-2. Schematic describing the LbL assembly process where a substrate is immersed into different aqueous solutions (A) to deposit layers of polyelectrolytes in succession (B).

In an idealized scenario with low ionic strength of solution and highly charged polyelectrolytes, the resultant film's molecular level stratification reflects its sequence of assembly with minimal interpenetration between layers(10), as depicted in Figure 1-2B. Unfortunately, it is often the case where films need to be assembled under non-ideal conditions. For example, stratification has been found to correlate with the strength of intermolecular interactions(11) and therapeutics can often be poorly charged/zwitterionic, have significant tertiary structure, and/or have limited water solubility, each of which can reduce the density of their possible intermolecular linkages in the film, and hence diminish the overall loading. Furthermore, film components can be dynamic during interdiffusing laterally(12) and perpendicularly to the film substrate(13) causing rearrangement and some times displacement of more weakly associated components in a film(14).

Despite these challenges, judicious choice of assembly conditions and components can generate the desired properties. One of the more exciting applications the LbL film assembly is for fabrication of controlled drug delivery devices. By being an aqueous-based technique that uses inherently available functional groups (ionic or hydrogen bonding) present in biologics, it can help preserve the native state of proteins(15) and avoids the potentially denaturing conditions (e.g., organic solvents and temperatures) required by other techniques. This has since been adopted for use with a variety of drugs, including small molecules, polynucleic acids, peptides, and proteins(7).

With a growing understanding of the intricacies underlying biological responses to single and multi-drug treatments and the potential synergy derived from their spatiotemporal administration (e.g., simultaneously, sequentially or a combination thereof), having a controlled delivery strategy from a biodegradable thin film device able to recapitulate complex dosage

regimens would be a significant advance in treatment of recalcitrant diseases. Programmable devices have shown some promise in controlled drug delivery, but they are often bulky and non-degradable, which requires retrieval after use. Having a biodegradable nano to micron scale device capable of a pre-programmed release of multiple drugs would be a significant advance in therapeutic drug treatment.

1.3   Thesis Overview

In its utmost superficiality, this body of work describes different kinds of drug release behavior. However, great significance and mechanistic insight can be derived from the extremes in this behavior (spanning minutes to more than a year) and the logical but subtly uncomplicated modifications needed to achieve it. While investigating these chemical and physical alterations, it was important to maintain biocompatibility and high drug activity and so considerable effort was made to restrict the choice of components and assembly conditions to those best suited for possible translational application. As a result, the progress reported here not only has fundamental implications on controlled release behavior, but also biomedical relevance.

In Chapter 2, we designed and characterized films composed of naturally derived materials for controlled release of proteins. Traditional drug delivery strategies rely on synthetic or semi-synthetic materials, or utilize potentially denaturing assembly conditions that are not optimal for sensitive biologics. Layer-by-Layer (LbL) assembly of films uses benign conditions and can generate films with various release mechanisms including hydrolysis-facilitated degradation. These use components such as synthetic polycations that degrade into non-natural products. Herein we report the use of a naturally-derived, biocompatible and degradable polyanion, poly(β-L-malic acid), alone and in combination with chitosan in an LbL film, whose

degradation products of malic acid and chitosan are both generally recognized as safe (GRAS) by the FDA. We have found that films based on this polyanion have shown sustained release of a model protein, lysozyme that can be timed from tens of minutes to multiple days through different film architectures. We also report the incorporation and release of a clinically used biologic, basic fibroblast growth factor (bFGF), which demonstrates the use of this strategy as a platform for controlled release of various biologics.

In Chapter 3, we addressed improving the release kinetics for controlled release of more than one drug. Multidrug regimens can sometimes treat recalcitrant diseases when single-drug therapies fail. Recapitulating complex multidrug administration from controlled release films for localized delivery remains challenging because their release kinetics are frequently intertwined and an initial burst release of each drug is usually uncontrollable. Herein we demonstrate kinetic control over protein release by crosslinking Layer-by-Layer films during the assembly process. We used biodegradable and naturally derived components and relied on copper-free click chemistry for bioorthogonal covalent crosslinks throughout the film that entrap, but do not modify the embedded protein. We found that this strategy restricted the interdiffusion of protein while maintaining its activity. By depositing a barrier layer and a second protein-containing layer atop this construct, we generated well-defined sequential protein release with minimal overlap that follows their spatial distribution within the film.

In Chapter 4, we developed a multidrug controlled release film with individually tunable release kinetics to address uncontrolled bleeding and infection, which are the major causes of death and morbidity from traumatic wounds during military conflicts, disasters, and accidents. Because immediate treatment is critical to survival, it is desirable to have a lightweight and rapidly applied bandage—one capable of delivering a hemostat that can quickly resolve bleeding

while addressing infection over short and longer time frames. It is challenging to design thin film coatings capable of multi-drug release, particularly when the drugs are quite different in nature (biologic versus small molecule, charged versus neutral) and the release profiles desired are different for each drug. Herein we have adopted a layer-by-layer film assembly technique to create a linear combination of two independently functional films capable of rapidly releasing thrombin within minutes while sustaining vancomycin elution for more than 24 hours. By conjugating vancomycin to a hydrolytically degradable polyacid, poly(β-L-malic acid), we were able to create a robust thin film with loading and release kinetics that remain unaffected by the additional deposition of a thrombin-based film, demonstrating the possibility for future multi-therapeutic films with independently tunable release kinetics.

In Chapter 5, we examined a controlled release thin film formulation to generate sustained drug release for more than a year. Usually, such long-term, localized, delivery of small molecules from a biodegradable thin film is challenging due to their low molecular weight and poor charge density. Accomplishing highly extended controlled release can facilitate high therapeutic levels in specific regions of the body while significantly reducing the toxicity to vital organs that is typically caused by systemic administration, all the while decreasing the need for medical intervention due to its long-lasting release. Also important is the ability to achieve high drug loadings in such thin film coatings to allow incorporation of significant drug amounts on implant surfaces. Herein we report a sustained release formulation for small molecules based on a soluble charged polymer-drug conjugate that is immobilized into nanoscale, conformal layer-by-layer (LbL) assembled films, applicable to a variety of substrate surfaces. Using an electrostatically assembled biodegradable film system composed of a drug conjugated to a biopolymer, we measure a highly predictable sustained drug release from a polymer thin film

coating of 0.5 to 2.7 microns that continues for more than 14 months with physiologically relevant drug concentrations, providing an important drug delivery advance. We use a potent small molecule non-steroidal anti-inflammatory (NSAID) drug, diclofenac, as a demonstration of this effect as it can be used to address chronic pain, osteoarthritis, and a range of other critical medical issues. We also show that despite the initial chemical modification and duration of release, the released drug remains active and retains its intrinsic potency.

In Chapter 6, we examine self-assembling peptide nanofibers, which have shown superior hemostatic activity. Herein we elucidate their action by visualizing the formation of nanofiber-based clots that aggregate blood components with a similar morphology to fibrin-based clots. Furthermore, to enhance its direct application to a wound, we developed layer-by-layer assembled thin films onto common materials used for wound dressings—gauze and gelatin sponges. We find these nanofibers elute upon hydration under physiological conditions and generate nanofiber clots with blood. After exposure to a range of harsh temperature conditions (-80°C to 60°C) for a week and even 2 months at 60°C, these hemostatic bandages remain capable of releasing active nanofibers. This thermal robustness in combination with the self-assembling peptide's potent hemostatic activity, biocompatibility, biodegradability, and low cost of production make this a promising approach for a cheap yet effective hemostatic bandage.

1.4 References

1. Siepmann J, Siegel RA, & Rathbone MJ eds (2012) *Fundamentals and Applications of Controlled Release Drug Delivery* (Springer).
2. Langer R & Tirrell DA (2004) Designing materials for biology and medicine. *Nature* 428(6982):487-492.
3. Richter A, Anton SF, Koch P, & Dennett SL (2003) The impact of reducing dose frequency on health outcomes. *Clin. Ther.* 25(8):2307-2335.
4. Ratner BD, Hoffman AS, Schoen FJ, & Lemons JE eds (1996) *Biomaterials Science: An Introduction to Materials in Medicine* (Academic Press, San Diego, California).
5. Fredenberg S, Wahlgren M, Reslow M, & Axelsson A (2011) The mechanisms of drug release in poly(lactic-co-glycolic acid)-based drug delivery systems—A review. *Int. J. Pharm.* 415(1–2):34-52.
6. Decher G, Hong JD, & Schmitt J (1992) BUILDUP OF ULTRATHIN MULTILAYER FILMS BY A SELF-ASSEMBLY PROCESS .3. CONSECUTIVELY ALTERNATING ADSORPTION OF ANIONIC AND CATIONIC POLYELECTROLYTES ON CHARGED SURFACES. *Thin Solid Films* 210(1-2):831-835.
7. Decher G & Schlenoff JB eds (2012) *Multilayer Thin Films: Sequential Assembly of Nanocomposite Materials* (Wiley-VCH, Weinheim, Germany), 2nd Ed.
8. Sukhishvili SA & Granick S (2000) Layered, erasable, ultrathin polymer films. *J. Am. Chem. Soc.* 122(39):9550-9551.
9. Such GK, Quinn JF, Quinn A, Tjipto E, & Caruso F (2006) Assembly of ultrathin polymer multilayer films by click chemistry. *J. Am. Chem. Soc.* 128(29):9318-9319.
10. Schmitt J, *et al.* (1993) INTERNAL STRUCTURE OF LAYER-BY-LAYER ADSORBED POLYELECTROLYTE FILMS - A NEUTRON AND X-RAY REFLECTIVITY STUDY. *Macromolecules* 26(25):7058-7063.
11. Kharlampieva E, Kozlovskaya V, Ankner JF, & Sukhishvili SA (2008) Hydrogen-Bonded Polymer Multilayers Probed by Neutron Reflectivity. *Langmuir* 24(20):11346-11349.
12. Xu L, Selin V, Zhuk A, Ankner JF, & Sukhishvili SA (2013) Molecular Weight Dependence of Polymer Chain Mobility within Multilayer Films. *Acs Macro Letters* 2(10):865-868.
13. Picart C, *et al.* (2002) Molecular basis for the explanation of the exponential growth of polyelectrolyte multilayers. *Proc. Natl. Acad. Sci. U. S. A.* 99(20):12531-12535.
14. Gilbert JB, Rubner MF, & Cohen RE (2013) Depth-profiling X-ray photoelectron spectroscopy (XPS) analysis of interlayer diffusion in polyelectrolyte multilayers. *Proc. Natl. Acad. Sci. U. S. A.* 110(17):6651-6656.
15. Schwinte P, *et al.* (2001) Stabilizing effects of various polyelectrolyte multilayer films on the structure of adsorbed/embedded fibrinogen molecules: An ATR-FTIR study. *J. Phys. Chem. B* 105(47):11906-11916.

Chapter 2
Multilayer Films Assembled from Naturally-Derived Materials for Controlled Protein Release

Authors:
Bryan B. Hsu[1,3], Samantha R. Hagerman[2], Kelsey Jamieson[2], Jovana Veselinovic[2], Nicholas O'Neill[4], Eggehard Holler[5], Julia Y. Ljubimova[5], and Paula T. Hammond[2,3]

Departments of [1]Chemistry and [2]Chemical Engineering, Massachusetts Institute of Technology, Cambridge, MA 02139
[3]Institute for Soldier Nanotechnologies, Cambridge, MA 02139
[4]Department of Chemical and Biomolecular Engineering, University of Notre Dame, South Bend, In 46556
[5]Nanomedicine Research Center, Department of Neurosurgery, Cedars Sinai Medical Center, Los Angeles, CA 90048

Contributions:
B.B.H. and P.T.H. designed experiments and prepared the manuscript. B.B.H., S.R.H., K.J., J.V., and N.O. performed experiments. E.H., and J.Y.L. contributed essential compounds.

2.1 Introduction

Controlled release from biodegradable matrices offers attractive possibilities in creating personalized medicine for on-demand and/or pre-programmed care with dynamic tunable delivery(1, 2). Topical application, implantation or injection of these materials, whether alone or as a coating, can administer localized dosages of therapeutics and significantly reduce complications from systemic toxicity(3, 4). In addition, with bolus release, biologics like growth factors are underutilized because of their rapid degradation and clearance *in vivo*. In addition, only nanogram levels are necessary to elicit biological response and hence a controlled low-dose release would enhance not only the therapeutic efficiency, but also practical factors such as increasing patient compliance through fewer applications, reduced cost from less growth factor needed, and minimal upkeep from a preprogrammed release profile. There are numerous mechanisms explored for controlling drug release ranging from dissolution, degradative, or diffusive mechanisms(5), to triggered release via external stimuli such as electrical or photonic means(6). For such delivery devices, biocompatibility and biodegradability are desirable and would eliminate concerns of systemic toxicity and complications from released polymer byproduct.

A prominent, well-studied degradable polymer for controlled release is poly(lactic-*co*-glycolic acid) (PLGA), which has a number of clinical uses for drug delivery(7, 8). Although processing of PLGA for drug encapsulation is amenable for certain small molecules, it is potentially denaturing for sensitive biologics(8, 9), as it may require organic solvent and/or heat conditions for processing. Furthermore, the relative loading of biologic drugs into PLGA is defined in part by the thermodynamics of polymer mixing, and typically implies low fractions of drug, thus requiring significantly more polymer carrier for a given net amount of drug. The

resultant drug release is a complex interplay between the drug's diffusivity and the PLGA carrier's degradation; heterogeneous drug distribution, pore formation, water ingress/swelling, and polymer structural stability, among other factors can lead to burst and/or multi-phasic release profiles that cause undesirable fluctuations in drug release(10).

An alternative approach is the aqueous based layer-by-layer (LbL) assembly of polymer thin films that encapsulates biologic drugs such as proteins and nucleic acids by taking advantage of their charged state and/or other secondary interactions(1, 2, 11). Instead of using organic solvent to form a water-insoluble hydrophobic polymer blend, LbL assembly utilizes electrostatic complexation between polyelectrolyte components under aqueous conditions to form insoluble, electrostatically-crosslinked matrices. When these films are assembled, they resist dissolution in water and can be designed to release therapeutic cargo through various diffusional, triggered, and degradative mechanisms(12). The latter has shown capability for tunable release of sensitive biologics like growth factors while retaining their biological activity(13-17). An extensive library of natural biomaterials such as polysaccharides (*e.g.*, hyaluronic acid, chondroitin, heparin, and chitosan) and polypeptides (*e.g.*, poly(L-lysine), poly(L-arginine), poly(L-glutamic acid), and poly(L-aspartic acid) are available for use in LbL assembly; however, to control release, synthetic polycations such as poly(β-amino ester)s (PBAEs) are primarily used. While these were originally synthesized for gene delivery(18) they have subsequently been used in LbL films as a hydrolytically degradable component(19-21) and sustained hydrolytic release still primarily relies on these synthetically-derived PBAEs.

Herein we investigate the use of completely naturally-derived materials for LbL assembly of controlled release films. To achieve tunable degradation, we replace the commonly used synthetic PBAE with a naturally derived polyanion, poly(β-L-malic acid) (PMLA), which can be

25

extracted in linear, high-molecular weight from *Physarum polycephalum* and branched, low molecular weight from *Aureobasidium* sp., functioning as a DNA polymerase inhibitor in the former(22). It has demonstrated excellent biocompatibility with tolerance by mice of up to 1.6 g/kg intravenously and 6 g/kg intraperitoneally(22-24), in addition to eliciting no immunogenic response(22, 24). The degradation product, L-malic acid, is a metabolite in the Krebs cycle and can be found naturally in high abundance, yielding a "Generally Recognized As Safe (GRAS)" status by the FDA. We also include use of chitosan as an additional component to stabilize film growth and robustness. This naturally-derived polycation has been extensively investigated for its numerous positive biological properties(25) and has also received GRAS status by the FDA. We demonstrate that the chitosan-PMLA scaffold is a viable and effective means for controlled delivery of a model protein, lysozyme, and a therapeutically relevant growth factor, bFGF.

2.2   Materials and Methods

All materials were used without further purification unless otherwise noted.   The polyelectrolytes used in this study were obtained from various sources: Poly(L-Lysine) (PLL, 30-70kDa, Sigma-Aldrich), fluorescein-labeled PLL (30-70kDa, Sigma-Aldrich) linear polyethylenimine (LPEI, 25kDa and 250kDa, Polysciences), chitosan (15 kDa, Polysciences), polyallylamine hydrochloride (PAH, 60 kDa, Polysciences), poly(sodium-4-styrenesulfonate) (SPS, 70 kDa, Sigma-Aldrich), poly(acrylic acid) (PAA, ~50 kDa, Polysciences). Poly(β-L-malic acid) (PMLA, 40 kDa) was cultured from *Physarum polycephalum* as previously described(22).   Hen-egg lysozyme, 3 M sodium acetate, and all other materials were obtained from Sigma-Aldrich.   Phosphate-buffered saline (Dulbecco's PBS 10X) was obtained from Invitrogen and diluted to 1X concentration before use. Recombinant human basic fibroblast growth factor (bFGF) was obtained from Biolegend.   Cell culture medium consisted of Dulbecco's modified eagle medium (DMEM) supplemented with L-Glutamine, antibiotic-antimycotic, and heat-inactivated fetal bovine serum (FBS), which were obtained from Invitrogen and used at 1X concentrations. All solutions involving H_2O used MilliQ purified water.

Polymer degrees of ionization were determined by potentiometric titration, similarly to as described previously(26). After bubbling solutions with N_2, 15 mL solutions 0.5 mg/mL of PMLA or PAA in H_2O were titrated with 0.2 M HCl or NaOH and normalized to titration of pure H_2O. The pKa was taken as the pH at which half of the monomer side chains are ionized.

In a 96-well plate, 40 µL of 10 mg/mL polycation (or lysozyme) solution was combined with 40 µL of polyanion solution and 70 µL of a diluted NaCl solution, each prepared in 10 mM sodium acetate, pH 5.0. Optical density at 450 nm was normalized to the maximal absorbance

after blank (buffer) subtraction. Chitosan-PMLA polyplexes formed intractable pastes so 5-fold diluted solutions were used.

Unless otherwise noted, polymer or proteins were formulated at 1 mg/mL concentrations and films were assembled using programmable slide strainers (Carl Zeiss). Silicon wafers were pre-cleaned with methanol and water, irradiated with plasma (Harrick PDC-32G) and coated with a baselayer of $(LPEI/SPS)_{10}$ as described previously(27).

Films of $(polycation/PMLA)_n$ with non-proteinacious polycations (i.e., without lysozyme or bFGF) were assembled from 100 mM sodium acetate, pH 5.0, solutions with programmed cycles of immersion for 15 min in polycation solution, 10 s, 20 s, and 30 s of wash in buffer, then 15 min in PMLA solution and 10 s, 20 s, and 30 s of wash in buffer. Analogous films containing protein in a $(protein/PMLA)_n$ or $(chitosan/PMLA/protein/PMLA)_n$ architecture were assembled from 10 mM sodium acetate, pH 5.0 solutions with identical incubation times of 15 min in polymer/protein solution and 10 s, 20 s, and 30 s washes in H_2O. Solutions of bFGF were formulated at 50 µg/mL. After assembly, films were dried under house vacuum at room temperature overnight.

Thickness was measured from razor-scored films by determining the average step-height difference between six measurements with a 2.5 µm tip (Dektak 150 Profilometer). Release studies of films of 1 cm^2 area were performed by incubation in physiological conditions of 500 µL of PBS, pH 7.4 at 37°C. Solutions were periodically replaced with fresh aliquots of PBS pre-warmed to 37°C and returned to incubation. Concentration of PLL^{Fluor} was determined by comparison of absorbances at 494 nm for release aliquots to standard curves. Quantification of lysozyme released from the film using bicinchoninic acid (BCA) assay was found unacceptable, because of background signal originating from chitosan and PMLA film components. Therefore

we used a lysozyme-specific enzymatic assay to determine the concentration of active lysozyme. Mixtures of 200 µL of 0.3 mg/mL *Micrococcus lysodeikticus* in PBS and 50 µL of lysozyme-containing sample or standard in PBS was monitored at 450 nm and 37°C in a 96-well plate format. The reduction in turbidity of sample solutions was compared to a standard curve to determine lysozyme concentration. bFGF concentration was measured by ELISA and performed according to manufacturer instructions (Peprotech).

To determine the effect of film components released into solution on cell viability, we incubated films in 1 mL of cell culture medium with 10% FBS at 37°C, similarly to as described for the release studies. NIH3T3 cells were seeded in a 96 well tissue culture plate at 10,000 cells/well in cell culture medium with 10% FBS and after an overnight incubation, media was replaced with 100 µL of sterile-filtered film release media. The cells were incubated overnight and then their viability was determined by MTS assay (Promega) and performed according to manufacturer's directions.

The activity of bFGF released was determined by proliferative assay with NIH3T3 (ATCC) fibroblast cells. Cell culture was composed of Dulbecco's modified eagle medium (DMEM) supplemented with fetal bovine serum, and the assay was adapted as previously described(14). Cells were seeded at 1000 cells/well in 100 µL of 10% FBS culture medium in a 96-well tissue culture plate and incubated for 2 d after which cells were serum starved in 100 uL of 0.5% FBS culture medium. After overnight incubation the media was replaced with 100 µL of PBS containing film release media (from the above mentioned release studies) that was combined with 900 µL of 0.5% FBS culture medium and then sterile filtered. After 2 d of incubation, cell numbers was quantified by MTS assay (Promega) according to manufacturer's

directions. Proliferative activity was determined by proportional increase in absorbance as normalized to a PBS control.

2.3   Results and Discussion

LbL Assembly and Degradation

A number of mechanisms have been used for controlled release from LbL films; harnessing tunable degradation of at least one component in a multi-component, drug-laden, film is an important approach for releasing various therapeutics ranging from small molecules to biomacromolecules(1).   PMLA offers an innocuous and naturally-derived alternative to the commonly used synthetic polyesters like PBAEs and PLGA.   With potentiometric titration, we measured PMLA's pH dependent ionization, which is an important characteristic when considering electrostatic or hydrogen-bonded LbL film assembly.   Figure 2-1 shows that the pH at which PMLA reaches 50% ionization (pK$_a$) is 4.58 ± 0.02 with roughly 68.2% and 99.3% of the carboxylic acid groups ionized at pH 5.0 and 7.4, respectively.   These degrees of ionization may also tend to be higher in salt solutions due to electrostatic screening effects(28, 29). Therefore assembly of films at pH 5 or above will have substantial electrostatic interactions.
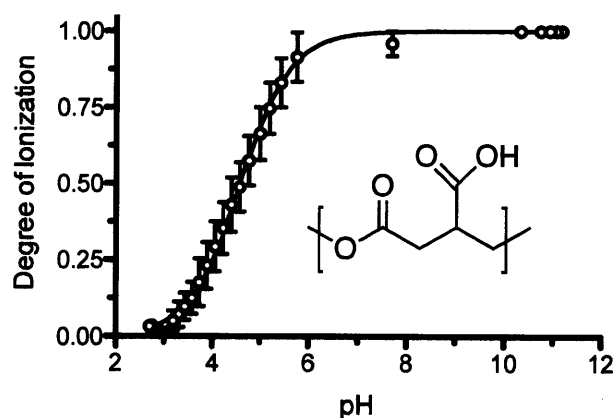
Figure 2-1. Potentiometric titration of PMLA in water at room temperature.   The symbols represent measured values of PMLA (*inset*) and the solid line is a four-parameter fit, giving a measured pK$_a$ of 4.58 ± 0.02.
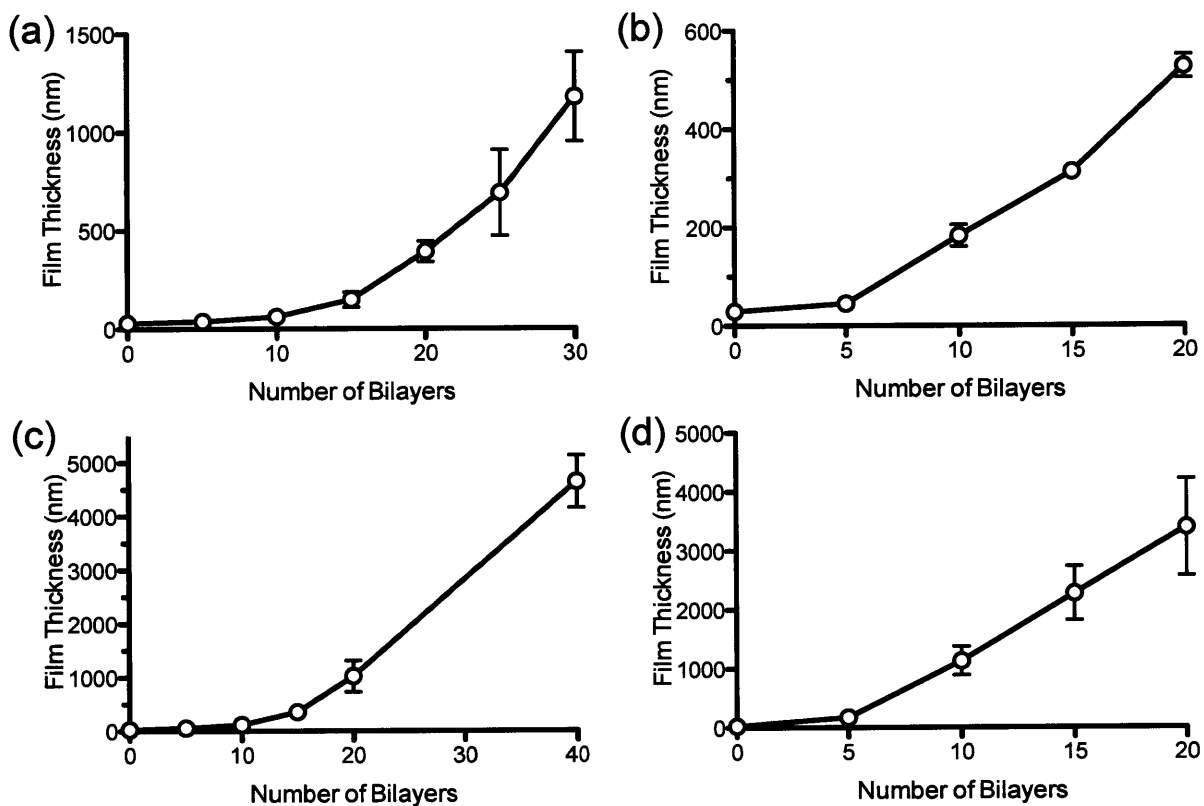
Figure 2-2. Film growth of (polycation/PMLA)$_n$ films. Growth curves represent film assembly with polycations of PAH (a), chitosan (b), PLL (c), and LPEI (d).

In exploiting PMLA's significant negative charge, we examined its film growth behavior with various polycations that have been well studied in polyelectrolyte multilayers. As shown in Figure 2-2, each (polycation/PMLA)$_n$ film reveals a concurrent growth with the number of bilayers deposited, exhibiting the tunability in thickness and loading traditionally observed in multilayer films. A figure with the compiled growth curves is shown in Figure 2-3. Based on reported pK_a values for poly-L-lysine (PLL, pK_a~9.9(30)), linear polyethylenimine (LPEI, pK_a~7.9(31)), polyallylamine (PAH, pK_a~8.8(32)), and chitosan (pK_a~6.5(33)), each polycation

bears significant positive charge under the assembly conditions (pH 5.0) thus driving electrostatic film assembly with PMLA.
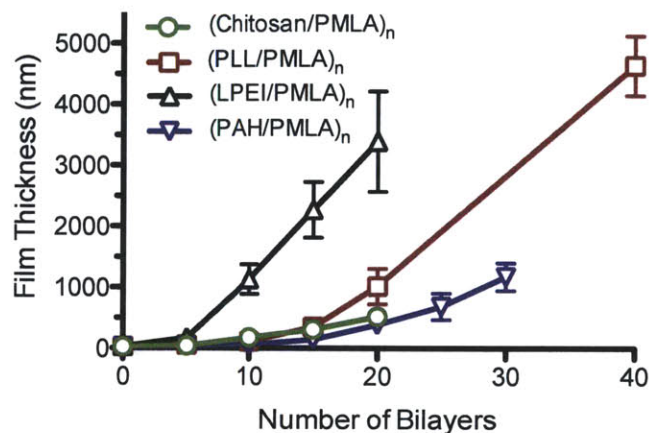
Figure 2-3. Compiled growth curves of (Polycation/PMLA) films.

As sometimes observed in LbL film assembly, there can be variability in growth behavior depending on the film components. Similarly, we observed that each (polycation/PMLA)$_n$ film grows exponentially to different degrees. Films composed of strong polyelectrolytes, or weak polyelectrolytes in highly charged states, can exhibit nanoscale growth that increases linearly with number of layers(34-36); typically the slope of the growth curve is in the range of nanometers to a few tens of nanometers per bilayer pair. On the other hand, when polyelectrolytes are weakly charged they may be highly diffusive in the LbL film, which can lead to exponential growth with bilayer thicknesses approaching hundreds of nanometers. Nonlinear growth is theorized to be a result of "in and out" diffusion where some polyelectrolytes can readily diffuse into and within the LbL film(37-40). Therefore the resulting growth behavior is subject to a number of characteristics such as the polyelectrolyte's degree of

ionization(41), charge density(42), molecular weight(43), secondary intermolecular interactions(42, 44, 45), and ionic strength of solution(46).
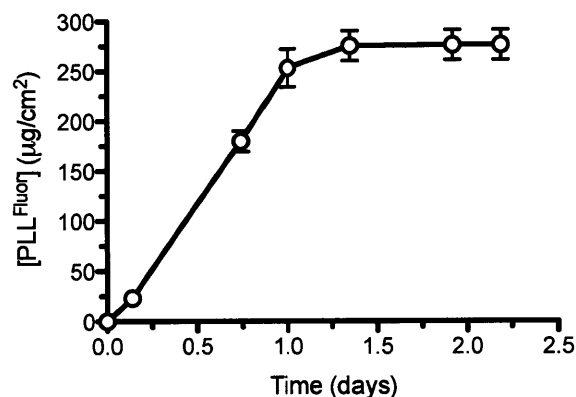
Figure 2-4. PLL^{Fluor} release profile from (PLL^{Fluor}/PMLA)$_{20}$ films incubated in PBS, pH 7.4 at 37°C.

With these clear examples of multilayer film assembly using PMLA, we studied its role in facilitating film disassembly and component release. The hydrolysis of the ester backbone in PMLA would reduce its molecular weight and consequently destabilize the overall film integrity. We used a fluorescently labeled PLL component in a (PLL^{Fluor}/PMLA)$_{20}$ film and tracked its elution over time for insight into the release behavior imparted by PMLA-based films. As is shown in Figure 2-4, we found that PLL^{Fluor} continued to release for 30 hours, with the majority eluting within the first 24 hours. The duration in release is similar to what was observed with previous (polycation/polyanion)$_n$ systems utilizing PBAEs, like (Polymer 1/DNA)$_n$ which showed sustained release in PBS, pH 7.4 at 37°C for 16 to 30 hours(20, 47).

Polyelectrolyte Complex Stability

Our previous studies have used lysozyme as a good model for the investigation of protein release from different LbL film architectures(13) with a size (i.e. 14.3 kDa with a hydrodynamic

radius of 1.9 nm(48)) and charge (i.e., isoelectric point, pI of 11(49)) relevant to other therapeutically interesting biologics. While investigating $(lysozyme/PMLA)_n$ film architectures, we discovered the ionic strength and pH of solution was highly influential on film growth; films could be assembled in 10 mM sodium acetate at pH 5.0, but not in 100 mM sodium acetate at pH 5.0, 10 mM sodium phosphate at pH 7.4, or phosphate buffered saline at pH 7.4. The stability of intermolecular crosslinks, especially ionic, is a well known factor in film assembly(50) and so we suspected the number and density of ionic crosslinks formed between the protein and polyanion may be less numerous than between a typical polycation and polyanion in an LbL film. Although lysozyme exhibits a net positive charge, it is in low number and of patchy distribution across the globular surface(51). In line with what we observed during attempted $(lysozyme/PMLA)_n$ film assemblies at pH 5.0 and pH 7.4, ionic strength at 10 mM was too weak to prevent electrostatic film assembly with lysozyme (net charge +10(49)). In contrast, 100 mM ionic strength disrupted film assembly due to increased ionic shielding. At pH 7.4, lysozyme's charge density is even lower (+7(49)), making it more sensitive to ionic shielding, which is evidenced by a lack of film growth in 10 mM sodium phosphate and PBS solutions.

Table 2-1. Ionic titration of polyplexes and polyionic species at pH 5.0 and at room temperature. The critical sodium chloride concentration at which complete polyplex dissolution is achieved is defined as $[NaCl]_c$.

Polyelectrolyte Complex	Type of Interaction	$[NaCl]_C$*
Lysozyme - Heparin Sulfate	Electrostatic	0.58 M
Lysozyme - PMLA	Electrostatic	0.29 M
Lysozyme - PAA	Electrostatic	1.17 M
Lysozyme - Tannic Acid	Hydrogen-Bonding	Unaffected
PLL - PMLA	Electrostatic	2.3 M
Chitosan - PMLA	Electrostatic	> 3.4 M
Chitosan - PAA	Electrostatic	> 3.4 M

To probe the stabilities of electrostatic interactions formed in our multilayers, we titrated two-component polyelectrolyte complexes (polyplexes) with increasing concentrations of sodium chloride. Addition of salt disrupts electrostatic crosslinks through ionic shielding and the critical concentration necessary for these polyplexes to reach dissolution (as determined by turbidity) reflects their relative strengths of complexation. This strategy has been fruitfully explored for other (protein/polyanion) film architectures(52) and has uncovered direct relationships between the stabilities of polyplexes in solution and their analogous LbL films(53-55). For insights into the PMLA-based systems, we studied the stability of polyplexes between lysozyme and various polyanionic compounds at pH 5. As shown in Figure 2-5 and summarized in the first three rows of Table 2-1, each of the polyplexes are stable up to a critical sodium chloride concentration, $[NaCl]_C$, beyond which the polyplexes are dissolved. Previous work has shown heparin to be an excellent polyanion for the LbL assembly of lysozyme(13) and as such, its polyplex is found to be stable in up to 580 mM of NaCl, agreeing with reported values(56). Heparin is strongly polyanionic with fully ionized sulfate moieties and in conjunction with its polysaccharide backbone (i.e., capable of hydrogen-bonding) it likely contributes additional stability to these polyplexes over PMLA, a weak polyelectrolyte. By comparison, PAA forms a more stable complex with lysozyme. Potentiometric titration of PAA (Figure 2-6) indicates it has a pKa of ~6.6 with substantially lower ionization (18.9%) than PMLA. Although it is capable of fewer electrostatic crosslinks at pH 5.0, hydrogen bonds can stabilize polyplex formation, as has been observed in previously assembled bilayer LbL films at pH 4(52), where PAA is even more poorly charged (<10% ionized). Hydrogen-bonding would be insensitive to ionic shielding effects and to demonstrate this, we titrated lysozyme polyplexes with tannic acid, a polyphenol known to form such complexes with proteins in solution and in LbL

assemblies(57). Shown in Figure 2-5 and Table 2-1, we found these complexes were insensitive to ionic titration.
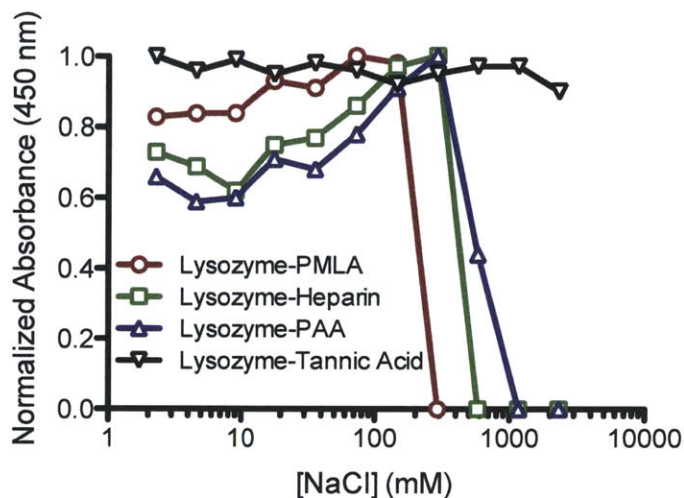
Figure 2-5. Ionic titration of polyplexes between lysozyme and various compounds.
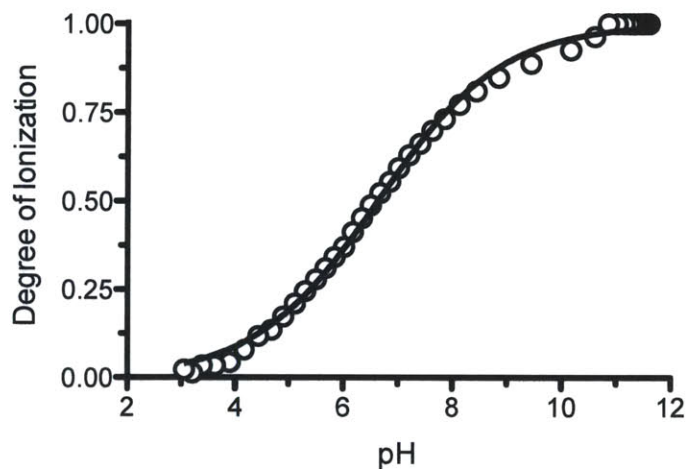
Figure 2-6. Potentiometric titration of PAA in H_2O shows a pK_a of 6.6, similarly to previously described values. (32).
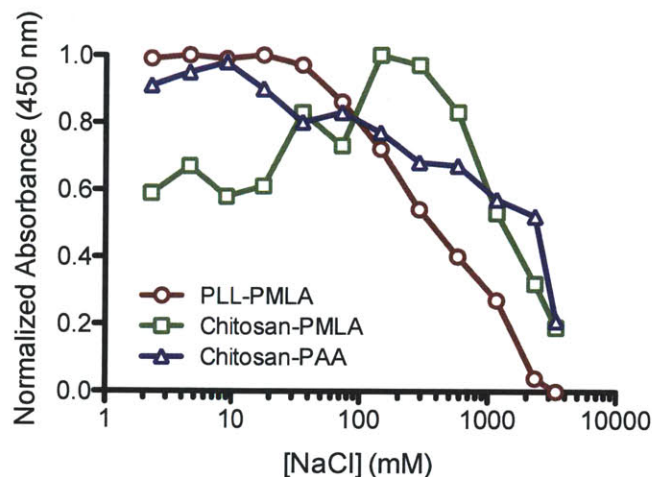
Figure 2-7. Ionic titration of polyplexes between various polyionic species.

For comparison of the relative stabilities of polycation-polyanion polyplexes, where electrostatic crosslinks would be more numerous, we studied the ionic titration of PLL, chitosan, PMLA, and PAA based complexes. As shown in Figure 2-7 and summarized in Table 1, each polyplex showed greater stability than lysozyme-based electrostatic polyplexes. This can be attributed to denser electrostatic crosslinks, which are overall less susceptible to salt induced dissolution. The gradual loss of turbidity with increasing ionic strength suggests loosening that progresses towards dissolution, where the high multivalency of crosslinks maintains some semblance of complexation despite high ionic strength. This is in contrast to lysozyme polyplexes, which have a sharp decline in stability after reaching a critical sodium chloride concentration.
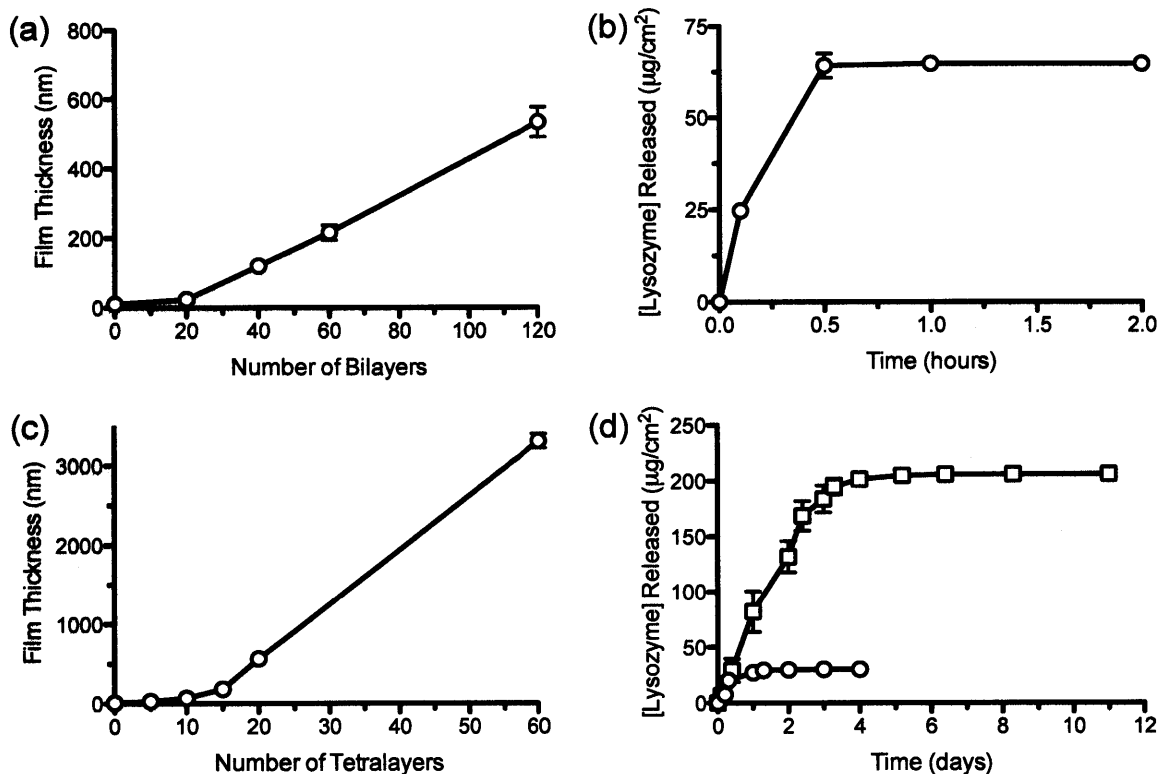
Figure 2-8. Film growth curves (a,c) and lysozyme release profiles in PBS, pH 7.4 at 37°C (b,d) for (lysozyme/PMLA)$_n$ films (a,b) and (chitosan/PMLA/lysozyme/PMLA)$_n$ films (c,d). Release data were from 120 bilayer films (b), and 20 (*circles*) and 60 (*squares*) tetralayer films (d).

Controlled Protein Release

Using our insights into the relative stabilities of protein-polyanion and polycation-polyanion polyplexes, we examined (lysozyme/PMLA)$_n$ bilayer systems and (chitosan/PMLA/lysozyme/PMLA)$_n$ tetralayer systems as rapid and sustained release film formulations, respectively. As described earlier, we found the bilayer films were capable of assembly from low salt solutions of 10 mM sodium acetate, pH 5.0. The (lysozyme/PMLA)$_n$ growth, as shown in Figure 2-8a, reveals an initial slow growth until 20 bilayers, after which growth becomes proportional with the number of bilayers. An initially sluggish growth has been similarly described for other multilayer film architectures(58, 59) including lysozyme-based

films(13) and was attributed to various factors such an initially slow period of exponential growth(59) or island formation of surface-complexes that coalesce to seed later film growth(38). After this induction period, we observe a linear growth that has been observed in LbL films composed of strong polyelectrolytes(34-36) and particle based films where minimal interdiffusion can occur. The film thickness deposited per bilayer in this linear growth regime is 5.1 nm/bilayer, which is roughly 1.3 times lysozyme's hydrodynamic diameter (~3.8 nm(49)). When including PMLA's thickness contribution, the lysozyme deposition appears to be limited to a monolayer adsorption, with minimal interdiffusion, which is likely due to lysozyme's size and globular structure.

When examining the release behavior of (lysozyme/PMLA)$_{120}$ films in physiological conditions (PBS, pH 7.4 and 37°C), we found a rapid lysozyme release as shown in Figure 2-8b. The combination of higher pH and ionic strength appears to completely destabilize the film within 30 min and coincides with our previously described observations. When calculating the loading density we find that there is 1.22 ± 0.10 mg/mm^3 of lysozyme in the film, a density approaching the 1.25 to 1.62 mg/mm^3 of protein typically found in dried formulations(60). This indicates that lysozyme is a substantial component of these films and although PMLA is a minor component (by mass), it plays a major functional role in facilitating assembly into tunable thin films.

For additional control over lysozyme release, we developed a tetralayer architecture of (chitosan/PMLA/lysozyme/PMLA)$_n$ that would impart robustness against pH and/or ionic strength changes and include hydrolytic degradability for controlled release. Ionic titration showed polycation-polyanion polyplexes substantially more robust than lysozyme-PMLA polyplexes (Table 2-1), and so we integrated a chitosan-PMLA component into the film.

Chitosan was chosen as the polycation because of its beneficial therapeutic properties in some applications(25). Similar to what we observed in the (chitosan/PMLA)$_n$ growth curve (Figure 2-2b), Figure 2-8c shows that this tetralayer architecture exhibits exponential growth that is representative of significant interdiffusion within the film. The film growth in the latter part of super-linearity (>15 bilayers) is 69.2 nm/tetralayer, a quantity greater than necessary for a simple monolayer adsorption mechanism that would lead to surface charge reversal. This difference in growth compared to the bilayer system shows that chitosan can facilitate interdiffusion and consequently more material deposition per adsorption cycle.
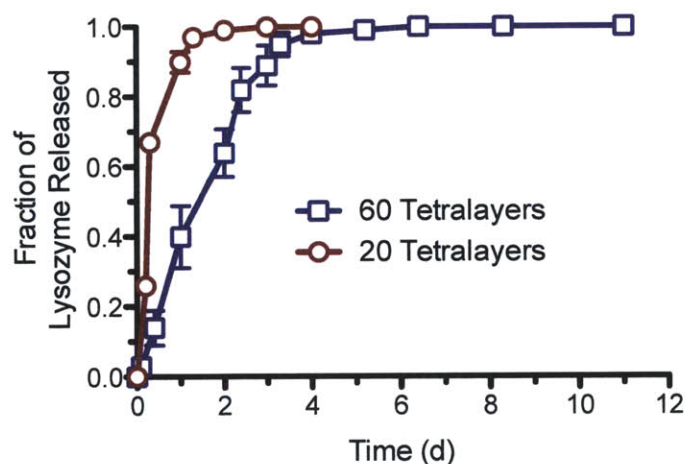
Figure 2-9. Fractional release of lysozyme from (chitosan/PMLA/lysozyme/PMLA)$_n$ tetralayer films.

When examining the tetralayer's release profile, Figure 2-8d showed a controlled release for both 20 and 60 tetralayers, equating to roughly 2 days and 5 days, while releasing 30.1 ± 1.1 $\mu g/cm^2$ and 206.0 ± 0.4 $\mu g/cm^2$ of lysozyme, respectively. From our previous investigations into other protein-based LbL films, especially those containing growth factors, these loadings are in far excess of what would be needed for *in vivo* therapeutic activity, as loadings of tens to hundreds of ng/cm^2 are able elicit biological response(14, 17). We found that the incorporation

of chitosan allowed for a more sustained degradative release mechanism avoiding the bolus release we observed with the bilayer system. When these release profiles are shown as a fraction of total release (Figure 2-9), it is clear there is additional sustainment of release from the 60 tetralayer film, which would be expected from the thicker film in which an erosion mechanism would dominate. It should be noted that hydrolysis of the PMLA backbone as well as ionization of the film components contributes to film disassembly, where the PMLA half-life for degradation is 10 h(22) under the same conditions of pH 7.4 and 37°C. The commensurate thickness and loading increases of 5.9-fold and 6.8-fold, respectively, of 60 tetralayer films compared to 20 tetralayer films reveal that the interdiffusional effects enhancing film growth also enhance lysozyme loading. At 60 tetralayers, the lysozyme loading density is 0.62 ± 0.02 mg/mm^3, almost exactly half that of the (Lysozyme/PMLA)$_{120}$ bilayer film with an equivalent number of total layers (240), which suggests there is minimal competition between lysozyme and chitosan, and that the chitosan/PMLA component has a balanced contribution to film growth. We also tested analogous films of (PLL/PMLA/Lysozyme/PMLA)$_n$ assembled in 10 mM sodium phosphate, pH 7.4. Although these films showed significant growth, they did not incorporate detectable amounts of lysozyme, and at this pH, the charge density of lysozyme may be too low (+7(49)) for stable electrostatic film incorporation. While ensuring sufficient drug payload is of primary importance, minimizing possibly deleterious effects of pH on drug and film components must also be considered when developing assembly conditions.
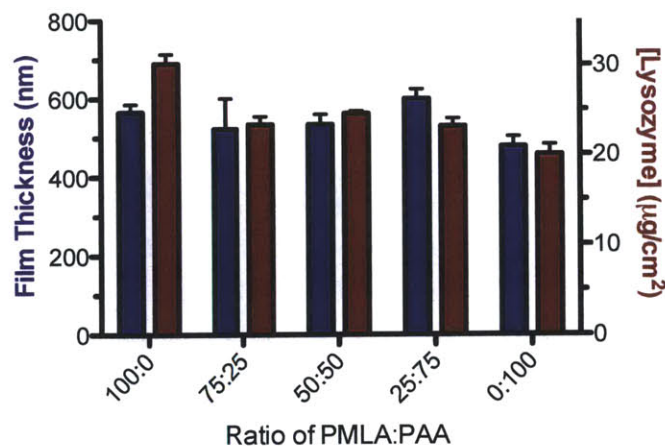
Figure 2-10. Film loadings and lysozyme thicknesses of (chitosan/polyanion/lysozyme/polyanion)$_{20}$ films of varied PMLA:PAA molar ratios.

With insight from our studies on polyplex stabilities, we hypothesized that gradually replacing PMLA with PAA as the polyanion in (chitosan/polyanion/lysozyme/polyanion)$_{20}$ films could introduce a tunable release profile. Previous studies have shown that mixtures of two weak polyelectrolytes, PLL and a PBAE, could vary ovalbumin release profiles from multilayer films(61). We assembled films from PMLA:PAA molar mixtures of 100:0, 75:25, 50:50, 25:75, and 0:100 and found that while these film thickness and lysozyme loadings were fairly similar (Figure 2-10), their release kinetics changed dramatically. As shown in Figure 2-11, the release can be sustained from ~2 days to more than 3 weeks by increasing the PAA fraction with first-order kinetic fits showing the time for half-maximum lysozyme release ($T_{1/2}$) also increases from 0.5 days to more than 5 days. The intermolecular interactions (e.g., ionic and hydrogen bonding) in the film are significantly affected by the changed nature of the aqueous environment when transitioning from assembly to release conditions; increasing pH (from 5 to 7.4) causes increased ionization in the polyanions and increasing salt concentrations weaken the electrostatic interactions. Based on our potentiometric and ionic titrations, PMLA is significantly charged

43

during both assembly (68% ionized) and release conditions (99% ionized) with those electrostatic bridges with lysozyme being highly sensitive to ionic shielding. In contrast, PAA is weakly charged during assembly (19% ionized) and can form a number of hydrogen-bonding interactions with lysozyme that are salt insensitive. Transition to release conditions causes significant but incomplete ionization (66% ionized), allowing for lysozyme stabilization despite the pH change. These factors in addition to the non-degradability of PAA are likely factors that allow for the sustainment in lysozyme release when increasing PAA fraction is incorporated into these LbL films.
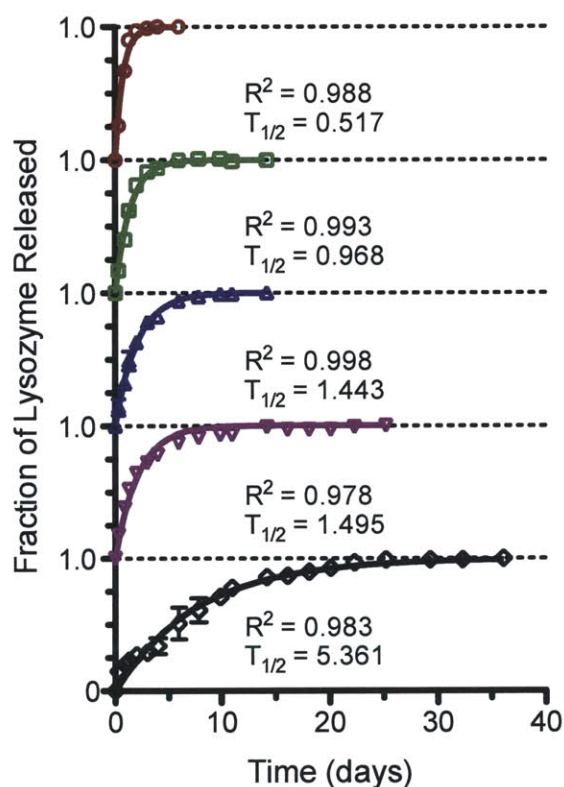
Figure 2-11. Release of lysozyme into PBS, pH 7.4 at 37°C from (chitosan/polyanion/lysozyme/polyanion)$_{20}$ films of 100:0 (*red circles*), 75:25 (*green squares*), 50:50 (*blue triangles*), 25:75 (*purple inverted triangles*), and 0:100 (*black diamonds*) PMLA:PAA molar ratios. Symbols represent measured data and solid lines are their first-order fits.

Therapeutic Growth Factor Release

As a demonstrative example for therapeutic release, we replaced lysozyme with fibroblast growth factor-basic (bFGF) in a (chitosan/PMLA/bFGF/PMLA)$_n$ tetralayer architecture. As observed in the growth curve (Figure 2-12a), these films show concomitant increases in film thickness with number of tetralayers. At 60 bilayers the film is 534 nm, which is considerably thinner than the 3.3 μm for analogous lysozyme-based tetralayers. The weight (16.3 kDa) and hydrodynamic diameter (~5.6 nm(62)) of bFGF is close to that of lysozyme; however, since only nanogram levels are needed to elicit biological response (ED$_{50}$ ~ 1-4 ng/mL), we used a considerably diluted protein solution (50 ug/mL) during assembly that results in less material deposited per tetralayer. Beyond the initial slow growth period (> 20 tetralayers), we found 10.7 nm/tetralayer deposited, which is roughly 6.5-fold less than the lysozyme-based tetralayer films.

Through examination of the release of these bFGF-based films, we found the desired sustained release profiles. Their duration (Figure 2-12b) extends beyond 10 days with 9.1 ± 1.5 ng/cm^2 and 20.1 ± 4.8 ng/cm^2 of bFGF loaded in 20 and 60 tetralayer films, respectively. Because of the near-linear growth curve, the loading of these bFGF films can be predetermined based on the film thickness, which is controlled by the number of layers deposited as is characteristic of LbL release systems. When examined as fraction of total release (Figure 2-13), it is clear that the kinetics of bFGF elution is similar and independent of the film thickness to at least 60 tetralayers. Studies of the release kinetics from these films (Figure 2-12) found sustained release for more than 10 days. There are two features that are different than observed with the lysozyme-based tetralayer release profiles: both 20 and 60 tetralayers have similar release kinetics (Figure 2-13) and their duration of release is longer. Previous studies with growth factors and lysozyme in LbL films(13-15, 17) have shown both kinetic dependence and

independence with the number of layers deposited; contributions of film thickness, architecture, component composition, and types of intermolecular interactions can have substantial influence on overall film morphology and stability.
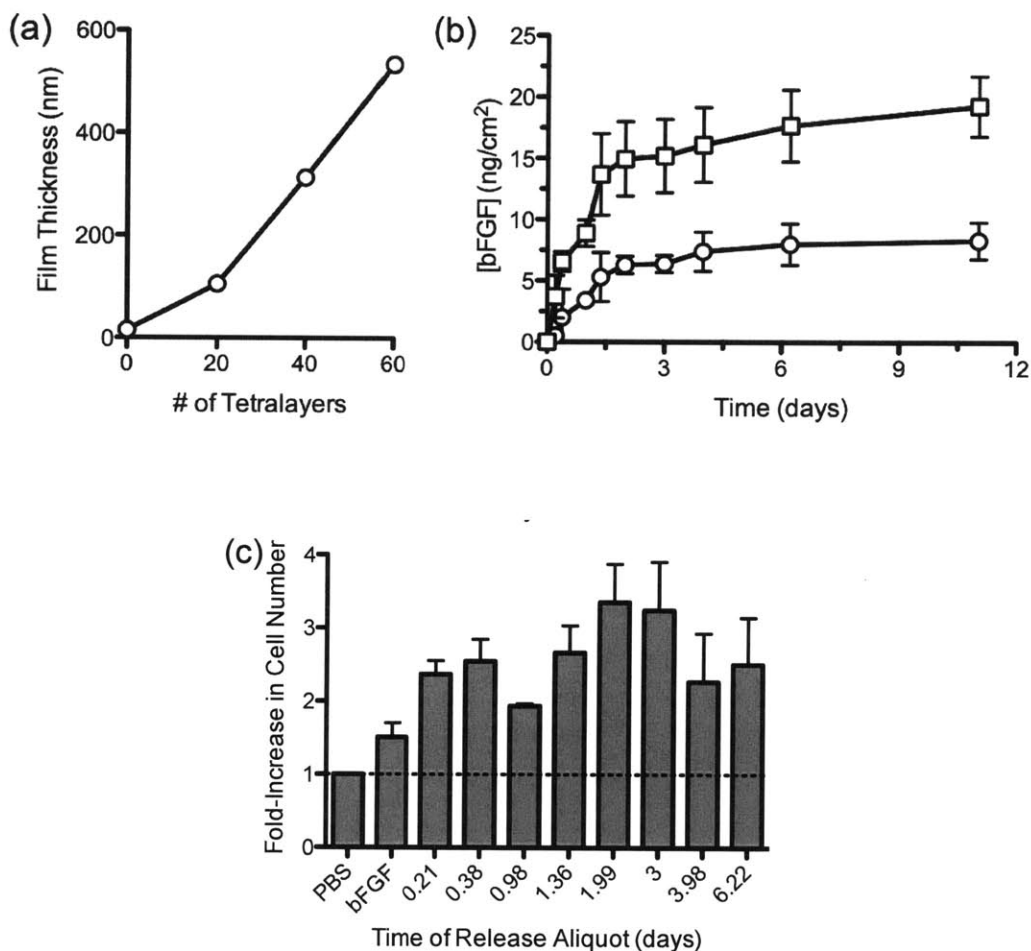
Figure 2-12. Film characteristics of (chitosan/PMLA/bFGF/PMLA)$_n$ films including its growth curve (a), release profiles in PBS, pH 7.4 at 37°C for 20 (*circles*) and 60 tetralayers (*squares*) (b), and proliferative activity of PBS, 10 ng/mL of as-received bFGF and film-released bFGF on NIH3T3 cells (c).

As LbL films can be assembled under benign aqueous conditions and is based on reversible intermolecular interactions like electrostatic and hydrogen-bonding, biologics can avoid the denaturing conditions sometimes plaguing other types of controlled release

formulations. Upon contact with bodily fluids, the actual *in vivo* concentration is variable with the area of film and contact volume ultimately dependent on the location application. However, we can demonstrate the proliferative activity of the film-released bFGF *in vitro*. Stimulation of cell proliferation by bFGF follows a dose-response relationship and we found 10 ng/mL to be sufficient for maximal effect (Figure 2-14). We compared this concentration of as-received bFGF with the bFGF released into PBS from 60 tetralayer films and found that its accumulation in each aliquot had significant proliferative activity (Figure 2-12c) that compares well to previous bFGF-based LbL films(14). In fact, the latter's greater activity over the as-received bFGF may indicate that it is the beneficiary of the co-release of chitosan that stabilizes bFGF activity by protecting it from heat-inactivation and proteolysis(63). For comparison, our study of the proliferative activity of the (chitosan/PMLA)$_n$ scaffold showed no significant activity (Figure 2-15) on its own. In conjunction with the relatively non-cytotoxic nature (Figure 2-16) of the scaffold, this controlled release formulation can sustainably release therapeutic proteins, like a growth factor, from a completely biodegradable thin film coating.
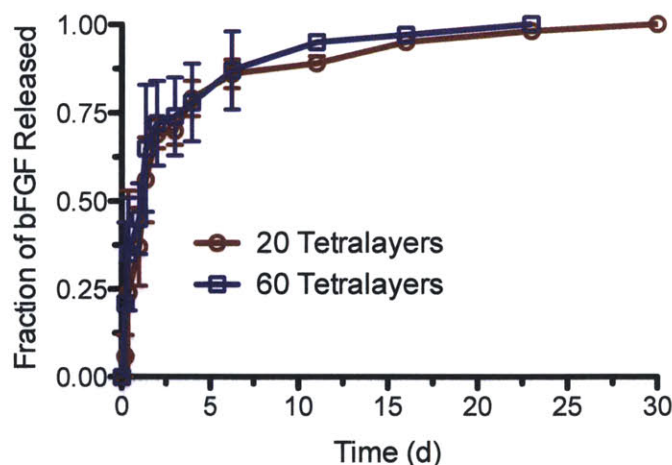
Figure 2-13. Release profiles of (chitosan/PMLA/bFGF/PMLA)$_n$ films normalized to their total loadings.
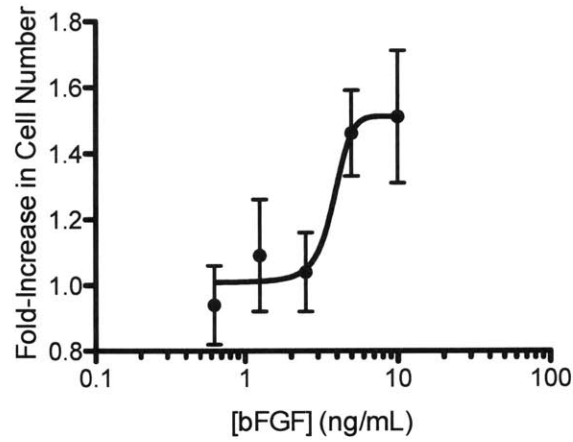
Figure 2-14. Dose-response relationship of as-received bFGF on proliferation of NIH3T3 cells.
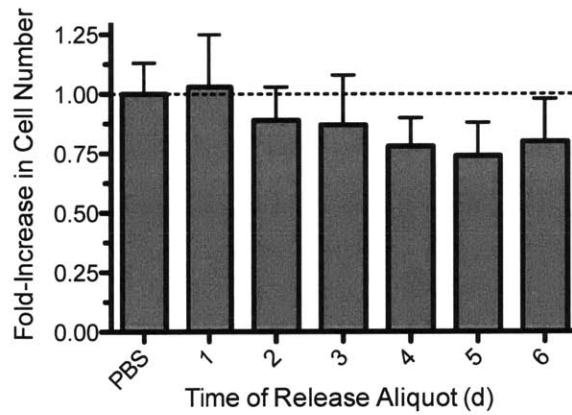
Figure 2-15. Control indicating minimal proliferative activity of (chitosan/PMLA)$_{40}$ films on NIH3T3 cells in the absence of bFGF.
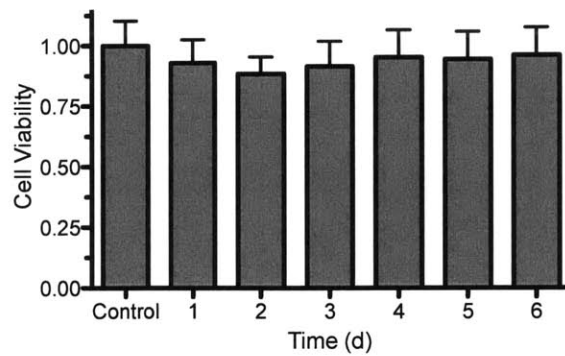
Figure 2-16. Cytotoxicity of (chitosan/PMLA)$_{40}$ films on NIH3T3 cells.

2.4 Conclusions

In the interest of generating improved biocompatibility in a biodegradable film formulation for controlled drug delivery, we utilized a naturally derived polyanion PMLA, whose degradation products are GRAS by the FDA. We investigated the ability of PMLA to assemble into multilayers with PAH, chitosan, PLL and LPEI and found the characteristic layer-dependent growth and sustained release behavior. Bilayer and tetralayer films using a model protein, lysozyme, showed tunable release from 30 minutes to more than 5 days. We found that the differences in their release kinetics, and overall film assembly could be explained by the relative stabilities of electrostatic complexation. By using a PMLA:PAA blend for the polyanionic component, we were able to tune release out to more than 3 weeks. To explore biomedical applicability of this film architecture, we demonstrated the sustained release of a growth factor, bFGF, for nearly two weeks and found it retained its biological activity.

2.5 References

1. Hammond PT (2012) Building biomedical materials layer-by-layer. *Mater. Today* 15(5):196-206.
2. Hammond PT (2012) Polyelectrolyte multilayered nanoparticles: using nanolayers for controlled and targeted systemic release. *Nanomedicine* 7(5):619-622.
3. Langer R (1990) New methods of drug delivery. *Science* 249(4976):1527-1533.
4. Uhrich KE, Cannizzaro SM, Langer RS, & Shakesheff KM (1999) Polymeric systems for controlled drug release. *Chem. Rev.* 99(11):3181-3198.
5. Fan LT & Singh SK (1989) *Controlled Release: A Quantitative Treatment* (Springer-Verlag).
6. Stevenson CL, Santini JT, Jr., & Langer R (2012) Reservoir-based drug delivery systems utilizing microtechnology. *Adv. Drug Del. Rev.* 64(14):1590-1602.
7. Lue J-M, *et al.* (2009) Current advances in research and clinical applications of PLGA-based nanotechnology. *Expert Review of Molecular Diagnostics* 9(4):325-341.
8. Wischke C & Schwendeman SP (2012) Degradable Polymeric Carriers for Parenteral Controlled Drug Delivery. *Fundamentals and Applications of Controlled Release Drug Delivery,* Advances in Delivery Science and Technology, eds Siepmann J, Siegel RA, & Rathbone MJ (Springer, New York), pp 171-228.
9. Jain RA (2000) The manufacturing techniques of various drug loaded biodegradable poly(lactide-co-glycolide) (PLGA) devices. *Biomaterials* 21(23):2475-2490.
10. Fredenberg S, Wahlgren M, Reslow M, & Axelsson A (2011) The mechanisms of drug release in poly(lactic-co-glycolic acid)-based drug delivery systems—A review. *Int. J. Pharm.* 415(1–2):34-52.
11. Hammond PT (2011) Engineering Materials Layer-by-Layer: Challenges and Opportunities in Multilayer Assembly. *AICHE J.* 57(11):2928-2940.
12. Pavlukhina S & Sukhishvili S (2011) Polymer assemblies for controlled delivery of bioactive molecules from surfaces. *Adv. Drug Del. Rev.* 63(9):822-836.
13. Macdonald M, Rodriguez NM, Smith R, & Hammond PT (2008) Release of a model protein from biodegradable self assembled films for surface delivery applications. *J. Controlled Release* 131(3):228-234.
14. Macdonald ML, Rodriguez NM, Shah NJ, & Hammond PT (2010) Characterization of Tunable FGF-2 Releasing Polyelectrolyte Multilayers. *Biomacromolecules* 11(8):2053-2059.
15. Macdonald ML, *et al.* (2011) Tissue integration of growth factor-eluting layer-by-layer polyelectrolyte multilayer coated implants. *Biomaterials* 32(5):1446-1453.
16. Shah NJ, Hong J, Hyder MN, & Hammond PT (2012) Osteophilic Multilayer Coatings for Accelerated Bone Tissue Growth. *Adv. Mater.* 24(11):1445-1450.
17. Shah NJ, *et al.* (2011) Tunable dual growth factor delivery from polyelectrolyte multilayer films. *Biomaterials* 32(26):6183-6193.

18. Lynn DM & Langer R (2000) Degradable poly(beta-amino esters): Synthesis, characterization, and self-assembly with plasmid DNA. *J. Am. Chem. Soc.* 122(44):10761-10768.

19. Vazquez E, Dewitt DM, Hammond PT, & Lynn DM (2002) Construction of hydrolytically-degradable thin films via layer-by-layer deposition of degradable polyelectrolytes. *J. Am. Chem. Soc.* 124(47):13992-13993.

20. Zhang JT, Chua LS, & Lynn DM (2004) Multilayered thin films that sustain the release of functional DNA under physiological conditions. *Langmuir* 20(19):8015-8021.

21. Zhang JT, Fredin NJ, Janz JF, Sun B, & Lynn DM (2006) Structure/property relationships in erodible multilayered films: Influence of polycation structure on erosion profiles and the release of anionic polyelectrolytes. *Langmuir* 22(1):239-245.

22. Lee B-S, Vert M, & Holler E (2002) Water-soluble Aliphatic Polyesters: Poly(malic acid)s. *Biopolymers: Polyesters I*, eds Doi Y & Steinbuchel A), Vol 3a, pp 75-103.

23. Fournie P, *et al.* (1992) In vivo fate of repeat-unit-radiolabeled poly(beta-malic acid), a potential drug-carrier. *J. Bioact. Compatible Polym.* 7(2):113-129.

24. Ljubimova JY, *et al.* (2013) Toxicity and efficacy evaluation of multiple targeted polymalic acid conjugates for triple-negative breast cancer treatment. *J. Drug Targeting* 21(10):956-967.

25. Rao SB & Sharma CP (1997) Use of chitosan as a biomaterial: Studies on its safety and hemostatic potential. *J. Biomed. Mater. Res.* 34(1):21-28.

26. Petrov AI, Antipov AA, & Sukhorukov GB (2003) Base-acid equilibria in polyelectrolyte systems: From weak polvelectrolytes to interpolyelectrolyte complexes and multilayered polyelectrolyte shells. *Macromolecules* 36(26):10079-10086.

27. Shukla A, Avadhany SN, Fang JC, & Hammond PT (2010) Tunable Vancomycin Releasing Surfaces for Biomedical Applications. *Small* 6(21):2392-2404.

28. Katchalsky A & Spitnik P (1947) Potentiometric Titrations of Polymethacrylic Acid. *Journal of Polymer Science* 2(4):432-446.

29. Gregor HP & Frederick M (1957) Potentiometric Titration of Polyacrylic and Polymethacrylic Acids with Alkali Metal and Quaternary Ammonium Bases. *Journal of Polymer Science* 23(103):451-465.

30. Dos A, Schimming V, Tosoni S, & Limbach H-H (2008) Acid-Base Interactions and Secondary Structures of Poly-L-Lysine Probed by (15)N and (13)C Solid State NMR and Ab initio Model Calculations. *J. Phys. Chem. B* 112(49):15604-15615.

31. Brissault B, *et al.* (2003) Synthesis of Linear Polyethylenimine Derivatives for DNA Transfection. *Bioconj. Chem.* 14(3):581-587.

32. Choi J & Rubner MF (2005) Influence of the degree of ionization on weak polyelectrolyte multilayer assembly. *Macromolecules* 38(1):116-124.

33. Wang QZ, *et al.* (2006) Protonation constants of chitosan with different molecular weight and degree of deacetylation. *Carbohydr. Polym.* 65(2):194-201.

34. Ladam G, *et al.* (2000) In situ determination of the structural properties of initially deposited polyelectrolyte multilayers. *Langmuir* 16(3):1249-1255.

35. Schmitt J, *et al.* (1993) Internal Structure of Layer-By-Layer Adsorbed Polyelectrolyte Films - A Neutron and X-Ray Reflectivity Study. *Macromolecules* 26(25):7058-7063.

36. Jomaa HW & Schlenoff JB (2005) Salt-induced polyelectrolyte interdiffusion in multilayered films: A neutron reflectivity study. *Macromolecules* 38(20):8473-8480.

37. Lavalle P, *et al.* (2002) Comparison of the structure of polyelectrolyte multilayer films exhibiting a linear and an exponential growth regime: An in situ atomic force microscopy study. *Macromolecules* 35(11):4458-4465.

38. Picart C, *et al.* (2001) Buildup mechanism for poly(L-lysine)/hyaluronic acid films onto a solid surface. *Langmuir* 17(23):7414-7424.

39. Lavalle P, *et al.* (2004) Modeling the buildup of polyelectrolyte multilayer films having exponential growth. *J. Phys. Chem. B* 108(2):635-648.

40. Picart C, *et al.* (2002) Molecular basis for the explanation of the exponential growth of polyelectrolyte multilayers. *Proc. Natl. Acad. Sci. U. S. A.* 99(20):12531-12535.

41. Shiratori SS & Rubner MF (2000) pH-dependent thickness behavior of sequentially adsorbed layers of weak polyelectrolytes. *Macromolecules* 33(11):4213-4219.

42. Xu L, Ankner JF, & Sukhishvili SA (2011) Steric Effects in Ionic Pairing and Polyelectrolyte Interdiffusion within Multilayered Films: A Neutron Reflectometry Study. *Macromolecules* 44(16):6518-6524.

43. Sui Z, Salloum D, & Schlenoff JB (2003) Effect of Molecular Weight on the Construction of Polyelectrolyte Multilayers: Stripping versus Sticking. *Langmuir* 19(6):2491-2495.

44. Clark SL & Hammond PT (2000) The Role of Secondary Interactions in Selective Electrostatic Multilayer Deposition. *Langmuir* 16(26):10206-10214.

45. Gilbert JB, Rubner MF, & Cohen RE (2013) Depth-profiling X-ray photoelectron spectroscopy (XPS) analysis of interlayer diffusion in polyelectrolyte multilayers. *Proc. Natl. Acad. Sci. U. S. A.* 110(17):6651-6656.

46. Picart C, *et al.* (2004) Measurement of film thickness up to several hundreds of nanometers using optical waveguide lightmode spectroscopy. *Biosens. Bioelectron.* 20(3):553-561.

47. Wood KC, Boedicker JQ, Lynn DM, & Hammond PT (2005) Tunable drug release from hydrolytically degradable layer-by-layer thin films. *Langmuir* 21(4):1603-1609.

48. Parmar AS & Muschol M (2009) Hydration and Hydrodynamic Interactions of Lysozyme: Effects of Chaotropic versus Kosmotropic Ions. *Biophys. J.* 97(2):590-598.

49. Spassov VZ, Karshikov AD, & Atanasov BP (1989) Electrostatic Interactions in Proteins - A Theoretical Analysis of Lysozyme Ionization. *Biochim. Biophys. Acta* 999(1):1-6.

50. Decher G & Schlenoff JB eds (2012) *Multilayer Thin Films* (Wiley-VCH), 2nd Ed.
51. Xie Y, Zhou J, & Jiang SY (2010) Parallel tempering Monte Carlo simulations of lysozyme orientation on charged surfaces. *J. Chem. Phys.* 132(6).
52. Izumrudov VA, Kharlampieva E, & Sukhishvili SA (2005) Multilayers of a globular protein and a weak polyacid: Role of polyacid ionization in growth and decomposition in salt solutions. *Biomacromolecules* 6(3):1782-1788.
53. Kovacevic D, van der Burgh S, de Keizer A, & Stuart MAC (2002) Kinetics of formation and dissolution of weak polyelectrolyte multilayers: Role of salt and free polyions. *Langmuir* 18(14):5607-5612.
54. Sukhishvili SA, Kharlampieva E, & Izumrudov V (2006) Where Polyelectrolyte Multilayers and Polyelectrolyte Complexes Meet. *Macromolecules* 39(26):8873-8881.
55. Mjahed H, *et al.* (2010) Turbidity diagrams of polyanion/polycation complexes in solution as a potential tool to predict the occurrence of polyelectrolyte multilayer deposition. *J. Colloid Interface Sci.* 346(1):163-171.
56. Boschetti E, Girot P, Secheresse JP, & Blancard JS (1981) Study of the molecular interaction between lysozyme and heparin and application in affinity-chromatography. *J. Chromatogr.* 210(3):469-475.
57. Erel-Unal I & Sukhishvili SA (2008) Hydrogen-bonded multilayers of a neutral polymer and a polyphenol. *Macromolecules* 41(11):3962-3970.
58. Porcel C, *et al.* (2007) Influence of the polyelectrolyte molecular weight on exponentially growing multilayer films in the linear regime. *Langmuir* 23(4):1898-1904.
59. Porcel C, *et al.* (2006) From exponential to linear growth in polyelectrolyte multilayers. *Langmuir* 22(9):4376-4383.
60. Berlin E & Pallansch MJ (1968) Densities of several proteins and L-amino acids in the dry state. *The Journal of Physical Chemistry* 72(6):1887-1889.
61. Hong J, Kim B-S, Char K, & Hammond PT (2011) Inherent Charge-Shifting Polyelectrolyte Multilayer Blends: A Facile Route for Tunable Protein Release from Surfaces. *Biomacromolecules* 12(8):2975-2981.
62. Onuma K, Kanzaki N, & Kobayashj N (2004) Association of calcium phosphate and fibroblast growth factor-2: a dynamic light scattering study. *Macromol. Biosci.* 4(1):39-46.
63. Masuoka K, *et al.* (2005) The interaction of chitosan with fibroblast growth factor-2 and its protection from inactivation. *Biomaterials* 26(16):3277-3284.

Chapter 3
Ordered and Kinetically Discrete Sequential Protein Release from Biodegradable Thin Films

Authors:
Bryan B. Hsu[1,2,4], Kelsey Jamieson[3], Samantha Hagerman[3], Eggehard Holler[5], Julia Y. Ljubimova[5], and Paula T. Hammond[1,3,4]

[1]Koch Institute for Integrative Cancer Research, Massachusetts Institute of Technology, Cambridge, MA 02139
Departments of [2]Chemistry and [3]Chemical Engineering, Massachusetts Institute of Technology, Cambridge, MA 02139
[4]Institute for Soldier Nanotechnologies, Massachusetts Institute of Technology, Cambridge, MA 02139
[5]Nanomedicine Research Center, Department of Neurosurgery, Cedars Sinai Medical Center, Los Angeles, CA 90048

3.1   Introduction

The development of chemical and biological therapeutics has profoundly improved the lifestyles and life expectancies of people worldwide, but single-drug treatments can sometimes be ineffective for especially recalcitrant diseases that have developed drug resistances or have temporal progression through different phases. For these cases, combination therapies with spatiotemporally optimized multi-drug regimens can profoundly improve biological effect. In fact, the sequential treatments of erlotinib prior to doxorubicin(1), siRNA followed by a small molecule(2), and antibiotics in sequence(3) have shown significant improvements over simultaneous administration.

Spatiotemporal treatment is especially important during the administration of growth factors(4-6). In the complex and multimodal process of wound healing, the judicious introduction of factors in a specific sequence can help drive the wound through the different phases of proper remediation(7). Studies have shown that the simultaneous introduction of multiple factors can be ineffective or even inhibitory(8-17), whereas temporally discrete, sequential administration can markedly improve results(16-18). In addition, sustained growth factor administration is essential to improving biological response because of rapid elimination; basic fibroblast growth factor and vascular endothelial growth factor have half-lives of 3 min(19) and 50 min(20), respectively. As growth factors and other signaling molecules can elicit a variety of responses, their indiscriminate systemic or bolus application can be deleterious. For these reasons, among others, it is desirable to deliver such drugs from an implant or scaffold located in close proximity to the target site with pre-programmed release kinetics, thus minimizing the concentration-related side effects typically associated with systemic delivery and eliminating the

need for additional, potentially invasive procedures to administer more drug, which would likely improve patient compliance and therapeutic outcome(21).

Recapitulating a multi-drug dosing regimen with a biodegradable, controlled release formulation remains a challenge, as drug release kinetics frequently have significant overlap, especially during the early phases of release. Some approaches have utilized combinations of different hydrophobic polyesters (e.g., poly[lactic-*co*-glycolic acid] or PLGA, poly[ε-caprolactone], and poly[3-hydroxybutyrate-*co*-3-hydroxyvalerate]) in strategic arrangements(22-25), as well as their combinations with hydrogels(26-30). Others have simply used scaffolds based on modified alginate(31-33) or gelatin(15, 34, 35) to manipulate release kinetics. The most common outcome is the acceleration or deceleration in drug elution, but it still remains difficult to achieve well defined multi-therapeutic release kinetics without some level of simultaneous release, often with an initial burst release. For the release of growth factors, biologic drugs, and more broadly, any synergistic therapeutic systems that require complex time dependent release, we sought to design ultrathin film coatings that could exhibit truly staggered and sustained release profiles for multiple therapeutics, as well as the ability to control loading.

Using the Layer-by-Layer (LbL) assembly approach, we and several others have shown the capability of incorporating high loadings of growth factors into thin films with controlled release and unique biological effect(36-50). This is a desirable approach because films can be assembled from benign aqueous solutions with minimal risk of inactivating sensitive biologics. In addition, its modularity in generating stacked composite films, such as a VEGF-film deposited atop a BMP2-film, has shown that one can easily achieve simultaneous co-release of both growth factors(39). The interdiffusion that occurs during film assembly creates a thoroughly blended nanoscale film that can be highly desirable in some situations, but is also detrimental when

aiming to exert more precise control over release behavior. Striking a balance between the chemical and/or physical means of controlling interdiffusion, while maintaining significant loadings of active drug, desirable release kinetics, and facile assembly conditions makes it an extremely challenging problem.

A number of researchers, in addition to us, have sought to control interdiffusion within LbL films using different film components and types of architectures, each with varying degrees of success. Early pioneering work found that barrier layers of linearly-growing $(PAH/SPS)_n$ could inhibit interdiffusion during film assembly by separating exponentially-growing (poly-L-lysine/hyaluronic acid), or $(PLL/HA)_n$, films into multiple "compartments"(51). Analogously, PLGA barriers deposited from aerosolized chloroform solutions also compartmentalized $(PLL/HA)_n$ films(52). The degradable nature of PLGA allowed for localized, cell-based film degradation, but also remains subject to a localized pH decrease typical of PLGA, which can lower protein activity. Additionally, the exposure to harsh solvents and complex processing steps needed for its fabrication provides reasons to pursue fully water-based nanolayer assembly approaches. Further investigations into different types of LbL barrier layers showed that electrostatically-crosslinked (polyvinylbenzyl ammonium chloride/SPS) or (PBA/SPS) films were ineffective at preventing the mixing of two dyes, while the increased tortuosity presented by the clay platelets in (PBA/laponite) films slowed mixing, and thermally-crosslinked, covalent barriers of (PAH/PAA) fully inhibited dye diffusion(53).

Expanding on the concept of compartmentalization, use of fully hydrolytically degradable components could facilitate true control of drug release rates and generate interesting, tunable release behaviors. By thermally-crosslinking even a single bilayer of (polyallylamine/polyacrylic acid), we found it could act as a barrier and thus delay the release of

a polysaccharide from a hydrolytically-degradable film buried underneath(54). While providing the initial proof that sequential release was possible, the crosslinking required heating to 215°C for 20 min, which would denature biologics and yield undesired side reactions with other components in the film. In another approach, we found that graphene oxide sheets were able to also act as a barrier layer by modulating the release of an underlying model protein, ovalbumin(55). Again this demonstrated the possibility of using a barrier layer to influence the film's release kinetics, but relied on a non-degradable graphene oxide layer that is not at this time generally regarded as safe (GRAS)(56, 57) and may present possible protein-denaturing effects(58). More recently, we have used laponite clays to achieve time lag between release of a small molecule and a growth factor. Unfortunately, even with these approaches, constant interdiffusion during assembly leads to significant phase mixing that makes it difficult to achieve well-defined sequencing, particularly with multiple proteins. For *in vivo* delivery systems, it would be ideal to deliver multiple drugs with minimally overlapping release profiles from a completely biocompatible and biodegradable film without the use of non-aqueous solvents, heat or other process conditions that can severely lower the activity of biologic drugs.

We posited that controlling interdiffusion in the film during the actual assembly process would allow us to judiciously embed therapeutics in different regions of the film at will. In a surface-erosion model, as previously demonstrated for hydrolytically degradable LbL films(59-61) (*see Chapter 2*) the therapeutic's location and depth in the film would govern its release order and kinetics; thus, when incorporating a hydrolytically degradable component throughout the film, deposition of a sacrificial barrier layer could putatively delay the onset of release and enable truly sequential release behavior. Herein, we describe our approach to introduce crosslinking *in situ* (i.e., as the film is deposited) using copper-free click functionalities in a

hydrolytically degradable LbL film. The bio-orthogonality of the click reaction ensured no unwanted side-reactions (e.g., with the embedded protein). We also found that the protein was effectively isolated to its designated region in the film, and that the subsequent addition of a degradable barrier layer effectively suppressed the onset of release, with the extent of suppression scaling with barrier thickness. With the addition of a second protein-containing layer, the film demonstrated exquisite control over release kinetics and allowed for sequential release.

3.2   Materials and Methods

All materials were used without additional purification. Poly(β-L-malic acid) (PMLA, 40 kDa) was obtained by culture in *Physarum polycephalum* and purified as described previously(62). Chitosan (15 kDa, 85% deacetylation) was obtained from Polysciences, Inc. Silicon wafers were purchased from Silicon Quest, Int'l and cleaned with water, methanol, then water prior to plasma cleaning. Click reagents of 3-azido-1-propylamine and dibenzocyclooctyne-amine (DBCO-amine) were obtained from Click Chemistry Tools. Phosphate buffered saline (PBS) at 10X formulation was purchased from Gibco and diluted to 1X and adjusted to pH 7.4 prior to use. Egg-white lysozyme, *Micrococcus lysodeikticus,* and all other chemicals were obtained from Sigma Aldrich, Co. unless otherwise noted. ^{1}H-NMR was performed on a Varian Inova NMR Spectrometer and infrared spectra was taken on a Thermo Nicolet Nexus 870 FTIR.

PMLA-Az Synthesis. The procedure was modified from a previous report(63). To 53 mg (0.45 mmol) of PMLA in 2 mL anhydrous DMSO, a 1 mL mixture of 104 mg (0.5 mmol) of DCC and 58 mg (0.5 mmol) of NHS in anhydrous DMSO was added dropwise under an argon atmosphere. After 3 h at room temperature, the precipitate was removed by filtration and a 1 mL solution containing 13.8 μL (0.14 mmol) of 3-azido-1-propylamine and 21 μL (0.15 mmol) of triethylamine was added dropwise to the filtrate. The reaction proceeded for 4 h at room temperature prior to quenching with 100 mL of 10 mM sodium phosphate, pH 7.4 for at least 30 min. The solution was concentrated and washed with H_2O *via* spin filtration (Corning Spin-X UF 10k MWCO) and lyophilized after residual particulates were removed by centrifugation. Yield was 55 mg. ^{1}H-NMR (500 MHz, D_2O, 25°C, δ/ppm): 5.5 – 5.1 (m, 1H, PMLA -C*H*-), 3.35 (t, *J* =

6.5 Hz, 2H, N_3-CH_2-CH_2-CH_2-NH-), 3.31 (quin, J = 6.1 Hz, 2H, N_3-CH_2-CH_2-CH_2-NH-), 3.1 –

2.9 (br, 2H, PMLA -CH_2-), and 1.77 (t, J = 7.4 Hz, 2H, N_3-CH_2-CH_2-CH_2-NH-). IR (KBr) $\bar{\nu}_{max}$:

2105, 1745, 1617, 1405, 1263, 1161, 1035, 954, 876, 802. Degree of functionalization

determined by NMR was 25.5 mol% with respect to monomer repeat units of PMLA.

PMLA-DBCO Synthesis. To 105 mg (0.91 mmol) of PMLA in 4 mL anhydrous DMSO, a

2 mL mixture of 282 mg (1.36 mmol) of DCC and 159 mg (1.36 mmol) of NHS in anhydrous

DMSO was added dropwise under an argon atmosphere. After 3 h at room temperature, the

precipitate was removed by filtration and a 1 mL solution containing 50 mg (0.18 mmol) of

DBCO-amine and 253 µL (1.8 mmol) of triethylamine was added dropwise to the filtrate. The

reaction proceeded overnight at room temperature prior to quenching with 140 mL of 10 mM

sodium phosphate, pH 7.4 for at least 30 min. The solution was concentrated and washed with

H_2O *via* spin filtration (Corning Spin-X UF 10k MWCO) and lyophilized after residual

particulates were removed by centrifugation. Yield was 69 mg. ^{1}H-NMR (500 MHz, D_2O, 25°C,

δ/ppm): 7.5 – 6.5 (br, 8H, Ar H), 5.4 – 5.0 (br, 1H, PMLA -CH-), and 3.2 – 2.7 (br, 2H, PMLA -

CH_2-). IR (KBr) $\bar{\nu}_{max}$: 1745, 1617, 1405, 1263, 1161, 1035, 771, 755. Degree of functionalization

determined by NMR was 28.9 mol% with respect to monomer repeat units of PMLA.

Preparation of Solutions for Film Assembly. Aqueous solutions of LPEI and SPS used for

baselayer assembly were prepared at 10 mM in water and adjusted to pH 4.3 and 4.8,

respectively. Chitosan, PMLA, PMLA-az, PMLA-DBCO and lysozyme were formulated at 1

mg/mL in 10 mM sodium acetate and pH adjusted to 5.0. BMP2 was formulated from a 4.67

mg/mL aliquot (in 5 mM L-glutamic acid, 5 mM NaCl, 2.5% glycine, 0.5% sucrose, 0.01%

polysorbate 80, pH 4.5) and diluted to 117 µg/mL in 10 mM sodium acetate, pH 5.0.

Adjustments in pH were made with 0.1 M of NaOH or HCl.

Film Assembly and Characterization. Similarly to as described earlier(61) (*see Chapter 2*), baselayer films of (LPEI/SPS)$_{10}$ were deposited onto plasma-cleaned (Harrick PDC-32G) silicon substrates by use of a programmable slide stainer (Carl Zeiss HMS). Substrates were incubated for 5 min in LPEI solution, washed three times with water (for 10 sec, 20 sec, and 30 sec), then immersed for 5 min in SPS solution and again washed thrice with water, to constitute a single bilayer. For 10 bilayers, this was repeated 10 times. The tetralayer film architectures as shown in Table 1 were assembled similarly by immersing baselayer-coated substrates in a solution of each film component for 15 min followed by three successive rinses with water (for 10 sec, 20 sec, and 30 sec). For example, assembly of one tetralayer of (chitosan/PMLA/lysozyme/PMLA) would consist of immersion for 15 min in chitosan solution followed by three washes, then immersion for 15 min in PMLA solution followed by three washes, then immersion for 15 min in lysozyme solution followed by three washes, and finally immersion for 15 min in PMLA solution followed by three washes. Films were then blown dry with gentle N2 gas and further dried under house vacuum overnight. Film thicknesses were determined by ellipsometry (J.A. Woolam, XLS-100) or profilometry with a 2.5 μm tip (Dektak 150 Profilometer).

Films released into media were determined by immersion in 500 μL of PBS, pH 7.4 at 37°C. At predetermined times, the films were transferred to fresh pre-warmed PBS aliquots and continued incubation. Lysozyme was quantified by a 96-well plate enzymatic assay where the reduction in turbidity of sample solutions, as determined by optical density at 450 nm, is compared to a standard curve. In a typical well, 50 μL of sample or standard solution in PBS is mixed with 200 μL of 0.3 mg/mL *Micrococcus lysodeikticus* in PBS and incubated at 37°C, with

optical density quantified after 5 to 15 min. BMP2 was quantified by ELISA and performed according to manufacturer directions (Peprotech).

XPS depth profiling was completed similarly as previously reported(64) and briefly described here. Surface specific chemical composition was determined using a PHI VersaProbe II X-ray photoelectron spectroscopy (XPS) instrument in conjunction with a C_{60}^{+} ion-sputtering source. Regions for C_{1s}, S_{2p}, and Si_{2p} were monitored after each 1-min sputter cycle over a 3 x 3 mm^3 area at 10 kV and 10 nA. Completion of film sputtering and reaching the Si-wafer was considered when the Si_{2p} intensity reached 1.5% of the Si-wafer value. Sulfur signal from SPS in the base layer shows a distinctly different peak position (~166 eV) from lysozyme (~162 eV) and was clearly differentiated.

3.3   Results and Discussion

In an earlier report studying the use of LbL assembled multilayered films(61) (*see Chapter 2*), we found that we could generate protein-loaded thin films using completely naturally-derived materials whose degradation products are generally recognized as safe (GRAS) by the FDA. These films were able to controllably sustain the release of protein over multiple days under physiological conditions. The growth behavior of these films(61) (*see Chapter 2*) and many other protein-containing LbL assembled films(65-70) has revealed exponential increases in film thickness as a function of layers deposited. This phenomenon has been well documented for certain LbL systems and has been explained by an "in-and-out" diffusion hypothesis that suggests the diffusivity of weakly charged polymeric species (i.e., proteins, polysaccharides, weak polyelectrolytes) in the film contributes significantly to this growth behavior; the diffusion and absorption of excess polyelectrolytes into and out of the film during assembly causes this exponential film growth(68). It is also hypothesized that there is a "diffusional zone" with finite thickness throughout which interdiffusion can readily occur over the timeframe of the adsorption step(69).
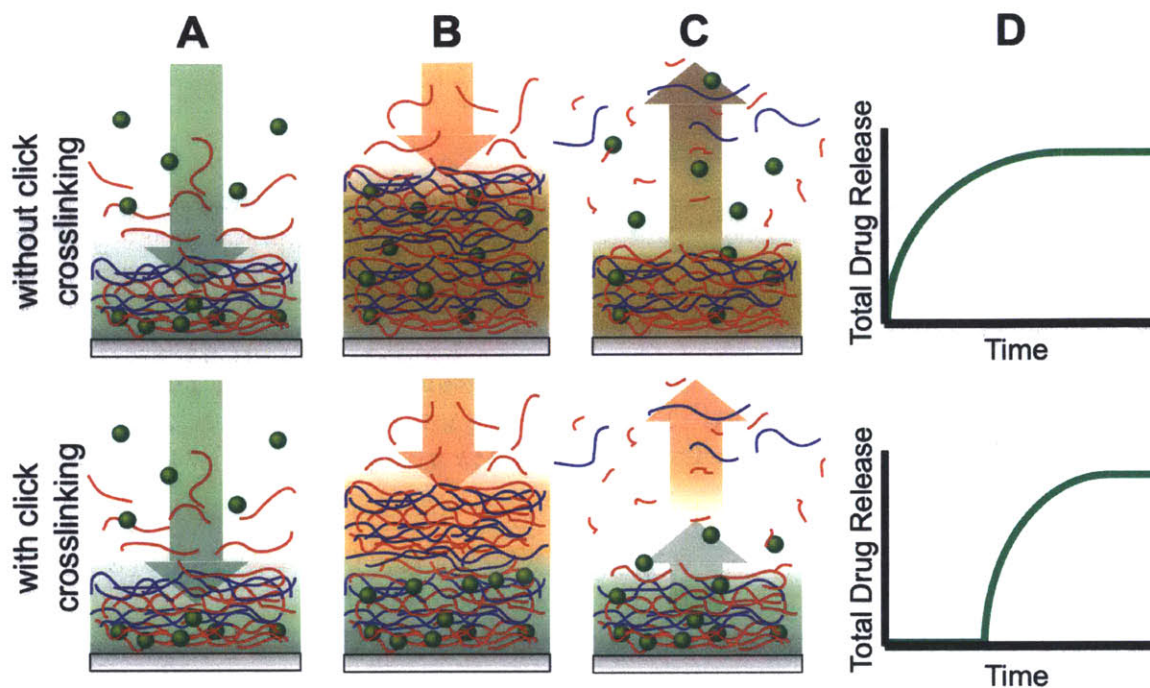
Figure 3-1. Illustration of the proposed assembly and degradation process of multilayer films without (*upper panel*) and with (*lower panel*) crosslinking, where the therapeutic (green spheres) is loaded into films composed of polycations (blue) and degradable polyanions (red). Each film undergoes typical LbL film assembly (A), however those films with crosslinking retain their stratified structure while non-crosslinked films are highly interdiffused (B). Surface erosion either degrades a blended film where the therapeutic is distributed throughout the film, or a stratified film with the therapeutic sequestered to where it was deposited (C). The release profiles reflect the effect of crosslinking, and hence interdiffusion, on kinetics of drug release (D).

In single protein films, we found that interdiffusion facilitates loading and blending on the nano-scale(36, 37, 71, 72). When combining two separately assembled protein-containing films into a composite film, with VEGF-loaded films stacked atop BMP-2-loaded films, both proteins released simultaneously due to interdiffusion, despite their sequence of deposition(39); they each have their own unique release profiles, but both simultaneously begin releasing upon hydration. We hypothesized that by kinetically freezing the interlayer diffusion during film assembly via covalent crosslinks, we would be able to dictate the sequence of their release based on the order of deposition. As schematically represented in Figure 3-1, the assembly of one film

on top of another typically leads to film blending, where the drug is distributed throughout the film (Figures 3-1A-B, *upper panel*). With crosslinking that limits interdiffusion, the drug would remain in the region to which it was deposited (Figures 3-1A-B, *lower panel*). The resultant surface erosion would reflect this drug distribution (Figures 3-1C-D) with immediate or delayed release for diffusive or non-diffusive systems, respectively. The in-situ generation of crosslinks by copper-free click chemistry would not only lower the diffusivity of large and intermediate sized biomacromolecules but also the other polyelectrolyte components within the LbL film matrix, thus lowering their mixing during assembly. Copper-assisted click crosslinking has previously been shown to facilitate LbL film assembly(73) especially as "click capsules"(74-76), but herein we endeavored to generate such crosslinks without the need of copper or any post-treatment.
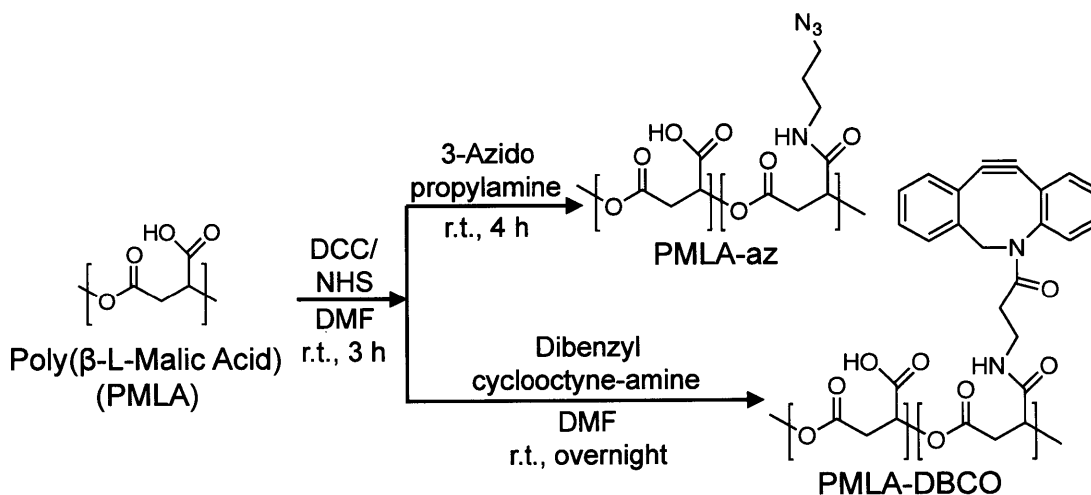
Figure 3-2. Synthetic scheme for functionalization of PMLA with 3-azidopropylamine *via* N,N'-dicyclohexylcarbodiimide/N-hydroxysuccinimide (DCC/NHS) coupling chemistry to generate PMLA with azide functionality, and through an analogous method, PMLA with dibenzocyclooctyne functionality.

To this end, we used a poly(β-L-malic acid) (PMLA) based LbL film architecture. PMLA is a bioresorbable, degradable polyanion with the added advantage of presenting available acid

groups for side group derivatization. It is well tolerated *in vitro* and *in vivo* without toxicity or immunogenicity(77). We functionalized separate batches of PMLA to contain either pendant azide or dibenzocyclooctyne (DBCO) functionalities (Figure S1). The azide-DBCO click reaction is driven *via* the release of ring-strain without needing a copper catalyst and has been shown to be bioorthogonal and biocompatible(78, 79). Through *N,N'*-dicyclohexylcarbodiimide/*N*-hydroxysuccinimide mediated amide coupling (Figure 3-2), we achieved azide (PMLA-az) and DBCO (PMLA-DBCO) functionalization, which were confirmed by FTIR (Figure 3-3), with degrees of functionalization of 25.5 mol% and 28.9 mol%, respectively, as determined by NMR. While assembling tetralayer films of (chitosan/PMLA-az/protein/PMLA-DBCO)$_n$ would putatively minimize interdiffusion, we also envisioned that the hydrolytic degradation of the PMLA ester backbone would impart controlled release behavior.
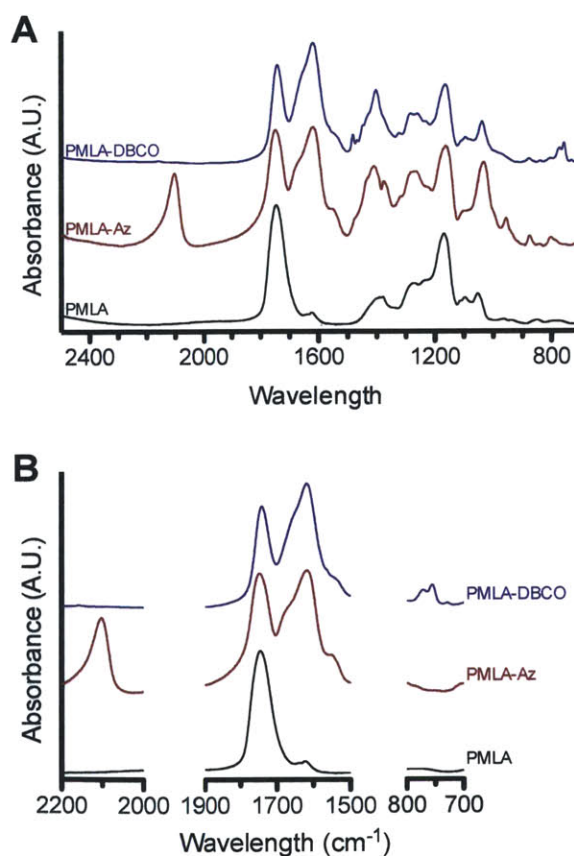
Figure 3-3. FTIR spectra of PMLA, PMLA-Az and PMLA-DBCO shown at full scale (A). Selected regions show the characteristic N_3 stretching (2105 cm^{-1}) of the azide moiety in PMLA-Az, the C=O stretching (1617 cm^{-1}) of the pendant amide formed during azide or DBCO conjugation, and the C-H out-of-plane bending (771 and 755 cm^{-1}) of the aromatic moieties of PMLA-DBCO.

Table 3-1. Film Nomenclature

Film Architecture	Number of Tetralayers	Abbreviation
(Chitosan/PMLA/Lysozyme/PMLA)$_n$	20	Lys Film
(Chitosan/PMLA-az/Lysozyme/PMLA-DBCO)$_n$	20	Lys$^{\text{x-linked}}$ Film
(Chitosan/PMLA-az/Chitosan/PMLA-DBCO)$_n$	20	Barrier Film
(Chitosan/PMLA-az/Lysozyme/PMLA-DBCO)$_n$ + (Chitosan/PMLA-az/Chitosan/PMLA-DBCO)$_n$	20 + 0 → 60	Lys$^{\text{x-linked}}$ + n Barrier Film

For an understanding of the growth behavior in our films, we examined the thicknesses of different film architectures at 20 tetralayer intervals. For convenience and brevity, we adopt the nomenclature outlined in Table 3-1. As shown in Figure 3-4, using click crosslinking reduces the thickness of 20 tetralayer films from 514 ± 12 nm to 258 ± 18 nm for Lys and Lys$^{\text{x-linked}}$ films, respectively. Subsequent deposition of n-Barrier Film revealed a linear growth ($R^2 = 0.992$) with 11.7 nm deposited per tetralayer, or ~3 nm per layer for the combined Lys$^{\text{x-linked}}$ + n-Barrier film. This is in striking contrast to our previous data, in which the growth behavior of (chitosan/PMLA/protein/PMLA)$_n$ films increases exponentially with up to ~69.2 nm ($R^2 = 0.9999$) deposited per tetralayer(61) (*see Chapter 2*), suggesting a significant suppression of exponential growth and interdiffusion.
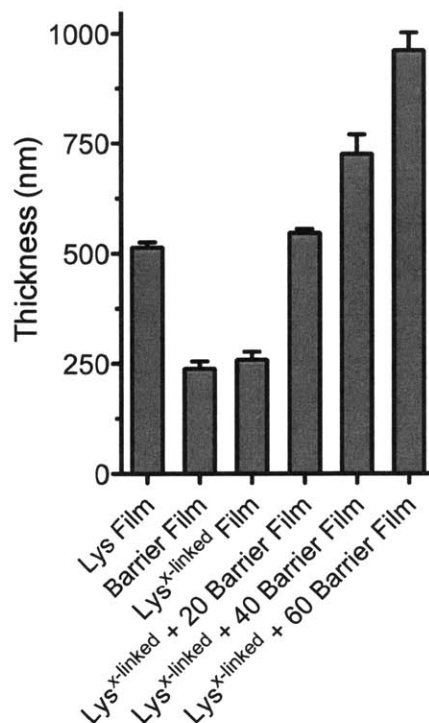
Figure 3-4. Effect of crosslinking and barrier layers on film thicknesses.

In our above-described strategy, we deposited an initial 20 tetralayers of crosslinked protein-containing film (chitosan/PMLA-az/lys/PMLA-DBCO)$_{20}$, followed by additional crosslinked film devoid of protein (chitosan/PMLA-az/chitosan/PMLA-DBCO)$_n$ to act as a sacrificial barrier layer. Lysozyme has one of the greater diffusivities among proteins in LbL films(80) and it is critical to confirm that it is segregated to the underlying layers with suppressed interdiffusion. To this end, we tracked the lysozyme profile through the film with X-ray Photoelectron Spectroscopy (XPS) by monitoring the sulfur signal as a function of probe depth. Coupling C60$^+$ ion sputtering with XPS allowed us to intermittently etch ~6.6 nm of film from the surface and obtain surface-specific elemental information, analogous to an earlier strategy that tracked polymer interdiffusion in multilayer films(64). By monitoring the sulfur content, an element uniquely characteristic of lysozyme in the film, we found its peak emerging above

background after ~40 cycles (Figure 3-5A). When examining the sulfur peak intensity as a function of probe depth (Figure 3-5B), the S_{2p} signal remained stagnant until reaching ~328 nm into the film, at which point the intensity significantly increased for an additional 80 nm before reaching a plateau. This step change reveals a gradual yet well defined transition from protein-free to protein-rich sections in the film, demonstrating the confinement of lysozyme to the portion of film beneath the barrier layer.

A

B
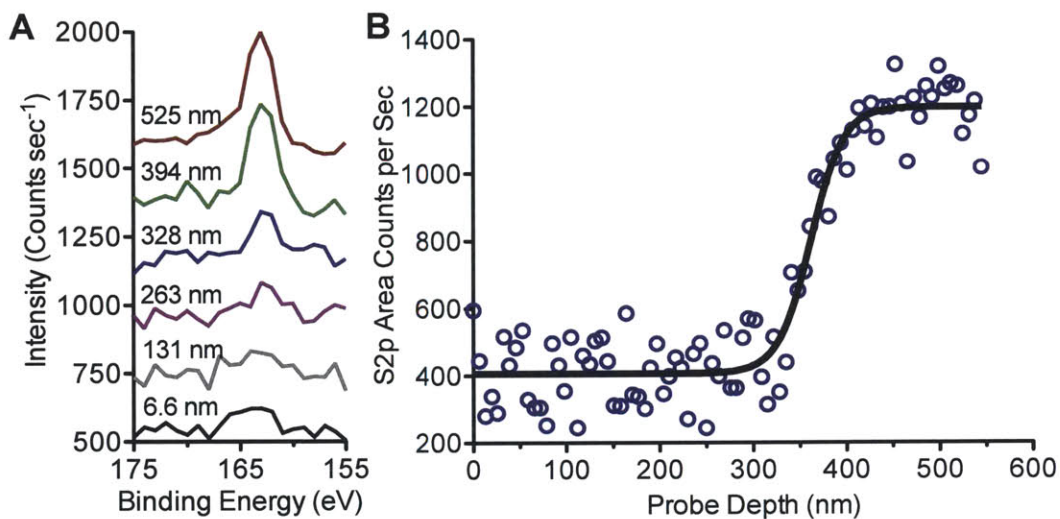
Figure 3-5. Depth profiling XPS analysis of sulfur content using a $C60^+$ ion bombardment of Lys[x-linked] + 20 Barrier Layer Films. Stacked spectra in the S2p region after 1, 20, 40, 50, 60, and 80 cycles corresponding to probe depths of approximately 7 nm, 131 nm, 263 nm, 328 nm, 394 nm, and 525 nm, respectively (A). Integrated S_{2p} area counts after every sputter cycle is shown as a function of probe depth from the film surface (B).

Stratification in the film architecture via crosslinking should not only isolate lysozyme to its designed region in the film but also minimize its loss as additional barrier layers are deposited. Figure 3-6 shows that in addition to the reduced thickness, there is a dramatic decrease in lysozyme loading when comparing Lys (30.1 ± 1.1 µg/cm^2) and Lys[x-linked] films (6.4 ± 0.1 µg/cm^2). Their loading densities of 586 µg/mm^3 and 247 µg/mm^3, respectively, also suggests that the fewer available carboxylates on PMLA-az and PMLA-DBCO and the limited

interdiffusion from crosslinking lowers the extent of lysozyme complexation and film-incorporation. Comparing $Lys^{x-linked}$ films with $Lys^{x-linked} + n$ barrier layer films, we find that the additional barrier layers deposited do not significantly affect the total lysozyme loading.
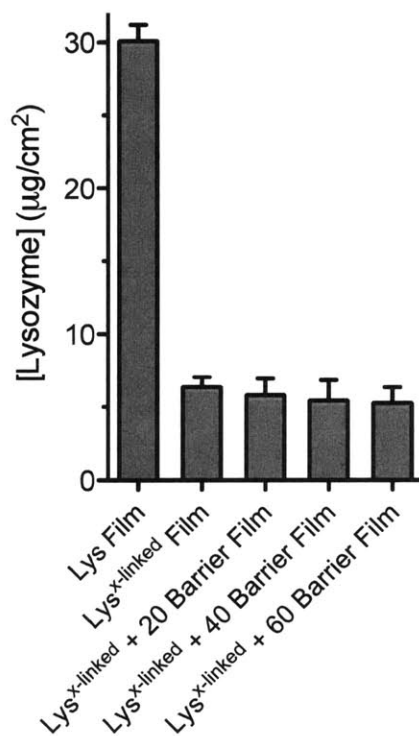
Figure 3-6. Effect of crosslinking and barrier layers on total lysozyme loading.

Based on our analysis thus far, we have found reduced interdiffusion through *in situ* crosslinking and have sequestered lysozyme beneath a degradable barrier layer. Seeking the proof of principle for sequential release, we evaluated the effect of crosslinking and thickness of barrier layers on the kinetics of lysozyme release. Herein, and reported previously(61) (*see Chapter 2*), we found that LbL assembled Lys films sustain the release of lysozyme for up to two days (Figure 3-7A). By introducing crosslinking, we suppressed the initial burst release from $Lys^{x-linked}$ films and slightly extended the duration of release to three days. In both cases, release was initiated at the start of incubation. As progressively thicker barrier layer films of 20, 40, and

60 tetralayers were deposited, we found that the start of lysozyme release was correspondingly suppressed up to ~0.5, ~1, and ~1.5 days, respectively (Figure 3-7A, *arrows*). Transformation of lysozyme release profiles to their rates as shown in Figure 3-7B further illustrates the effect that both crosslinking and barrier films have on the release kinetics; not only is the onset of release suppressed, its rate and period of release is also dramatically shifted. This heralds the possibility of pre-programmable release behavior without the need of external intervention.
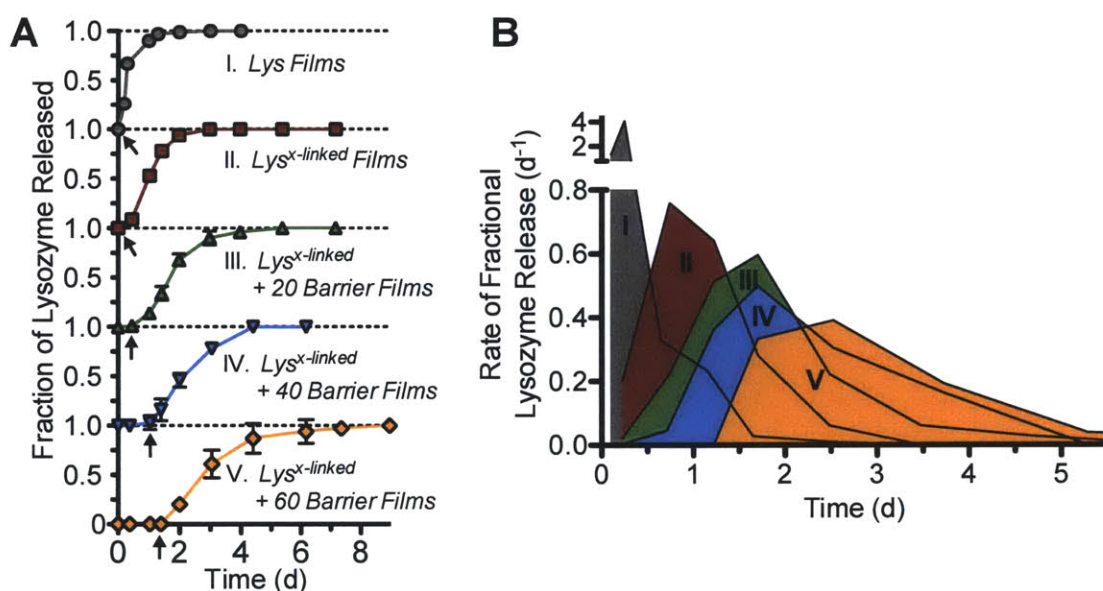
Figure 3-7. The effect of crosslinking and barrier layer thickness on the lysozyme release (a) and rate of fractional lysozyme release (b) into PBS, pH 7.4 at 37°C.

For downstream biomedical applications, biocompatibility is vital; we found analogous (chitosan/PMLA)$_n$ films, without click functionality, to be non-cytotoxic(61) (*see Chapter 2*), and the addition of click functionality through amide linkages should have minimal, if any, impact on cell viability. To prove this, we incubated a weeks worth of release solutions from Lys$^{x-linked}$ + 60 barrier films with NIH3T3 cells and quantified their effect on cellular metabolic activity (Figure 3-8). Cells incubated with these release media (in cell culture medium) showed

no difference in viability compared to cell culture medium alone, thus further demonstrating this as a biocompatible and biodegradable method for generating controllable protein release.
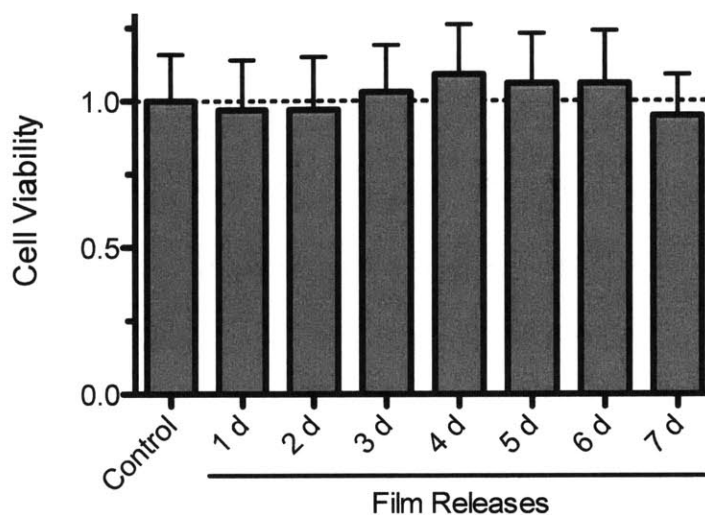
Figure 3-8. Cytotoxic effect of releases from Lys$^{\text{x-linked}}$ + 60 Barrier Layer films on the viability of NIH3T3 cells.

We next tested the ability to release two therapeutics in sequential fashion from these thin films through the deposition of an additional protein-containing layer on top of a Lys$^{\text{x-linked}}$ + n barrier film. As shown in Figure 3-9A, a triple-stacked composite film undergoing surface erosion would first release the protein from the upper layers (BMP2), then progress through the sacrificial barrier layer, and eventually release the buried protein in the lower layers (lysozyme). We deposited a rapidly releasing (chitosan/PMLA/BMP2/PMLA)$_{20}$ film on top of Lys$^{\text{x-linked}}$ + 60 barrier films, as schematically represented in Figure 3-9A, and studied its release behavior. Shown in Figure 3-9B, we found that BMP2 is rapidly released upon hydration with more than 90% of its 9.1 ± 0.7 ng/cm^2 eluting in the first 12 hours. Then, 20 hours later, 1.0 ± 0.3 μg/cm^2 lysozyme elutes for an additional 40 hours. Surprisingly the lysozyme loading for these films was reduced after BMP2 film deposition, which we suspect may be due to the effects of the

73

BMP2 excipients (e.g., glycine, glutamic acid, sucrose, and polysorbate 80) whose preservative effects by reducing intermolecular interactions(81, 82) can also disrupt LbL film interactions. Despite their impact, substantial protein remains in the film.
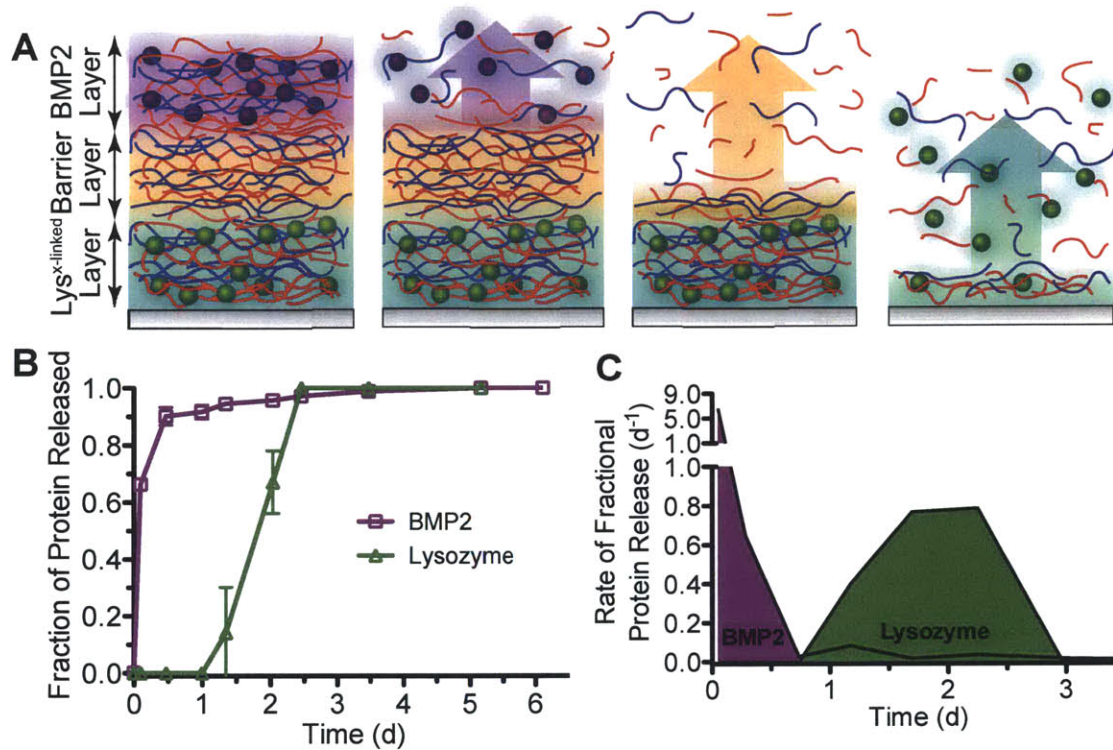
Figure 3-9. Characteristics of sequential release from composite multilayer films with a schematic view of the proposed film architecture and surface-based erosion (A). Protein release profiles (B) and their rates of fractional release (C) into PBS, pH 7.4 at 37°C.

Overall we have developed a kinetically discrete protein delivery platform, where release of the temporally second therapeutic (lysozyme in the present case) is initially suppressed and does not coincide with release of the first therapeutic (BMP2 in the present case). This is even more evident when examining the rate of fractional release, shown in Figure 3-9C. We find two distinct schedules of release with each demonstrating unique release behaviors resulting in spatiotemporal separation of BMP2 and lysozyme for their sequential delivery. This is markedly

different than many other dual release formulations, which purport "sequential release" behavior,

but in fact have an uncontrolled initial co-release of the second therapeutic with the first.

.

.

3.4   Conclusions

We have designed a biodegradable and biocompatible thin film localized delivery formulation with kinetically discrete and controlled drug release. LbL assembly allowed us to use benign conditions to incorporate significant quantities of active protein and with copper-free click chemistry, bio-orthogonal crosslinking during film assembly significantly reduced interdiffusion to maintain film stratification. Depth-dependent elemental analysis of these films revealed sequestration of lysozyme to its designed region, beneath a barrier layer, and release studies showed that the combination of crosslinking and barrier layers suppressed the initial burst release and effectively delayed the onset of release with increasing barrier layer thickness. Depositing an additional protein-containing LbL film on top of this construct yielded a sequential release behavior as dictated by logical film construction. This demonstration of spatiotemporally discrete protein delivery reveals the possibility of localized, non-overlapping multi-therapeutic administration from a biodegradable thin film that can be tuned for a broad variety of biomedical applications.

3.5 References

1. Lee MJ, *et al.* (2012) Sequential Application of Anticancer Drugs Enhances Cell Death by Rewiring Apoptotic Signaling Networks. *Cell* 149(4):780-794.
2. MacDiarmid JA, *et al.* (2009) Sequential treatment of drug-resistant tumors with targeted minicells containing siRNA or a cytotoxic drug. *Nat Biotech* 27(7):643-651.
3. Vaira D, *et al.* (2007) Sequential Therapy versus Standard Triple-Drug Therapy for Helicobacter pylori EradicationA Randomized Trial. *Ann. Intern. Med.* 146(8):556-563.
4. Lee K, Silva EA, & Mooney DJ (2011) Growth factor delivery-based tissue engineering: general approaches and a review of recent developments. *Journal of the Royal Society Interface* 8(55):153-170.
5. Chen F-M, Zhang M, & Wu Z-F (2010) Toward delivery of multiple growth factors in tissue engineering. *Biomaterials* 31(24):6279-6308.
6. Mehta M, Schmidt-Bleek K, Duda GN, & Mooney DJ (2012) Biomaterial delivery of morphogens to mimic the natural healing cascade in bone. *Adv. Drug Del. Rev.* 64(12):1257-1276.
7. Barrientos S, Stojadinovic O, Golinko MS, Brem H, & Tomic-Canic M (2008) Growth factors and cytokines in wound healing. *Wound Repair Regen.* 16(5):585-601.
8. De Marchis F, *et al.* (2002) Platelet-derived growth factor inhibits basic fibroblast growth factor angiogenic properties in vitro and in vivo through its alpha receptor. *Blood* 99(6):2045-2053.
9. Facchiano A, *et al.* (2000) The chemotactic and mitogenic effects of platelet-derived growth factor-BB on rat aorta smooth muscle cells are inhibited by basic fibroblast growth factor. *J. Cell Sci.* 113(16):2855-2863.
10. Russo K, Ragone R, Facchiano AM, Capogrossi MC, & Facchiano A (2002) Platelet-derived growth factor-BB and basic fibroblast growth factor directly interact in vitro with high affinity. *J. Biol. Chem.* 277(2):1284-1291.
11. Zellin G, Beck S, Hardwick R, & Linde A (1998) Opposite effects of recombinant human transforming growth factor-beta 1 on bone regeneration in vivo: Effects of exclusion of periosteal cells by microporous membrane. *Bone* 22(6):613-620.
12. Vonau RL, Bostrom MPG, Aspenberg P, & Sams AE (2001) Combination of growth factors inhibits bone ingrowth in the bone harvest chamber. *Clin. Orthop. Relat. Res.* (386):243-251.
13. Ripamonti U, Crooks J, Petit JC, & Rueger DC (2001) Periodontal tissue regeneration by combined applications of recombinant human osteogenic protein-1 and bone morphogenetic protein-2. A pilot study in Chacma baboons (Papio ursinus). *Eur. J. Oral Sci.* 109(4):241-248.
14. Marden LJ, Fan RSP, Pierce GF, Reddi AH, & Hollinger JO (1993) PLATELET-DERIVED GROWTH-FACTOR INHIBITS BONE REGENERATION INDUCED BY OSTEOGENIN, A BONE MORPHOGENETIC PROTEIN, IN RAT CRANIOTOMY DEFECTS. *J. Clin. Invest.* 92(6):2897-2905.

15. Raiche AT & Puleo DA (2004) In vitro effects of combined and sequential delivery of two bone growth factors. *Biomaterials* 25(4):677-685.

16. Tengood JE, Kovach KM, Vescovi PE, Russell AJ, & Little SR (2010) Sequential delivery of vascular endothelial growth factor and sphingosine 1-phosphate for angiogenesis. *Biomaterials* 31(30):7805-7812.

17. Tengood JE, Ridenour R, Brodsky R, Russell AJ, & Little SR (2011) Sequential Delivery of Basic Fibroblast Growth Factor and Platelet-Derived Growth Factor for Angiogenesis. *Tissue Engineering Part A* 17(9-10):1181-1189.

18. Sabo JK, Aumann TD, Kilpatrick TJ, & Cate HS (2013) Investigation of Sequential Growth Factor Delivery during Cuprizone Challenge in Mice Aimed to Enhance Oligodendrogliogenesis and Myelin Repair. *Plos One* 8(5).

19. Edelman ER, Nugent MA, & Karnovsky MJ (1993) PERIVASCULAR AND INTRAVENOUS ADMINISTRATION OF BASIC FIBROBLAST GROWTH-FACTOR - VASCULAR AND SOLID ORGAN DEPOSITION. *Proc. Natl. Acad. Sci. U. S. A.* 90(4):1513-1517.

20. Lazarous DF, *et al.* (1996) Comparative effects of basic fibroblast growth factor and vascular endothelial growth factor on coronary collateral development and the arterial response to injury. *Circulation* 94(5):1074-1082.

21. Richter A, Anton SF, Koch P, & Dennett SL (2003) The impact of reducing dose frequency on health outcomes. *Clin. Ther.* 25(8):2307-2335.

22. Chen RR, Silva EA, Yuen WW, & Mooney DJ (2007) Spatio-temporal VEGF and PDGF delivery patterns blood vessel formation and maturation. *Pharm. Res.* 24(2):258-264.

23. Chapanian R & Amsden BG (2010) Combined and sequential delivery of bioactive VEGF(165) and HGF from poly (trimethylene carbonate) based photo-cross-linked elastomers. *J. Controlled Release* 143(1):53-63.

24. Yilgor P, Hasirci N, & Hasirci V (2010) Sequential BMP-2/BMP-7 delivery from polyester nanocapsules. *Journal of Biomedical Materials Research Part A* 93A(2):528-536.

25. Bonani W, Motta A, Migliaresi C, & Tan W (2012) Biomolecule Gradient in Micropatterned Nanofibrous Scaffold for Spatiotemporal Release. *Langmuir* 28(38):13675-13687.

26. Yilgor P, Tuzlakoglu K, Reis RL, Hasirci N, & Hasirci V (2009) Incorporation of a sequential BMP-2/BMP-7 delivery system into chitosan-based scaffolds for bone tissue engineering. *Biomaterials* 30(21):3551-3559.

27. Yonet-Tanyeri N, *et al.* (2013) The spatiotemporal control of erosion and molecular release from micropatterned poly(ethylene glycol)-based hydrogel. *Biomaterials* 34(33):8416-8423.

28. Shin S-H, *et al.* (2013) Sequential delivery of TAT-HSP27 and VEGF using microsphere/hydrogel hybrid systems for therapeutic angiogenesis. *J. Controlled Release* 166(1):38-45.

29. Nelson DM, Ma Z, Leeson CE, & Wagner WR (2012) Extended and sequential delivery of protein from injectable thermoresponsive hydrogels. *Journal of Biomedical Materials Research Part A* 100A(3):776-785.

30. Kempen DHR, *et al.* (2009) Effect of local sequential VEGF and BMP-2 delivery on ectopic and orthotopic bone regeneration. *Biomaterials* 30(14):2816-2825.

31. Ruvinov E, Leor J, & Cohen S (2011) The promotion of myocardial repair by the sequential delivery of IGF-1 and HGF from an injectable alginate biomaterial in a model of acute myocardial infarction. *Biomaterials* 32(2):565-578.

32. Hao X, *et al.* (2007) Angiogenic effects of sequential release of VEGF-A(165) and PDGF-BB with alginate hydrogels after myocardial infarction. *Cardiovasc. Res.* 75(1):178-185.

33. Freeman I & Cohen S (2009) The influence of the sequential delivery of angiogenic factors from affinity-binding alginate scaffolds on vascularization. *Biomaterials* 30(11):2122-2131.

34. Wang H, *et al.* (2013) Combined delivery of BMP-2 and bFGF from nanostructured colloidal gelatin gels and its effect on bone regeneration in vivo. *J. Controlled Release* 166(2):172-181.

35. Kim S, *et al.* (2012) Sequential delivery of BMP-2 and IGF-1 using a chitosan gel with gelatin microspheres enhances early osteoblastic differentiation. *Acta Biomater.* 8(5):1768-1777.

36. Macdonald ML, Rodriguez NM, Shah NJ, & Hammond PT (2010) Characterization of Tunable FGF-2 Releasing Polyelectrolyte Multilayers. *Biomacromolecules* 11(8):2053-2059.

37. Macdonald ML, *et al.* (2011) Tissue integration of growth factor-eluting layer-by-layer polyelectrolyte multilayer coated implants. *Biomaterials* 32(5):1446-1453.

38. Shah NJ, Hong J, Hyder MN, & Hammond PT (2012) Osteophilic Multilayer Coatings for Accelerated Bone Tissue Growth. *Adv. Mater.* 24(11):1445-1450.

39. Shah NJ, *et al.* (2011) Tunable dual growth factor delivery from polyelectrolyte multilayer films. *Biomaterials* 32(26):6183-6193.

40. Shah NJ, *et al.* (2013) Surface-Mediated Bone Tissue Morphogenesis from Tunable Nanolayered Implant Coatings. *Science Translational Medicine* 5(191):191ra183.

41. Crouzier T, Ren K, Nicolas C, Roy C, & Picart C (2009) Layer-By-Layer Films as a Biomimetic Reservoir for rhBMP-2 Delivery: Controlled Differentiation of Myoblasts to Osteoblasts. *Small* 5(5):598-608.

42. De Cock LJ, *et al.* (2010) Layer-by-Layer Incorporation of Growth Factors in Decellularized Aortic Heart Valve Leaflets. *Biomacromolecules* 11(4):1002-1008.

43. Dierich A, *et al.* (2007) Bone formation mediated by synergy-acting growth factors embedded in a polyelectrolyte multilayer film. *Adv. Mater.* 19(5):693-+.

44. Itoh Y, Matsusaki M, Kida T, & Akashi M (2008) Locally controlled release of basic fibroblast growth factor from multilayered capsules. *Biomacromolecules* 9(8):2202-2206.

45. Mao ZW, Ma L, Zhou J, Gao CY, & Shen JC (2005) Bioactive thin film of acidic fibroblast growth factor fabricated by layer-by-layer assembly. *Bioconj. Chem.* 16(5):1316-1322.

46. Muller S, *et al.* (2008) VEGF-functionalized polyelectrolyte multilayers as proangiogenic prosthetic coatings. *Adv. Funct. Mater.* 18(12):1767-1775.

47.   van den Beucken JJJP, *et al.* (2006) Functionalization of multilayered DNA-coatings with bone morphogenetic protein 2. *J. Controlled Release* 113(1):63-72.

48.   Vodouhe C, *et al.* (2005) Effect of functionalization of multilayered polyelectrolyte films on motoneuron growth. *Biomaterials* 26(5):545-554.

49.   Facca S, *et al.* (2010) Active multilayered capsules for in vivo bone formation. *Proc. Natl. Acad. Sci. U. S. A.* 107(8):3406-3411.

50.   Peterson AM, Pilz-Allen C, Kolesnikova T, Mohwald H, & Shchukin D (2014) Growth Factor Release from Polyelectrolyte-Coated Titanium for Implant Applications. *Acs Applied Materials & Interfaces* 6(3):1866-1871.

51.   Garza JM, *et al.* (2004) Multicompartment films made of alternate polyelectrolyte multilayers of exponential and linear growth. *Langmuir* 20(17):7298-7302.

52.   Garza JM, *et al.* (2005) Polyelectrolyte multilayers and degradable polymer layers as multicompartment films. *Langmuir* 21(26):12372-12377.

53.   Peralta S, Habib-Jiwan J-L, & Jonas AM (2009) Ordered Polyelectrolyte Multilayers: Unidirectional FRET Cascade in Nanocompartmentalized Polyelectrolyte Multilayers. *Chemphyschem* 10(1):137-143.

54.   Wood KC, Chuang HF, Batten RD, Lynn DM, & Hammond PT (2006) Controlling interlayer diffusion to achieve sustained, multiagent delivery from layer-by-layer thin films. *Proc. Natl. Acad. Sci. U. S. A.* 103(27):10207-10212.

55.   Hong J, *et al.* (2012) Graphene Multilayers as Gates for Multi-Week Sequential Release of Proteins from Surfaces. *Acs Nano* 6(1):81-88.

56.   Wang K, *et al.* (2011) Biocompatibility of Graphene Oxide. *Nanoscale Research Letters* 6.

57.   Zhang XY, *et al.* (2011) Distribution and biocompatibility studies of graphene oxide in mice after intravenous administration. *Carbon* 49(3):986-995.

58.   Alava T, *et al.* (2013) Control of the Graphene–Protein Interface Is Required To Preserve Adsorbed Protein Function. *Anal. Chem.* 85(5):2754-2759.

59.   Smith RC, Riollano M, Leung A, & Hammond PT (2009) Layer-by-Layer Platform Technology for Small-Molecule Delivery. *Angew. Chem. Int. Ed.* 48(47):8974-8977.

60.   Vazquez E, Dewitt DM, Hammond PT, & Lynn DM (2002) Construction of hydrolytically-degradable thin films via layer-by-layer deposition of degradable polyelectrolytes. *J. Am. Chem. Soc.* 124(47):13992-13993.

61.   Hsu BB, *et al.* (2014) Multilayer films assembled from biocompatible, naturally-derived materials for controlled protein release. *Biomacromolecules* in press.

62.   Lee B-S, Vert M, & Holler E (2002) Water-soluble Aliphatic Polyesters: Poly(malic acid)s. *Biopolymers: Polyesters I*, eds Doi Y & Steinbuchel A), Vol 3a, pp 75-103.

63.   Lee BS, *et al.* (2006) Polycefin, a new prototype of a multifunctional nonconjugate based on poly(beta-L-malic acid) for drug delivery. *Bioconj. Chem.* 17(2):317-326.

64.   Gilbert JB, Rubner MF, & Cohen RE (2013) Depth-profiling X-ray photoelectron spectroscopy (XPS) analysis of interlayer diffusion in polyelectrolyte multilayers. *Proc. Natl. Acad. Sci. U. S. A.* 110(17):6651-6656.

65. Picart C, *et al.* (2001) Buildup mechanism for poly(L-lysine)/hyaluronic acid films onto a solid surface. *Langmuir* 17(23):7414-7424.

66. Lavalle P, *et al.* (2002) Comparison of the structure of polyelectrolyte multilayer films exhibiting a linear and an exponential growth regime: An in situ atomic force microscopy study. *Macromolecules* 35(11):4458-4465.

67. Picart C, *et al.* (2002) Molecular basis for the explanation of the exponential growth of polyelectrolyte multilayers. *Proc. Natl. Acad. Sci. U. S. A.* 99(20):12531-12535.

68. Lavalle P, *et al.* (2004) Modeling the buildup of polyelectrolyte multilayer films having exponential growth. *J. Phys. Chem. B* 108(2):635-648.

69. Porcel C, *et al.* (2006) From exponential to linear growth in polyelectrolyte multilayers. *Langmuir* 22(9):4376-4383.

70. Decher G & Schlenoff JB eds (2012) *Multilayer Thin Films: Sequential Assembly of Nanocomposite Materials* (Wiley-VCH, Weinheim, Germany), 2nd Ed.

71. Macdonald M, Rodriguez NM, Smith R, & Hammond PT (2008) Release of a model protein from biodegradable self assembled films for surface delivery applications. *J. Controlled Release* 131(3):228-234.

72. Shukla A, *et al.* (2010) Controlling the release of peptide antimicrobial agents from surfaces. *Biomaterials* 31(8):2348-2357.

73. Such GK, Quinn JF, Quinn A, Tjipto E, & Caruso F (2006) Assembly of ultrathin polymer multilayer films by click chemistry. *J. Am. Chem. Soc.* 128(29):9318-9319.

74. Such GK, Tjipto E, Postma A, Johnston APR, & Caruso F (2007) Ultrathin, responsive polymer click capsules. *Nano Lett.* 7(6):1706-1710.

75. Liang K, *et al.* (2012) Engineering Cellular Degradation of Multilayered Capsules through Controlled Cross-Linking. *Acs Nano* 6(11):10186-10194.

76. Ochs CJ, Such GK, Yan Y, van Koeverden MP, & Caruso F (2010) Biodegradable Click Capsules with Engineered Drug-Loaded Multilayers. *Acs Nano* 4(3):1653-1663.

77. Ljubimova JY, *et al.* (2013) Toxicity and efficacy evaluation of multiple targeted polymalic acid conjugates for triple-negative breast cancer treatment. *J. Drug Targeting* 21(10):956-967.

78. Jewett JC & Bertozzi CR (2010) Cu-free click cycloaddition reactions in chemical biology. *Chem. Soc. Rev.* 39(4):1272-1279.

79. Debets MF, *et al.* (2010) Aza-dibenzocyclooctynes for fast and efficient enzyme PEGylation via copper-free (3+2) cycloaddition. *Chem. Commun.* 46(1):97-99.

80. Uhlig K, *et al.* (2012) 3d localization and diffusion of proteins in polyelectrolyte multilayers. *Soft Matter* 8(47):11786-11789.

81. Liao YH, Brown MB, Quader A, & Martin GP (2002) Protective mechanism of stabilizing excipients against dehydration in the freeze-drying of proteins. *Pharm. Res.* 19(12):1854-1861.

82. Chi EY, Krishnan S, Randolph TW, & Carpenter JF (2003) Physical stability of proteins in aqueous solution: Mechanism and driving forces in nonnative protein aggregation. *Pharm. Res.* 20(9):1325-1336.

Chapter 4
Multifunctional Self-Assembled Films for Rapid Hemostat and Sustained Anti-Infective Delivery

A version of this chapter is in preparation for publication.

Authors:
Bryan B. Hsu[1,2,4], Samantha R Hagerman[3], Kelsey Jamieson[3], Eggehard Holler[5], Julia Y. Ljubimova[5], and Paula T. Hammond[1,3,4]

[1]Koch Institute for Integrative Cancer Research, Massachusetts Institute of Technology, Cambridge, MA 02139
Departments of [2]Chemistry and [3]Chemical Engineering, Massachusetts Institute of Technology, Cambridge, MA 02139
[4]Institute for Soldier Nanotechnologies, Massachusetts Institute of Technology, Cambridge, MA 02139
[5]Nanomedicine Research Center, Department of Neurosurgery, Cedars Sinai Medical Center, Los Angeles, CA 90048

4.1   Introduction

Uncontrolled bleeding is the most significant cause of mortality on the battlefield, causing more than 85% of the deaths from potentially survivable wounds(1). In civilian populations, it is a factor in more than half of trauma related deaths(2). Once soldiers survive beyond the initial few hours, infection becomes the major cause of morbidity, as pathogens can populate open wounds from environmental contamination (e.g., blast debris and soil) or through human transmission(3-5). To address this medical crisis, it would be ideal to have a multifunctional bandage that is easily applied, lightweight, and immediately active to provide hemostasis and fight infection(6).

For this application it would be desirable deliver multiple therapeutics directly to the wound, each with individually optimized release kinetics. To stop bleeding, a hemostat would need to be delivered immediately on-contact in a bolus release, while killing pathogens would require a sustained release of antibiotic above the critical concentration from one to a few days to eradicate the presence of infection(7). Generating complex multimodal release behavior from biodegradable matrices has traditionally been challenging because of the diverse array of physical and chemical interactions that can affect drug loading and elution. These factors become more complicated when more than one drug is involved(8).

We aimed to generate Layer-by-Layer (LbL) assembled films capable of addressing both hemostasis and infection. We have previously developed films capable of sustained release of antibiotics(9-11) as well as those rapidly achieving hemostasis through thrombin delivery(12). With LbL, nano-to-micron scale thin films can be fabricated through deposition of compounds with complementary intermolecular interactions (e.g., electrostatic, hydrogen-bonding, covalent, etc.) from aqueous solutions(13). This eliminates the potential for protein denaturation from

organic solvents that have been traditionally used for controlled release from hydrophobic polyesters like poly(lactic acid-*co*-glycolic acid) and poly(ε-caprolactone) based bulk films(8). Since the first demonstration of protein incorporation into LbL films(14), a number of different types of films incorporating therapeutics including proteins, peptides, and small molecules, have demonstrated controlled release with a high level of activity retained. Typically, it can be challenging to generate distinctly different release behaviors of multiple therapeutics from LbL films because of high levels of blending(15) or the competitive behavior of different components(16), but recently we have been able to demonstrate sequential release of two polysaccharides(17), two proteins(18, 19) (*see Chapter 3*), and the staged release of an antibiotic and growth factor(20), each of which has relied on a physical or chemically crosslinked barrier layer for controlling release kinetics.

Herein, we address the challenge of maintaining high drug loading and tuned release by using a polymer-drug conjugation strategy that covalently links vancomycin to the hydrophilic and hydrolytically degradable polyanion, poly(β-L-malic acid) (PMLA). We found that the PMLA-Vanco conjugate retains its antibacterial activity and can confer high drug loadings into (poly-L-lysine/PMLA-Vanco) films assembled at the physiological pH of 7.4, which would otherwise be difficult because of the poor charge density of vancomycin. Hydrolytic degradation of the ester backbone in PMLA facilitates film degradation and controlled release of vancomycin. We found that deposition of (thrombin/tannic acid)$_n$ on top of these layers generated a composite film that retained a rapid thrombin release over the timeframe of several minutes and sustained vancomycin release over a period of 24 hours, similar to that achieved with the independent films when studied separately. We found that thrombin retained its clotting activity and vancomycin retained its antibacterial potency after release from this composite film.

4.2   Materials and Methods

All materials were used without further purification unless otherwise noted. Tannic acid, vancomycin, and poly-L-lysine (PLL, 30-70 kDa) were obtained from Sigma-Aldrich. Poly(β-L-malic acid) (PMLA, 40 kDa) was cultured and purified as previously described from *Physarum polycephalum*(21). Bovine thrombin (high purity) was obtained from Biopharm Laboratories. Cation-adjusted Mueller Hinton broth (CaMHB) was obtained from BD. All other chemicals unless otherwise noted, were obtained from Sigma-Aldrich.

In a typical strategy for conjugating vancomycin to PMLA, which was adapted from previously described approaches(22, 23), 25 mg (216 μmol) of PMLA was dissolved in 2 mL of acetone (dried over molecular sieves) under an argon atmosphere. While stirring on ice, a solution of 2 mL of anhydrous N,N-dimethylformamide (DMF) containing 22 mg (108 μmol) of dicyclohexylcarbodiimide (DCC) and 12 mg (108 μmol) of N-hydroxysuccimide (NHS) was added drop-wise, prior to incubation for 4 h at room temperature. The precipitated by-products were removed by filtration with Celite 545 (EM Science) and the filtrate was added drop-wise to a stirring solution of 2 mL of anhydrous DMF containing 160 mg (108 μmol) of vancomycin and 302 μL (2.2 mmol) of triethylamine. Use of a 20-fold molar excess of triethylamine has been shown to favor reaction through vancomycin's primary amine(24). After 2 h of stirring at room temperature, the reaction was quenched with 10 mL of 10 mM phosphate, pH 7.4, on ice for 30 min prior to further dilution to 40 mL with H_2O. This solution was syringe filtered (0.45 μm), concentrated by centrifugal filtration (Corning Spin-X UF 20, 10k MWCO) then purified with a PD-10 desalting column (GE Healthcare) according to the manufacturer's instructions and dried by lyophilization yielding 50 mg of PMLA-Vanco (74 wt% vancomycin conjugation). The degree of vancomycin loading was determined by HPLC. Other degrees of modification were

similarly synthesized using proportionately smaller quantities of DCC, NHS, vancomycin, and triethylamine.

Quantification of vancomycin and PMLA-Vanco was performed by HPLC (Agilent 1100 Series) using an injection volume of 50 μL and a C18 column (Supelco Discovery C18) with a 1 mL/min mobile phase ramped from 100% PBS to 100% methanol over 20 min. Vancomycin was quantified by fluorescence (λ_{ex} = 280 nm; λ_{em} = 355 nm).

Antibacterial activity was determined by a microdilution assay as previously described(9). Samples in PBS were initially diluted 2-fold with 2X concentrated CaMHB and then 2-fold serially diluted with 1X CaMHB in a 96-well microplate for final volumes of 90 μL. To these dilutions, 10 μL of 10^6 cells/mL of S. aureus (ATCC 25923) was added and then incubated overnight at 37°C with shaking. After 18-24 h, the most diluted sample concentration that remained optically clear (i.e., no evidence of turbidity) was determined to be the minimum inhibitory concentration.

LbL-assembled films were constructed on silicon wafers pre-cleaned with methanol and water, then irradiated with plasma (Harrick PDC-32G) and coated with a baselayer of (linear polyethylenimine/sodium polystyrene sulfonate)$_{10}$ as described previously(9) using an automated slide stainer (Carl Zeiss) for film assembly. All polymer/protein solutions were formulated in 10 mM phosphate, pH 7.4 while rinses were performed in H_2O, pH adjusted to 7—7.5. Films of (PLL/PMLA-Vanco)$_n$ were constructed with repeated cycles of 15 min incubation in 1 mg/mL of PLL followed by rinsing for 10 s, 20 s, and 30 s then incubation for 15 min in 1 mg/mL of PMLA-Vanco followed by rinsing for 10 s, 20 s, and 30 s. After construction, films were gently dried with N_2 and then house vacuum overnight. Films of (thrombin/tannic acid)$_n$ were deposited with 5 min incubation in 1 mg/mL of thrombin followed by rinsing for 10 s, 20 s, and 30 s, then

incubation for 5 min in 2 mg/mL of tannic acid followed by rinsing for 10 s, 20 s, and 30 s. Film thicknesses were determined by step-height measurement of razor-scored films with profilometry using a 2.5 μm tip (Dektak 150 Profilometer).

Release profiles of vancomycin and thrombin eluted from films were determined by incubation in 500 μL of PBS, pH 7.4 or TCNB, pH 7.4 at 37°C. These solutions were periodically collected for analysis and replaced with fresh buffer solutions. TCNB buffer was composed of sterile-filtered 50 mM of Trizma, 150 mM of sodium chloride, 1.1 mM of calcium chloride, 0.05% of Brij-35, and 0.2 mg/mL of BSA at pH 7.4. Vancomycin concentration and activity was determined from these releases as described above.

Film degradation during vancomycin elution of (PLL/PMLA-Vanco)$_{40.5}$ films composed of PMLA-Vanco with 74 wt% functionalization was tracked by incubating films in 500 μL of PBS, pH 7.4 at 37°C then at predermined times briefly immersed in H_2O, drying with N_2 and measuring the thickness with spectroscopic ellipsometry (Woollam XLS-100) before continued incubation in fresh PBS solution.

Thrombin activity was determined by a fibrin-clot forming assay that measures the time for clot formation by enzymatic conversion of soluble fibrinogen to an insoluble fibrin. Fibrinogen dilution buffer was composed of 10 mM of sodium citrate, 120 mM of glycine, and 32 mM of tranexamic acid at pH 7.4 and sterile filtered. Fibrinogen solution was composed of 20 mM sodium citrate and 10 mg/mL of human fibrinogen (Sigma Aldrich) at pH 7.4, sterile filtered, and then stored in aliquots at -20°C. Prior to testing, coagulation reagent was prepared by combining 9 mL of fibrinogen dilution buffer (with pre-dissolved 10 mg/mL of BSA) with 1 mL of fibrinogen solution. To assay clotting time, 125 μL of coagulation reagent was added to 50 μL of thrombin solution in TCNB buffer at 37°C and the time for clotting was quantified with

a coagulation analyzer (Diagnostica Stago ST4). Comparison of clotting time to a standard curve yielded concentration of thrombin activity.

For scanning electron microscopy, films were imaged with a field-emission gun scanning electron microscope (JEOL-6700F) at 5 kV and an 8 mm working distance after sputter coating with ~8 nm of Au/Pd.

4.3   Results and Discussion

Because of the difficulty in combining multiple drugs with independently tunable release kinetics, we sought to use a covalent conjugation strategy to improve vancomycin's incorporation into the LbL film by tethering it to a linear polyelectrolyte. Vancomycin is a relatively small (~1450 Da) glycopeptide antibiotic with a low charge density, which can be directly incorporated into LbL films at pH 5(9), but the labile intermolecular interactions were easily perturbed by slight changes in aqueous conditions or the presence of other compounds(16)—conditions needed to incorporate other drugs into the film. Therefore, improving the film stability of the vancomycin multilayers was of primary importance for the construction of multifunctional films containing multiple types of drugs. By pendant attachment to a polyacid, significant negative charge could be imparted to vancomycin, anchoring it into the film through multivalent electrostatic crosslinking. This approach has proved fruitful for other LbL films for the incorporation of peptides(25, 26), click reagents(19) (*see Chapter 3*) and small molecules(27) (*see Chapter 5*). In addition to an improved drug loading with greater film stability (potentiating future downstream processing), we aimed to introduce a controlled release mechanism. To this end, we used poly(*β*-L-malic acid) (PMLA) as both the polyanion to which vancomycin could be conjugated, but also as a hydrolytically degradable component (whose backbone ester cleavage could mediate controlled drug release (Figure 4-1). This naturally-derived polyacid has been shown to be non-toxic and non-immunogenic(28) with its drug conjugates showing potent therapeutic activity(22, 23, 28). We have previously found that use of PMLA in LbL films is capable of generating sustained release profiles of durations from minutes to weeks(29) (*see Chapter 2*) as well as more complex, sequential release behavior(19) (*see Chapter 3*).
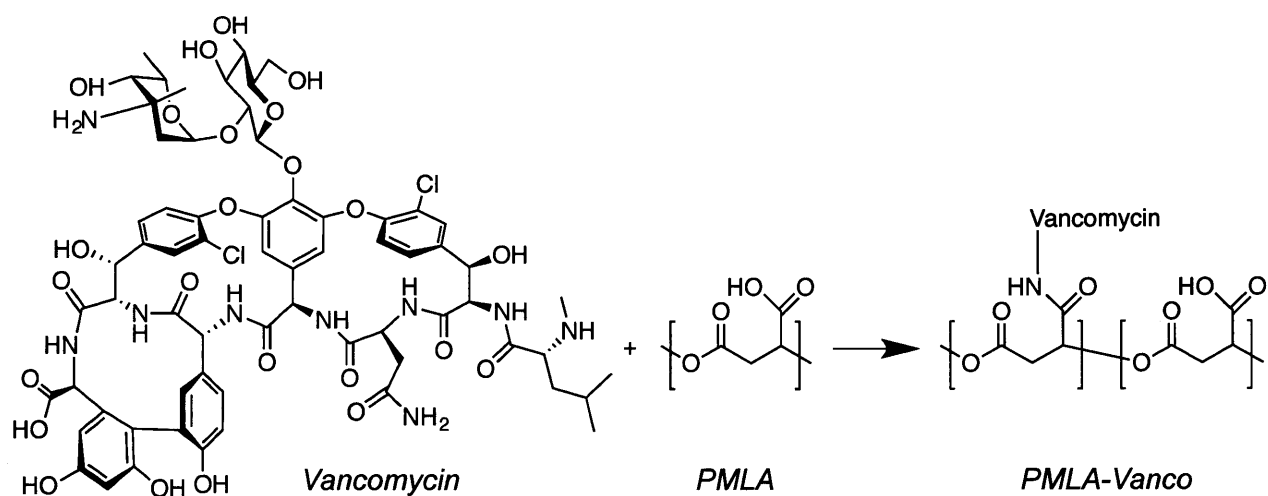
Figure 4-1. Covalent functionalization of PMLA with vancomycin through DCC mediated amide coupling.

Vancomycin acts to bind to the free termini of bacterial peptidoglycans through five hydrogen-bonds, thereby preventing crosslinking and weakening the cell wall's integrity(30). Studies have shown that chemical modification of vancomycin can enhance or inhibit its potency depending on the location(31), and covalently linked dimer or trimer variants can have multivalently enhanced potency against drug resistant strains(32). We chose reaction conditions that preferentially conjugated vancomycin's vancosamine moiety (the primary amine) to PMLA through a DCC-mediated amide coupling(24) (Figure 4-1), allowing the modification to be sterically distant from the cell wall binding region and maximizing the resultant potency. We used a microdilution assay to titrate for the minimum inhibitory concentration (MIC) of PMLA-Vanco compounds with different degrees of functionalization against the gram-positive pathogen, *Staphylococcus aureus*, and found that increasing vancomycin loading was not substantially deleterious to antibacterial potency (Table 4-1). For antibacterial activity against *S. aureus*, vancomycin MICs of ≤2, 4—8, and ≥16 μg/mL indicate the bacterium is considered

susceptible, intermediately-resistant, or resistant, respectively(33). Based on these definitions, the functionalized form of vancomycin remains active up to high levels of functionalization. Previous examination of functional modifications to vancomycin at this disaccharide region has shown that the introduction of a negatively charged moiety is not specifically enhancing or deleterious to antibacterial potency on its own(34), which corroborates our observation that malic acid residues do not significantly affect its activity. It is noted that as the functionalization degree increased to weight fractions greater than 10%, there was some increase in MIC observed.

Table 4-1. Antibacterial activity of PMLA-Vanco with different degrees of functionalization against *S. aureus*.

Compound	Degree of Functionalization		Minimum Inhibitory Concentration (MIC)*
	Molar (%)	Weight (%)	
Free Vancomycin	100	100	1.3 μg/mL
PMLA-Vanco$^{8.4}$	0.7	8.4	1.2 ± 0.1 μg/mL
PMLA-Vanco^{10}	0.84	10.2	1.6 ± 0.3 μg/mL
PMLA-Vanco^{43}	5.4	43.3	1.7 ± 0.1 μg/mL
PMLA-Vanco^{74}	17.6	74.0	2.3 ± 0.2 μg/mL

Since attachment to the PMLA backbone did not deteriorate vancomycin's antibacterial potency, we examined its capability for both film assembly and controlled release. Previous tetralayer LbL films of (Poly 2/dextran sulfate/vancomycin/dextran sulfate)$_n$ were assembled at pH 5 to leverage vancomycin's net +1 charge for electrostatic incorporation, which was otherwise unattainable at the physiological pH of 7.4 (pI ~7.2(35)). When assembling a composite film (i.e., the stacking of two or more independently stable films), we found that the vancomycin release kinetics were highly dependent on the way the films were assembled, including the components, pH, order of stacking, and method of assembly (i.e., spray- or dip-

LbL)(16). Furthermore, the deposition of a (thrombin/tannic acid)$_n$ film at pH 7.4 directly on top of this tetralayer vancomycin film caused the film to strip away due to the incompatible assembly conditions. With thrombin's activity being highly dependent on pH(36), it is important to find assembly conditions that both maintain its activity and do not destabilize vancomycin loading or release kinetics. To this end, we leveraged the increased charge density of the PMLA-Vanco conjugate to assemble a film at pH 7.4, which was otherwise unfeasible with the (Poly 2/dextran sulfate/vancomycin/dextran sulfate)$_n$ film architecture.
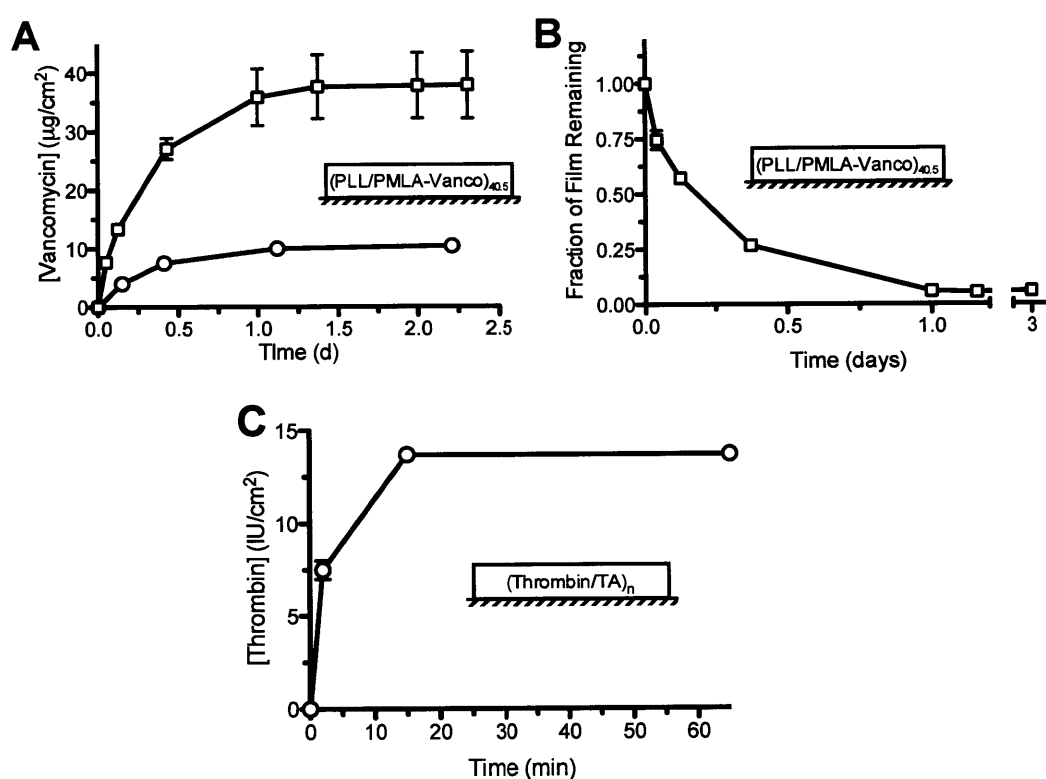
Figure 4-2. Characteristics of films containing vancomycin and thrombin. Release profiles of (PLL/PMLA-Vanco)$_{40.5}$ films with 8.4 (*circles*) and 74 wt% (*squares*) vancomycin functionalization eluted into PBS, pH 7.4 at 37°C (A), the thickness of the latter film during this elution (B) and the release profile of (thrombin/tannic acid)$_{25}$ films eluted into TCNB, pH 7.4 at 37°C (C).

To verify that we could indeed construct a desirable vancomycin-loaded film using our PMLA-Vanco conjugate, we studied the release kinetics for (PLL/PMLA-Vanco)$_{40.5}$ films

assembled from 10 mM phosphate, pH 7.4. For PMLA-Vanco having 8.4 and 74 wt% conjugation, we found both had similar release durations of roughly one day (Figure 4-2A) with film loadings of 10.4 ± 0.3 µg/cm^2 and 37.9 ± 5.7 µg/cm^2 of vancomycin, respectively. As would be expected with the higher degree of conjugation, a greater amount of drug could be incorporated into the film for the same number of layers. Interestingly, the duration of release was similar for both conjugates and is comparable to that of PLL released from (PLL/PMLA) films(29) (see Chapter 2), which suggests that vancomycin does not significantly participate in the stabilization or destabilization of these films during drug release. Of the amines present in vancomycin, only two are of sufficiently basic to be ionized under physiological conditions: an amino sugar primary amine (pK_a ~8.6(37)) and an N-terminal, secondary amine (pK_a ~ 6.8(37)). The former is linked to the PMLA backbone through an amide conjugation, while the latter is weakly charged at the assembly condition pH of 7.4. The other ionizable group, a C-terminal carboxylate (pK_a ~2.5(37)) confers a negative charge. Because of vancomycin's poor net charge and the densely polyanionic backbone, it is presumed that the PMLA-Vanco conjugate acts essentially as a polyanion during LbL assembly. The inability of vancomycin to directly form cohesive intermolecular crosslinks likely allows it to play a non-structural role in the ionically crosslinked film. Thus, vancomycin is released after hydrolysis of sufficient fragments of the PMLA backbone, liberating it from complexation in the film and allowing it to elute. Our previous studies with other PMLA-based multilayer films revealed that the hydrolysis of this polymer could facilitate controlled film degradation and hence controlled elution of drugs embedded in the film(29) (see Chapter 2). To elucidate this effect in (PLL/PMLA-Vanco)$_{40.5}$ films, we tracked the fraction of film remaining during vancomycin elution (Figure 4-2B) and found drug release was concomitant with film degradation. This further indicates that hydrolysis

.

of the PMLA backbone not only causes film erosion but also liberates the vancomycin conjugated along the backbone. The independence of the kinetics on the molecule released is promising because it shows that the release kinetics may be tuned independently of the pendant drug.
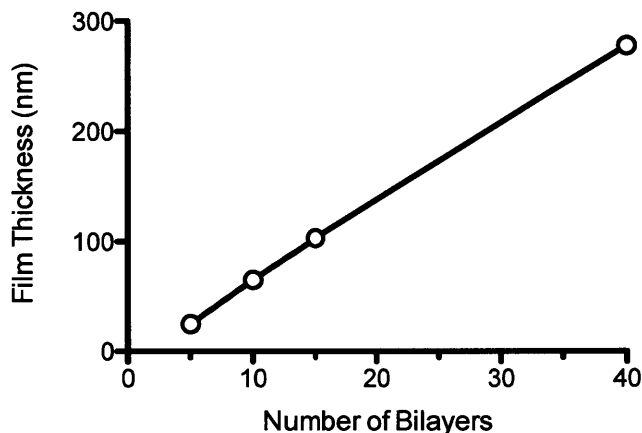
Figure 4-3. Growth curve of (thrombin/tannic acid)$_n$ film
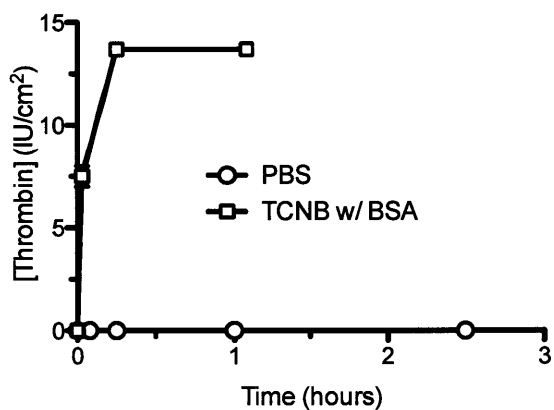
Figure 4-4. Release profiles for (thrombin/tannic acid)$_{25}$ films eluted into PBS (*circles*) and TCNB with BSA (*squares*)

In a slight modification to the films we previously reported, we assembled thrombin-containing films from 10 mM phosphate, pH 7.4 (rather than PBS) to match the conditions we used for the PMLA-Vanco films and found a linear growth profile (Figure 4-3). Our previous

studies of (thrombin/tannic acid)$_n$ films assembled from and eluted into PBS, pH 7.4 showed a slow film degradation through a diffusional release mechanism, and not the desired bolus thrombin release. Although PBS is good for simulating physiological pH and ionic strength it does not contain serum proteins. Incubation in tris-CaCl$_2$-NaCl-Brij35 buffer (TCNB) containing bovine serum albumin (BSA) was able to better recapitulate *in vivo* conditions with the presence of serum protein, and showed a rapid elution of active thrombin that corroborated well with *in vivo* efficacy(12). We similarly found that our (thrombin/tannic acid)$_{25}$ films did not elute into PBS (Figure 4-4), but released rapidly into TCNB (Figure 4-2B), which is likely due to the competitive interactions from proteins and possibly the other components in solution that disrupt the hydrogen-bonds in the film. Because the (PLL/PMLA-Vanco)$_{40.5}$ films are assembled through more robust electrostatic interactions and drug release is facilitated through hydrolytic degradation, the vancomycin release kinetics were unaltered whether the film was eluted in PBS or TCNB (Figure 4-5).
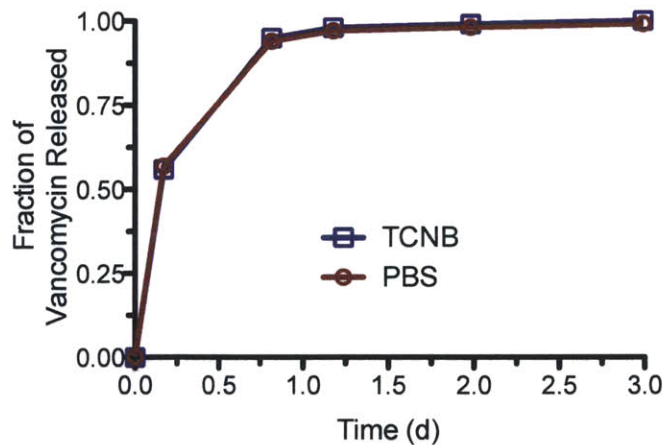
Figure 4-5. Release profiles of (PLL/PMLA-Vanco)$_{40.5}$ films released into PBS buffer (*circles*) and into TCNB with BSA (*squares*) at pH 7.4 and 37°C

While these independent vancomycin and thrombin containing films demonstrated desirable release profiles, combining them into a composite film may introduce competitive interactions that significantly alter elution kinetics. During LbL film assembly, polyelectrolytes can interdiffuse to create blending throughout the film's thickness(38) and the introduction of a new component can displace existing portions of the film(39). We have similarly seen this effect modulate the release profiles in a composite film comprised of independently validated vancomycin and diclofenac films(16). By covalently conjugating vancomycin to PMLA, the high charge valency and molecular size of the polyanionic backbone should enhance the stability of the film and eliminate displacement and exchange when an additional film is deposited, especially one based on weaker, hydrogen-bonding interactions as is the case for the (thrombin/tannic acid)$_n$ films. We studied the film growth for the composite film (Figure 4-6A) where we first deposited (PLL/PMLA-Vanco)$_n$ films (comprising the 74 wt% PMLA-Vanco conjugate) and then a (thrombin/tannic acid)$_n$ film on top. The exponential growth observed for the first portion of the film corresponds to what was observed for (PLL/PMLA)$_n$ films(29) (*see Chapter 2*) and is characteristic of some polyelectrolytes, including PLL, which is known to be capable of interdiffusing at higher pH values(38). The (thrombin/tannic acid)$_n$ portion of the films showed growth that was commensurate with layers deposited, showing that film assembly could continue on top of another film. The greater degree of uncertainty associated with the growth of the (thrombin/tannic acid)$_n$ film is due to the underlying (PLL/PMLA-Vanco)$_{40.5}$ film, as can be seen in Figure 4-6A.
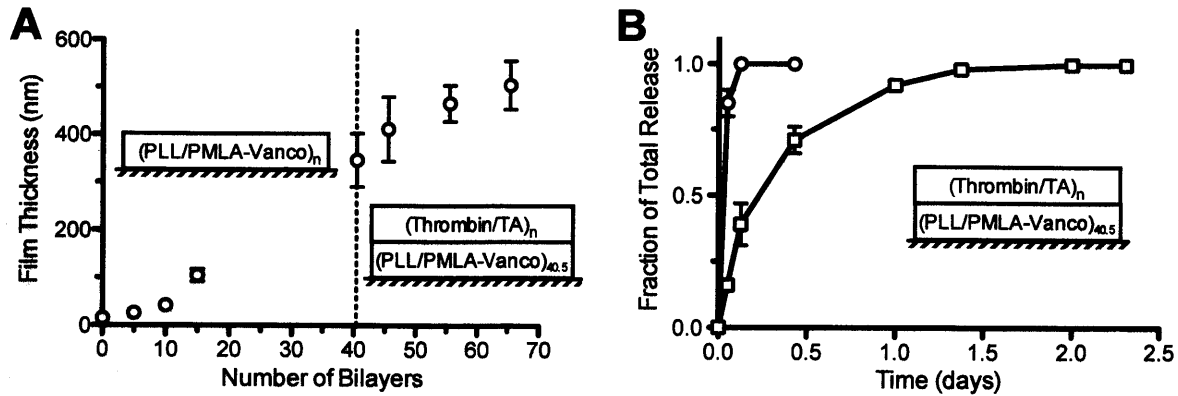
Figure 4-6. Growth curves of a composite films of (PLL/PMLA-Vanco)$_n$ and (thrombin/tannic acid)$_n$ (A) and the release profiles (B) for thrombin (*circles*) and vancomycin (*squares*) eluted into TCNB, pH 7.4 at 37°C.

Examination of the surface morphology of these films by scanning electron microscopy (SEM) showed significant differences in topology. At 5,000X (Figure 4-7A) and 10,000X (Figure 4-7B) magnification, the (PLL/PMLA-Vanco)$_{40.5}$ films are relatively smooth, which is common for polyelectrolyte based films, especially those assembled in pH regimes where both polyelectrolytes are substantially ionized(40). After deposition of the hydrogen bond based LbL (thrombin/tannic acid)$_{25}$ films, the SEM micrographs show significant texturing and the appearance of aggregates on the surface at 5,000X (Figure 4-7C) and 10,000X (Figure 4-7D) magnifications. Such features have been previously observed for protein-containing bilayer LbL films(41), as well as (thrombin/tannic acid)$_n$ films(12) and demonstrates that there is a distinctly different morphology associated with this film as compared to the film based on polyelectrolyte interactions

For the biomedical application of the film to rapidly stop bleeding and fight infection, it is imperative to have a large bolus release of thrombin and a sustained release of vancomycin. Therefore, we examined the release kinetics of thrombin and vancomycin from a composite film architecture of (PLL/PMLA-Vanco)$_{40.5}$ + (thrombin/tannic acid)$_{25}$. Upon incubation in TCNB at

37°C, we found thrombin released within minutes, and coincided with a sustained release of vancomycin for more than a day (Figure 4-6B). The release profiles of these drugs appear strikingly similar to those from their individual films, indicating that a linear combination of these two films does not significantly alter their release kinetics. This is further evidenced by the 35.1 ± 6.7 $\mu g/cm^2$ of vancomycin loaded in the composite film, which is comparable to its loading in the individual film (37.9 ± 5.7 $\mu g/cm^2$). Furthermore, thrombin release from these films is not impeded by deposition onto the (PLL/PMLA-Vanco)$_{40.5}$ film as compared to deposition onto silicon. The lack of interference between these two films is likely a consequence of their types of intermolecular interactions and order of deposition. As reported earlier, the introduction of a polyelectrolyte to a hydrogen-bonded film can cause rearrangement and materials displacement to accommodate the stronger electrostatic crosslinks(39). Herein, we deposit a hydrogen-bonded film on top of an electrostatically bonded film and find the release kinetics for both drugs to remain intact. The components in the (thrombin/tannic acid)n film are too weakly charged to affect the (PLL/PMLA-Vanco)$_{40.5}$ film and likewise, the latter film is electrostatically compensated and has no driving force to affect the (thrombin/tannic acid)$_{25}$ film beyond providing a substrate for deposition.
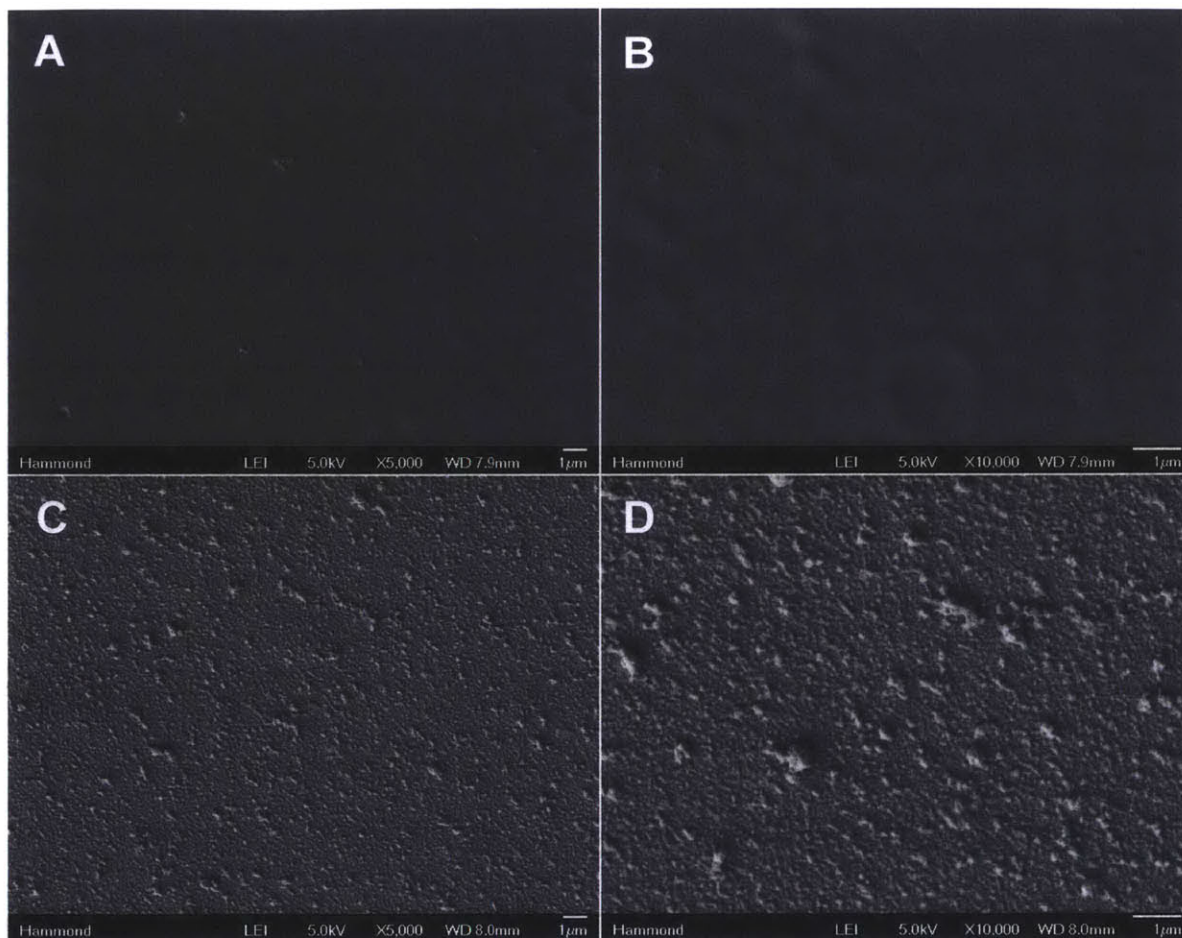
Figure 4-7. Scanning electron micrographs of (PLL/PMLA-Vanco)$_{40.5}$ films (A,B) and (PLL/PMLA-Vanco)$_{40.5}$ + (thrombin/tannic acid)$_{25}$ films (C,D) at magnifications of 5,000X (A,C) and 10,000X (B,D).

To ensure that the compounds remained active upon elution from the film as a result of release, we quantified thrombin release by activity and found that 5.7 ± 2.1 IU/cm^2 eluted from the composite films; this loading is significant, as one IU is capable of clotting one milliliter of plasma in fifteen seconds(42). For the vancomycin released from the composite films, we examined its antibacterial activity against *S. aureus* and found that its potency remained unchanged, demonstrating that the film assembly process, including the deposition of the (thrombin/tannic acid) film and subsequent drug elution did not affect its potency.

4.4   Conclusions

Herein we have developed a biodegradable, composite thin film composed of a linear combination of two independent films that is capable of multi-therapeutic release for traumatic wounds. We used a polymer-drug strategy to covalently link vancomycin to a hydrolytically degradable polyanion, PMLA. Release was sustained from $(PLL/PMLA\text{-}Vanco)_{40.5}$ films for more than a day. Upon deposition of rapidly eluting $(thrombin/tannic\ acid)_{25}$ films on top, the vancomycin release kinetics and loading were unaffected. Thrombin release is similarly unperturbed whether the film is deposited on top of silicon or on top of this vancomycin-loaded film. The composite film demonstrates the desirable release kinetics for addressing the immediate hemostasis and prolonged antibacterial activity necessary for improving survivability and reducing morbidity from traumatic wounding.

4.5 References

1. Kelly JF, *et al.* (2008) Injury severity and causes of death from operation Iraqi freedom and operation enduring freedom: 2003-2004 versus 2006. *Journal of Trauma-Injury Infection and Critical Care* 64(2):S21-S26.
2. Evans JA, *et al.* (2010) Epidemiology of Traumatic Deaths: Comprehensive Population-Based Assessment. *World J. Surg.* 34(1):158-163.
3. Murray CK (2008) Infectious disease complications of combat-related injuries. *Crit. Care Med.* 36(7):S358-S364.
4. Zapor MJ & Moran KA (2005) Infectious diseases during wartime. *Curr. Opin. Infect. Dis.* 18(5):395-399.
5. Eardley WGP, Brown KV, Bonner TJ, Green AD, & Clasper JC (2011) Infection in conflict wounded. *Philosophical Transactions of the Royal Society B-Biological Sciences* 366(1562):204-218.
6. Anonymous (2004) *Capturing the Full Power of Biomaterials for Military Medicine: Report of a Workshop* (The National Academies Press).
7. Hospenthal DR, *et al.* (2011) Guidelines for the Prevention of Infections Associated With Combat-Related Injuries: 2011 Update Endorsed by the Infectious Diseases Society of America and the Surgical Infection Society. *Journal of Trauma-Injury Infection and Critical Care* 71:S210-S234.
8. Siepmann J, Siegel RA, & Rathbone MJ eds (2012) *Fundamentals and Applications of Controlled Release Drug Delivery* (Springer).
9. Shukla A, Avadhany SN, Fang JC, & Hammond PT (2010) Tunable Vancomycin Releasing Surfaces for Biomedical Applications. *Small* 6(21):2392-2404.
10. Chuang HF, Smith RC, & Hammond PT (2008) Polyelectrolyte multilayers for tunable release of antibiotics. *Biomacromolecules* 9(6):1660-1668.
11. Moskowitz JS, *et al.* (2010) The effectiveness of the controlled release of gentamicin from polyelectrolyte multilayers in the treatment of Staphylococcus aureus infection in a rabbit bone model. *Biomaterials* 31(23):6019-6030.
12. Shukla A, Fang JC, Puranam S, Jensen FR, & Hammond PT (2012) Hemostatic Multilayer Coatings. *Adv. Mater.* 24(4):492-496.
13. Decher G & Schlenoff JB eds (2012) *Multilayer Thin Films* (Wiley-VCH), 2nd Ed.
14. Lvov Y, Ariga K, Ichinose I, & Kunitake T (1995) ASSEMBLY OF MULTICOMPONENT PROTEIN FILMS BY MEANS OF ELECTROSTATIC LAYER-BY-LAYER ADSORPTION. *J. Am. Chem. Soc.* 117(22):6117-6123.
15. Shah NJ, *et al.* (2011) Tunable dual growth factor delivery from polyelectrolyte multilayer films. *Biomaterials* 32(26):6183-6193.
16. Shukla A, Fuller RC, & Hammond PT (2011) Design of multi-drug release coatings targeting infection and inflammation. *J. Controlled Release* 155(2):159-166.
17. Wood KC, Chuang HF, Batten RD, Lynn DM, & Hammond PT (2006) Controlling interlayer diffusion to achieve sustained, multiagent delivery from layer-by-layer thin films. *Proc. Natl. Acad. Sci. U. S. A.* 103(27):10207-10212.
18. Hong J, *et al.* (2012) Graphene Multilayers as Gates for Multi-Week Sequential Release of Proteins from Surfaces. *Acs Nano* 6(1):81-88.

19. Hsu BB, *et al.* (2014) Ordered and kinetically discrete sequential protein release from biodegradable thin films. *Angew. Chem. Int. Ed.* In Press.

20. Min J, Braatz RD, & Hammond PT (2014) Tunable staged release of therapeutics from layer-by-layer coatings with clay interlayer barrier. *Biomaterials* 35(8):2507-2517.

21. Lee B-S, Vert M, & Holler E (2002) Water-soluble Aliphatic Polyesters: Poly(malic acid)s. *Biopolymers: Polyesters I*, eds Doi Y & Steinbuchel A), Vol 3a, pp 75-103.

22. Ding H, *et al.* (2010) Inhibition of brain tumor growth by intravenous poly(β-l-malic acid) nanobioconjugate with pH-dependent drug release. *Proceedings of the National Academy of Sciences* 107(42):18143-18148.

23. Lee B-S, *et al.* (2006) Polycefin, a New Prototype of a Multifunctional Nanoconjugate Based on Poly(β-l-malic acid) for Drug Delivery. *Bioconj. Chem.* 17(2):317-326.

24. Greenwald RB, Zhao H, Xia J, & Martinez A (2003) Poly(ethylene glycol) transport forms of vancomycin: A long-lived continuous release delivery system. *J. Med. Chem.* 46(23):5021-5030.

25. Chluba J, *et al.* (2001) Peptide Hormone Covalently Bound to Polyelectrolytes and Embedded into Multilayer Architectures Conserving Full Biological Activity. *Biomacromolecules* 2(3):800-805.

26. Schultz P, *et al.* (2005) Polyelectrolyte multilayers functionalized by a synthetic analogue of an anti-inflammatory peptide, α-MSH, for coating a tracheal prosthesis. *Biomaterials* 26(15):2621-2630.

27. Hsu BB, Park M, Hagerman SR, & Hammond PT (2014) Multi-month controlled small molecule release from biodegradable thin films. *Proc. Natl. Acad. Sci. U. S. A.* In Review.

28. Ljubimova JY, *et al.* (2013) Toxicity and efficacy evaluation of multiple targeted polymalic acid conjugates for triple-negative breast cancer treatment. *J. Drug Targeting* 21(10):956-967.

29. Hsu BB, *et al.* (2014) Multilayer films assembled from biocompatible, naturally-derived materials for controlled protein release. *Biomacromolecules* in press.

30. Walsh CT, Fisher SL, Park IS, Prahalad M, & Wu Z (1996) Bacterial resistance to vancomycin: Five genes and one missing hydrogen bond tell the story. *Chem. Biol.* 3(1):21-28.

31. Griffin JH, *et al.* (2003) Multivalent drug design. Synthesis and in vitro analysis of an array of vancomycin dimers. *J. Am. Chem. Soc.* 125(21):6517-6531.

32. Li L & Xu B (2005) Multivalent vancomycins and related antibiotics against infectious diseases. *Curr. Pharm. Des.* 11(24):3111-3124.

33. Tenover FC & Moellering RC (2007) The Rationale for Revising the Clinical and Laboratory Standards Institute Vancomycin Minimal Inhibitory Concentration Interpretive Criteria for Staphylococcus aureus. *Clin. Infect. Dis.* 44(9):1208-1215.

34. Fu X, Albermann C, Zhang C, & Thorson JS (2005) Diversifying Vancomycin via Chemoenzymatic Strategies. *Org. Lett.* 7(8):1513-1515.

35. Gasper MP, Berthod A, Nair UB, & Armstrong DW (1996) Comparison and modeling study of vancomycin, ristocetin A, and teicoplanin for CE enantioseparations. *Anal. Chem.* 68(15):2501-2514.

36. Fenton JW, *et al.* (1977) HUMAN THROMBINS - PRODUCTION, EVALUATION, AND PROPERTIES OF ALPHA-THROMBIN. *J. Biol. Chem.* 252(11):3587-3598.

37. Sitrin RD, *et al.* (1985) ARIDICINS, NOVEL GLYCOPEPTIDE ANTIBIOTICS .2. ISOLATION AND CHARACTERIZATION. *J. Antibiot.* 38(5):561-571.

38. Picart C, *et al.* (2002) Molecular basis for the explanation of the exponential growth of polyelectrolyte multilayers. *Proc. Natl. Acad. Sci. U. S. A.* 99(20):12531-12535.

39. Gilbert JB, Rubner MF, & Cohen RE (2013) Depth-profiling X-ray photoelectron spectroscopy (XPS) analysis of interlayer diffusion in polyelectrolyte multilayers. *Proc. Natl. Acad. Sci. U. S. A.* 110(17):6651-6656.

40. Shiratori SS & Rubner MF (2000) pH-dependent thickness behavior of sequentially adsorbed layers of weak polyelectrolytes. *Macromolecules* 33(11):4213-4219.

41. Caruso F, Furlong DN, Ariga K, Ichinose I, & Kunitake T (1998) Characterization of polyelectrolyte-protein multilayer films by atomic force microscopy, scanning electron microscopy, and Fourier transform infrared reflection-absorption spectroscopy. *Langmuir* 14(16):4559-4565.

42. Edgell TA & Gaffney PJ (1995) SOLUBLE FIBRIN - CHARACTERIZATION AND ASSAY PROCEDURES. *Thromb. Haemost.* 73(6):1435-1435.

Chapter 5
Multi-Month Controlled Small Molecule Release from Biodegradable Thin Films

This chapter has been accepted for publication in the *Proceedings of the National Academy of Sciences*

Authors:
Bryan B. Hsu[1,3,4], Myoung-Hwan Park[5], Samantha R. Hagerman[2], and Paula T. Hammond[2,3,4]

Departments of [1]Chemistry and [2]Chemical Engineering, Massachusetts Institute of Technology, Cambridge, MA 02139
[3]Koch Institute for Integrative Cancer Research, Massachusetts Institute of Technology, Cambridge, MA 02139
[4]Institute for Soldier Nanotechnologies, Cambridge, MA 02139
[5]Department of Chemistry, Sahmyook University, Seoul, 139-742, South Korea

5.1   Introduction

There is a compelling need for long-term, controlled release for sustained treatment of chronic or recalcitrant medical conditions and diseases, especially when using small molecules with abundant targets throughout the body. For example, antibacterial therapy typically requires sustained local concentrations from days to weeks, whereas some cases like tuberculosis need daily dosages of antibiotic for at least 6 months(1). Other diseases have also shown benefit from a long-term multi-month drug regime such as cystic fibrosis(2), ankylosing spondylitis(3), and chronic uveitis(4). Chronic pain may best illustrate the positive multifaceted impact of long-term drug treatment. Described as "pain that extends beyond the expected period of healing", it is a widespread and debilitating ailment underpinning unwanted dependencies on narcotic medications. Often misdiagnosed and under treated, roughly 20% of adults (and 25% of those >45 years old) in the US reported having pain most to every day(5). Sometimes considered a silent epidemic, advanced pain treatments are of critical need(6).

Non-steroidal anti-inflammatory drugs (NSAIDs) are one of a number of approaches in pain relief and have a preferable balance between analgesic effectiveness and incidences of adverse reactions(7). Although the potentially adverse effects from NSAID use is minimal compared to alternatives, its prolonged and frequent use can lead to adverse drug reactions, especially for adults aged 65 or older(8). With NSAIDs being the most frequently prescribed medications for osteoarthritis(9), treating this persistent pain while avoiding the associated adverse drug reactions could have tremendously positive effects for millions of people.

Localized drug delivery is an attractive route for substantially reducing systemic dosages, while maintaining localized saturation(10). Locally delivered diclofenac has shown similar analgesia to systemic delivery with significantly reduced adverse reactions(11) which led the

way for FDA approval of topical formulations: Voltaren® Gel (Novartis) and Pennsaid® (Mallinckrodt). Although topical diclofenac has demonstrated the promise of localized delivery, it also requires frequent administration (4 times daily) with bioelimination occurring within hours(12). Less frequent dosing has shown a positive influence on outcome(13) and this, in addition to several other applications in orthopedics and wound healing, would tremendously benefit.

Long-term small molecule release is typically difficult, and formulations based on biodegradable materials like poly(lactic-*co*-glycolic acid) (PLGA) can extend release from days to several weeks with some notable exceptions reaching multiple months(10). Water permeation, lowered pH due to acid build-up in the case of polymers like PLGA, structural instability (e.g., crack formation), erosion, and drug diffusivity among other factors constitute a complex picture with a ceiling on release duration(14). Because of their small size and hydrophobicity, controlling the release of small molecules is especially difficult as they rapidly diffuse(15). Achieving sustained release from other polymeric vehicles ranging from gels to bulk degradable plastics is also well known(16, 17); these materials have been able to sustain drug release for, at best, one to a few months when mitigating the aforementioned obstacles. Additionally, these inherent limitations make extensive release periods difficult because of the need for excessive quantities of material, the changes in material properties with time, and ultimate constraints on drug loading density due to the thermodynamic constraints of traditional polymer molecular blends. Achieving a sustained multiple-month long term release usually requires non-degradable physical release devices like Illuvien™ (Alimera Sciences), a cylindrical intraocular insert with a semi-permeable membrane that can sustain release for more than a year(18). In pain management, some non-degradable implants capable of sustained release for a few months have

been investigated(19), but a biodegradable, long-term sustained drug delivery formulation is still highly desired.

The Layer-by-Layer (LbL) assembly technique has uniquely demonstrated construction of thin films under benign aqueous conditions for controlled release of numerous therapeutics including proteins, growth factors, peptides, and small molecules(20). This technique relies on numerous intermolecular interactions (e.g., electrostatic) for assembly and stability; thus the use of high molecular weight polyelectrolytes can result in films that are extremely robust and capable of coating a variety of materials and substrate geometries. A common challenge in any small molecule drug delivery system is the incorporation and subsequent controlled release of poorly charged or low molecular weight species. For example, our laboratory has investigated a number of LbL-based biodegradable strategies for controlled small molecule release including direct incorporation of drug into the film(21, 22) or physical entrapment in other charged systems (23, 24) with the longest sustained release previously achieved of three weeks. Changes in aqueous environment, such as pH or ionic strength, can also facilitate undesirable film deterioration or drug elution that dramatically affects release kinetics(25).

Herein we report the development of a polymer-drug conjugate and its assembly into an LbL thin film for long-term sustained drug delivery. Diclofenac is used as a model small molecule and its release is measured for more than 14 months from biodegradable conformal coatings. Films as thin as ~500 nm show the capability for substantial diclofenac loading and once released, the drug maintains its anti-inflammatory activity and potency despite prolonged hydration at elevated temperatures. The possibility of such long-term controlled release of active small molecule drugs from a biodegradable, nanoscale thin film has implications for drug delivery in a broad spectrum of fields.

5.2   Materials and Methods

All materials were used without further purification unless otherwise noted. Diclofenac (acid form) was purchased from TCI America. Poly(L-lysine) (PLL, M_W = 30-70 kDa) and poly(L-glutamic acid) (PGA, M_w = 50-100 kDa) were obtained from Sigma Aldrich with the latter converted to acid form by precipitation in 100 mM HCl and washing with 10 mM HCl prior to lyophilization. Chitosan (15 kDa) was purchased from Polysciences. All other chemicals unless otherwise noted were obtained from Sigma Aldrich. All indications of H_2O use refers to 18.2 MΩ MilliQ purified water.

Synthesis

TriEG-Diclof. Synthesis and purification of the diclofenac-triethylene glycol compound proceeded as described earlier(26) with minor modifications. To 2.37 g of diclofenac in 100 mL of anhydrous chloroform, 1.43 g of 1,1'-carbonyldiimidazole was added portion-wise with vigorous stirring. The reaction continued at room temperature under Ar for 4 h, was then placed on ice while rapidly adding 4.4 mL of triethylene glycol. After stirring overnight at room temperature, the solution was washed four times with H_2O and dried over $MgSO_4$ prior to solvent removal *in vacuo,* resulting in a yellow oil. This product was purified by flash silica gel column chromatography with a 50% cyclohexane, 49.5% ethyl acetate, and 0.5% acetic acid eluent solution. Thin layer chromatography differentiated the desired TriEG-Diclof product ($R_f \sim$ 0.12) from diclofenac ($R_f \sim$ 0.46). Solvent was removed *in vacuo* from the purified product, redissolved in chloroform, washed twice with 0.1 M sodium bicarbonate, twice with H_2O, dried over $MgSO_4$ and then extracted *in vacuo,* yielding 570 mg of viscous oil. ^{1}H-NMR (500 MHz,

CDCl$_3$, 22°C): δ= 7.4 – 6.5 ppm (7H, -C*H*-), 4.3 ppm (2H, -CH$_2$COOC*H$_2$*-), and 3.9 – 3.5 ppm (12H, -C*H$_2$*COOCH$_2$(C*H$_2$*OC*H$_2$*)$_2$CH$_2$OH).

PGA-TriEG-Diclof. In an adapted procedure(27), to 75 mg of PGA (acid form) in 1 mL of anhydrous DMF, 60 mg of DCC in 1 mL DMF was added. Then mixture of 142 mg TriEG-Diclof and catalytic quantities of DMAP in 1 mL of DMF was and stirred overnight at room temperature. The product was diluted to 30 mL with 10 mM sodium bicarbonate, generating precipitates that were removed by centrifugation. The supernatant was filtered with a 0.45 μm syringe filter and then concentrated and washed with H$_2$O in a centrifugal spin concentrator (Corning Spin-X UF, 10k MWCO) prior to lyophilization, yielding 224 mg of a white solid. ^{1}H-NMR (500 MHz, D$_2$O, 22°C): δ= 7.4 – 6.0 ppm (7H, -C*H*- of Diclof), 3.9 – 4.5 ppm (1H, -C*H*- of PGA; 4H, -COOC*H$_2$*(CH$_2$OCH$_2$)$_2$C*H$_2$*COO- of TriEG), 3.8 – 3.0 ppm (8H, -COOCH$_2$(C*H$_2$*OC*H$_2$*)$_2$CH$_2$COO- of TriEG and -CC*H$_2$*COO- of Diclof), 2.6 – 1.6 ppm (4H, -CHC*H$_2$*C*H$_2$*CO- of PGA).

Film Assembly and Characterization

Multilayer films were deposited on silicon substrates (Silicon Quest International) pretreated with (LPEI/SPS)$_{10}$ baselayers. Films were assembled by incubation for 10 min in polycation solution, then 10 s, 20 s, and 30 s of H$_2$O rinse, then 10 min of polyanion solution, and then 10 s, 20 s, and 30 s of H$_2$O rinse. For (PLL/PGA-TriEG-Diclof)$_n$ films, both PLL and PGA-TriEG-Diclof were formulated at 1 mg/mL in 10 mM sodium phosphate, pH 7.4. For (chitosan/PGA-TriEG-Diclof)$_n$ films, 2 mg/mL of chitosan in 100 mM sodium acetate, pH 5.0,

and 1 mg/mL of PGA-TriEG-Diclof in 100 mM sodium acetate, pH 6.3, was used. The latter pH was chosen because of the limited solubility of PGA-TriEG-Diclof below pH 6.3.

Polymer-Drug Conjugate and Multilayer Film Studies

Solubility of PGA-TriEG-Diclof was determined in 100 mM sodium phosphate, pH 7.4 at room temperature. The degree of diclofenac conjugation was determined by the incubating 400 μg/mL of PGA-TriEG-Diclof in 500 μL of 0.1 M of sodium hydroxide overnight at 37°C, then quenching with 500 μL of 0.1 of hydrochloric acid prior to quantification by HPLC. Hydrolysis kinetics of the polymer-drug conjugate was measured by incubation of 500 μL of 3 mg/mL PGA-TriEG-Diclof in a small volume dialysis unit (2k MWCO, Slide-A-Lyzer MINI, Thermo Fischer Scientific) immersed in 1 mL of PBS, pH 7.4. At predetermined time points, 200 μL was extracted for HPLC analysis and replaced with fresh 200 μL of PBS. Kinetic rate constants were calculated using pseudo first order kinetics from initial rates measured at 19°C, 37°C, and 50°C. The activation energy was calculated from the Arrhenius equation. Film-based diclofenac release was studied by immersion in 1 mL of PBS, pH 7.4 at 37°C for predetermined times, after which films were transferred to fresh PBS solution. Films released into solution were analyzed by HPLC and for cyclooxygenase-1 (COX) inhibition. Total film loadings of diclofenac were measured by elution into 500 μL of 0.1 M sodium hydroxide at 37°C for 6 h prior to quantification with HPLC.

PGA-TriEG-Diclof at 1 mg/mL in 10 mM phosphate, pH 7.4 and 100 mM acetate, pH 6.3 was characterized by dynamic light scattering (NanoBrook ZetaPALS, Brookhaven Instruments Co.). Critical micelle concentrations (CMC) were performed in a manner previously described(28, 29) and was determined by the concentration at which the ratio of the first and

third vibrational peaks (λ_{ex} = 334 nm; λ_{em} = 373 and 384, respectively) of pyrene begin to decrease, an indication of pyrene's solubilization in the more hydrophobic environment of formed micelles or aggregates. These fluorescence measurements (Horiba Scientific Fluorolog-3 spectrofluorometer) were conducted after overnight incubation of serial dilutions of PGA-TriEG-Diclof in 10 mM phosphate, pH 7.4, and 100 mM acetate, pH 6.3, containing 600 nM of pyrene.

Film thickness was measured by profilometry (Veeco Dektak 150). Swelling studies, performed similarly to previously described(30), were conducted by spectroscopic ellipsometry (Woollam XLS-100) of films in the dry state and after 10 minutes of immersion in PBS, pH 7.4. The films studied, (chitosan/PGA-TriEG-Diclof)$_{10}$ and (PLL/PGA-TriEG-Diclof)$_5$, were of comparable dry thicknesses (115 ± 2 nm and 145 ± 25 nm, respectively).

Diclofenac was quantified, as described previously(24, 25), by HPLC (Agilent 1100 series) with a Supelco Discovery C18 column (Sigma Aldrich) with 100 μL injections into a 1 mL/min mobile phase of PBS:acetonitrile (70:30) using a fluorescence detector (λ_{ex} = 280 nm and λ_{em} = 355 nm). Because of the limited aqueous solubility of TriEG-Diclof, it was dissolved and diluted in acetonitrile prior to makeup into a 70:30 mixture of PBS:acetonitrile and HPLC analysis. COX-1 inhibition activity was quantified with a COX fluorescent inhibitor screening assay kit (Cayman Chemicals) according to the manufacturer directions. Controls were formulated in PBS, pH 7.4, using 75 ng/mL of diclofenac, and 512 μg/mL of PGA-TriEG-Diclof (equivalent to 100 ng/mL of diclofenac). Released diclofenac was from (PLL/PGA-TriEG-Diclof)$_{40}$ films at different timepoints with those at 0.5 months (accumulated over 3 d), 3.0 months (15 d) and 6 months (9.3 d) contained 91 ng/mL, 112 ng/mL, and 100 ng/mL of diclofenac, respectively. Diclofenac potency (IC$_{50}$) was determined by fitting a dose-response curve to inhibitory activity as a function of 2-fold serial dilutions. Samples of hydrolyzed PGA-

TriEG-Diclof used kinetic release samples done in PBS, pH 7.4 at 37°C, and released diclofenac from LbL films were the averaged values from 0.5, 3 and 6 month release solutions, as described above. Values of IC_{50} were determined as the concentration of diclofenac generating half of the maximum possible COX activity (i.e. no inhibitor).

5.3   Results and Discussion

Polymer-Drug Conjugate.

LbL assembly is based on alternating adsorption of charged (or otherwise complementary) species. We used the biologically derived polyacid, poly(L-glutamic acid) (PGA), as it is composed of a natural L-amino acid and can ultimately be broken down and resorbed by the body. In addition, the pendant carboxylates allows for a high level of drug conjugation while maintaining sufficient free acid groups for electrostatic complexation. Similar PGA-based LbL approaches have shown *in vitro*(31) and *in vivo*(32) bioactivity from functionalized films, as well as for cellular delivery of doxorubicin(33). To generate our polymer-drug conjugate we relied on a two-step strategy that first forms a diclofenac prodrug with hydroxyl functionality and is subsequently conjugated to the polymer backbone.
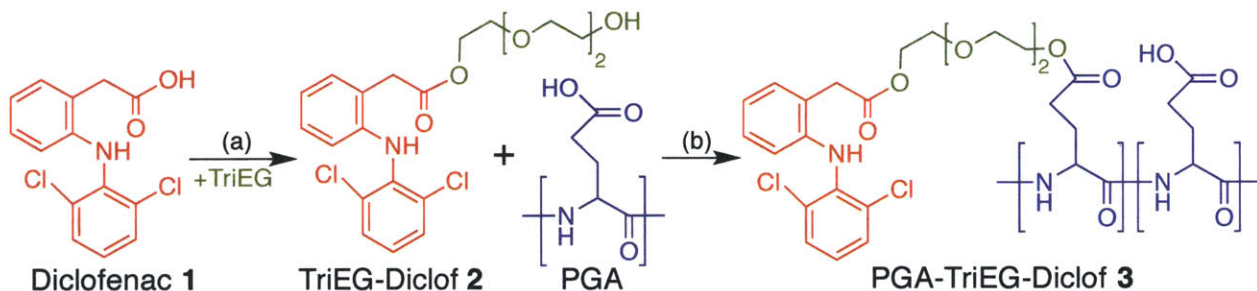
Figure 5-1. The synthetic scheme of the polymer-drug conjugate. (a) The carboxylic acid moiety of Diclofenac **1** is activated with 1,1'-Carbonyldiimidazole and subsequently esterified with triethylene glycol (TriEG) to form the TriEG-Diclof prodrug **2**. (b) After purification, **2** is then conjugated to poly(L-glutamic acid) *via* Steglich esterification with *N,N'*-dicyclohexylcarbodiimide and 4-dimethylaminopyridine to yield the PGA-TriEG-Diclof conjugate **3**.

As shown in Figure 5-1, the carboxylic acid of diclofenac **1** was activated with 1,1'-carbonyldiimidazole and then esterified with excess triethylene glycol. The resulting prodrug, a triethylene glycol-diclofenac conjugate (TriEG-Diclof) **2**, was purified and subsequently coupled to PGA via Steglich esterification using *N,N'*-dicyclohexylcarbodiimide and 4-

dimethylaminopyridine. This resultant polymer-drug conjugate, PGA-TriEG-Diclof **3**, had 9.8

mol% (19.5 wt%) of the PGA monomer repeat units functionalized with diclofenac. Diclofenac,

similar to other small molecules, has a limited aqueous solubility of 2.4 µg/mL(34). While **2** was

found to be water-insoluble(26), **3** was well solubilized at 50 mg/mL, equivalent to 9.8 mg/mL of

diclofenac. By virtue of attachment to a large polyacid, diclofenac's solubility in water increased

almost 4 orders of magnitude over its acid form and more than 5-fold over its sodium salt (1.9

mg/mL(34)) indicating that significant stability is imparted by conjugation to a hydrophilic

backbone, analogous to observations with other PGA-drug conjugates(27). Furthermore, the high

drug density of the polymer conjugate provides the opportunity to achieve substantial film

loading of the drug in LbL films.
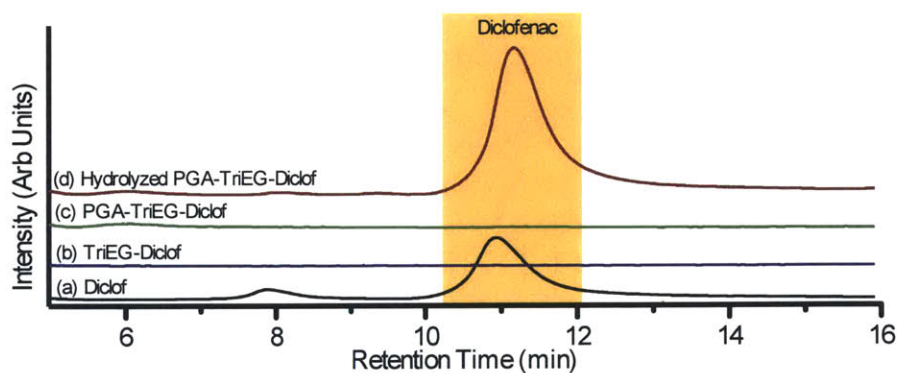
Figure 5-2. Chromatograms for the fluorescent intensity of stock diclofenac **1** (A), the TriEG-Diclof prodrug **2** (B), the polymer-drug conjugate **3** (C), and hydrolyzed polymer-drug conjugate (D) as analyzed by HPLC.

For characterization of diclofenac tethering to the PGA backbone, we analyzed our

various diclofenac-based compounds by HPLC. A typical chromatogram for diclofenac is shown

in Figure 5-2A with small peak at 8 min that appears to be a low level impurity. Neither TriEG-

Diclof (Figure 5-2B) nor PGA-TriEG-Diclof (Figure 5-2C) solutions give significant HPLC

114

signal, which indicates two things. First, chemical modification substantially changes diclofenac's characteristic affinity for the C18 HPLC column, and second, the product contains no detectable free diclofenac, thus reaffirming complete covalent modification. Quantitative ester hydrolysis of PGA-TriEG-Diclof with sodium hydroxide (100 mM, pH ~11) overnight at 37°C showed that diclofenac is regenerated (Figure 5-2D).

Table 5-1. Hydrolysis kinetics of PGA-TriEG-Diclof in PBS, pH 7.4

T (°C)	k_{obs} ($\times 10^{-8}$ s^{-1})	$t_{1/2}$ (d)
19	0.311 ± 0.005	2577
37	2.29 ± 0.03	350
50	4.14 ± 0.29	194

Before their incorporation into LbL films, we first investigated the rate of ester hydrolysis of the PGA-conjugates under physiological conditions, which is an important determinant of whether therapeutically relevant concentrations of diclofenac can be generated on a biologically important time scale. Using pseudo first order reaction kinetics, we calculated the initial rates of diclofenac release in PBS at pH 7.4 to determine their rate constants (k_{obs}) at 19°C, 37°C and 50°C (Table 5-1). As expected, hydrolysis accelerates with increasing temperature, as is characterized by the positive activation energy (E_a) of 67 ± 12 kJ/mol. In analogous polymer-drug systems, the half-life ($t_{1/2}$) at pH 7.4 and 37°C of small molecules conjugated to dextran can vary greatly with the drug type and polymer backbone. For example, 5-fluorouracil (0.73 d)(35), benzoate (7.5 d)(36), naproxen (7.6 d)(37), and ketoprofen/ibuprofen/naproxen (7.8 d/5.3 d/4.2 d)(38) have half lives up of a week or less, and other variations, such as starch-naproxen (33 d)(37), and hyaluronic acid-cortisone (3.6 d)(39) demonstrate a potentially broad range. We found that our polymer-drug compound has a substantially longer $t_{1/2}$ (Table 5-1) in comparison

to most reported conjugates, making it an ideal candidate for long-term sustained release formulations.

A multitude of factors could affect the rate of ester hydrolysis. For example, nearest neighbor groups are influential(40) with negative charges along the polymer backbone slowing(41) and positive charges accelerating bond cleavage(42). In addition, electron donating or withdrawing groups near the ester can modulate hydrolysis(43), as can steric bulk that limits accessibility(37). If a linker is present, as in our case, its hydrophobicity can also slow ester cleavage(44). The combination of high negative charge along the PGA backbone, which is increased as the ester hydrolyzes, and hydrophobicity of the pendant TriEG-Diclof are likely significant factors in contributing to the slow release kinetics that we observe.

In addition to the linker's hydrolytic susceptibility, the hydrophobicity of the pendant side-chains along a charged, hydrophilic backbone has also shown the propensity to form colloidal aggregates which exhibit a hydrophilic outer shell and hydrophobic core(45). Some amphiphilic polymers, such as those with randomly functionalized pendant hydrophobic moieties, can also generate hydrophobic intramolecular nanodomains within a single molecule(46). Our studies of PGA-TriEG-Diclof in aqueous solution at 1 mg/mL by dynamic light scattering showed hydrodynamic diameters of 124.9 ± 1.6 nm in 100 mM sodium acetate, pH 6.3 (conditions used for assembly with chitosan), and 28.8 ± 4.7 nm in 10 mM sodium phosphate, pH 7.4 (conditions used for assembly with PLL). In addition, we found their critical micelle concentrations (CMCs) to be 4.2 µg/mL and 9.9 µg/mL, respectively. These measurements reveal the presence of micellar aggregates due to the hydrophobicity of the pendant diclofenac and hydrophilicity of the PGA backbone. The differences in sizes depending on solution conditions is likely a consequence of the lower ionization and increased charge

shielding that occurs in 100 mM sodium acetate, pH 6.3 as compared to 10 mM sodium phosphate, pH 7.4; the reduced electrostatic repulsion in the former allows for higher aggregation numbers and hence larger particle sizes(47). Because of the self-assembly into micellar aggregates, pendant ester linkages are sequestered into the hydrophobic core, which is likely one major factor in the slow diclofenac release kinetics we observe.

Multilayer Films.

Solution phase kinetics indicate that controlled diclofenac release can be facilitated by ester hydrolysis from a polymer backbone; however, the polymer-drug conjugate is itself soluble in water, and cannot be used to create a stable thin film coating or similar construct for controlled localized release. Using an LbL assembly technique we were able to immobilize nanoscale layers of PGA-TriEG-Diclof from aqueous solution via polyelectrolyte complexation with a cationic polymer atop a substrate surface. Repeated deposition of (Polycation/PGA-TriEG-Diclof) layers allows for control over film thickness and drug payload. These bilayers were constructed with polycations of poly(L-lysine) (PLL) at pH 7.4 and chitosan at pH 5.0, with the PGA-TriEG-Diclof at pH 7.4 and 6.3, respectively. Their film growth revealed a concomitant thickness increase with number of bilayers, a characteristic feature of LbL-based films(48), and is shown in Figures 5-3A and 5-3B.
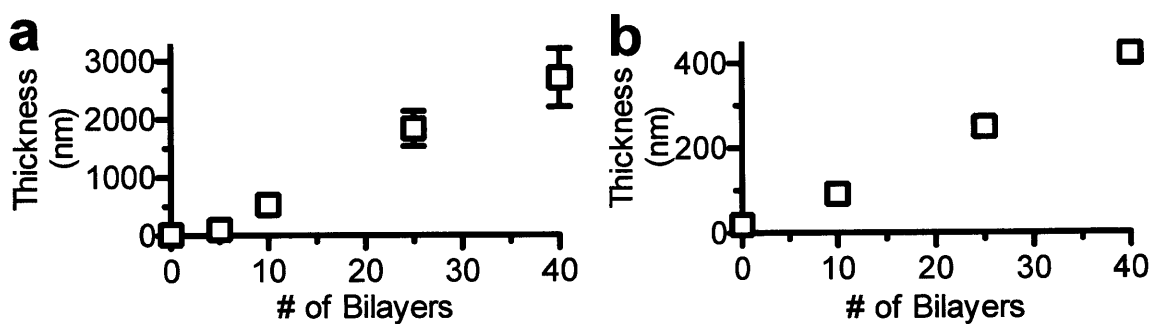
Figure 5-3. Growth curves of (PLL/PGA-TriEG-Diclof)$_n$ (A) and (Chitosan/PGA-TriEG-Diclof)$_n$ (B) films.

The bilayer thickness of an LbL film can vary from sub-nanometer to tens of nanometers depending on a number of different factors, including pH, ionic strength and degree of ionization of the adsorbing polymer chains. These effects, among others, can mechanistically influence the polyelectrolyte's ability to diffuse into, out of, and within hydrated multilayer films during film assembly(49). In addition, the size of the PGA-TriEG-Diclof micellar aggregate may restrict its diffusivity within the film. Other electrostatic-based LbL films with block copolymer micelles have shown linear growth behavior after the initial few layers, with bilayer thicknesses of ~100 nm, suggesting the deposition of multiple micelle layers, a large fraction of the other film component or a combination thereof. We observed a similar growth behavior in (PLL/PGA-TriEG-Diclof)$_n$ films where relatively little material is deposited for the first few layers, but the assembly transitions to considerably thicker deposition beyond 5 bilayers (Figure 5-3A). PLL (pk$_a$~9.9(50)) is significantly charged with a random coil conformation(51) at pH 7.4 during deposition and its intediffusivity can be a considerable factor as films of (PLL/PGA)$_n$ are well known to demonstrate exponential growth due to interdiffusion(52) with the diffusivity of PLL independent of the diffusivity of the polyanion(53). Linear regression of this latter phase in

118

growth (Figure 5-3A) shows 75.1 ± 5.1 nm (R^2 = 0.991) is deposited per bilayer, which suggests considerable deposition per bilayer. In contrast, we found (chitosan/PGA-TriEG-Diclof)$_n$ films were considerably thinner without an observed induction period, with 11.0 ± 0.3 nm (R^2 = 0.9994) deposited per bilayer. The growth behavior of a (chitosan/PGA)$_n$ films can range from linear to exponential depending on the polyelectrolyte's charge density during film deposition(54), which contributes tremendously to the thickness of film per bilayer(55). When chitosan (pKa~6.5(56)) is well ionized and attains a flat and extended conformation, it demonstrates linear film growth(54), which we similarly observed. The seemingly small thickness contribution by the polymer-drug conjugate despite its micelle size (~125 nm) is likely due to spreading of the aggregates and possible rearrangement of the structures on adsorption.

The elution of diclofenac from these films shows a long-lasting multi-month release. For the PLL-based and chitosan-based films, we measured release for more than 14 months and 5 months, respectively (Figure 5-4). In the latter case, diclofenac release from the thinner 10 and 25 bilayer films was too low to be reliably detected by HPLC. Overall, the release kinetics of diclofenac from these LbL films can be fit to pseudo first-order kinetics, as we can see with the curves in Figures 5-4A and 5-4B. This is unsurprising since diclofenac release by ester hydrolysis in the hydrated LbL film is of the same mechanism as in the solubilized PGA-TriEG-Diclof. Film assembly through electrostatic complexation of the polyanionic backbone accommodates its immobilization into the film while maintaining the polymer-drug conjugate's aqueous solvation and accessibility, thus allowing its use as a localized drug delivery strategy. The kinetic rate constants, k$_{obs}$, can similarly be calculated from the these release curves and we find values of 5.6 x 10^{-8} s^{-1} for the PLL-based film and 1.7 x 10^{-7} s^{-1} for the chitosan-based film. Both film-based rate constants are greater than that of solubilized PGA-TriEG-Diclof (Table 5-1)

under identical conditions of PBS, pH 7.4 at 37°C. This film-based rate acceleration is likely a consequence of a combination of the aforementioned micellar disruption upon film assembly and the polyion's electrostatic complexation, which neutralizes much of the backbone nearest neighbor negative charges and in turn, may reduce inhibition of ester side-chain hydrolysis(41).
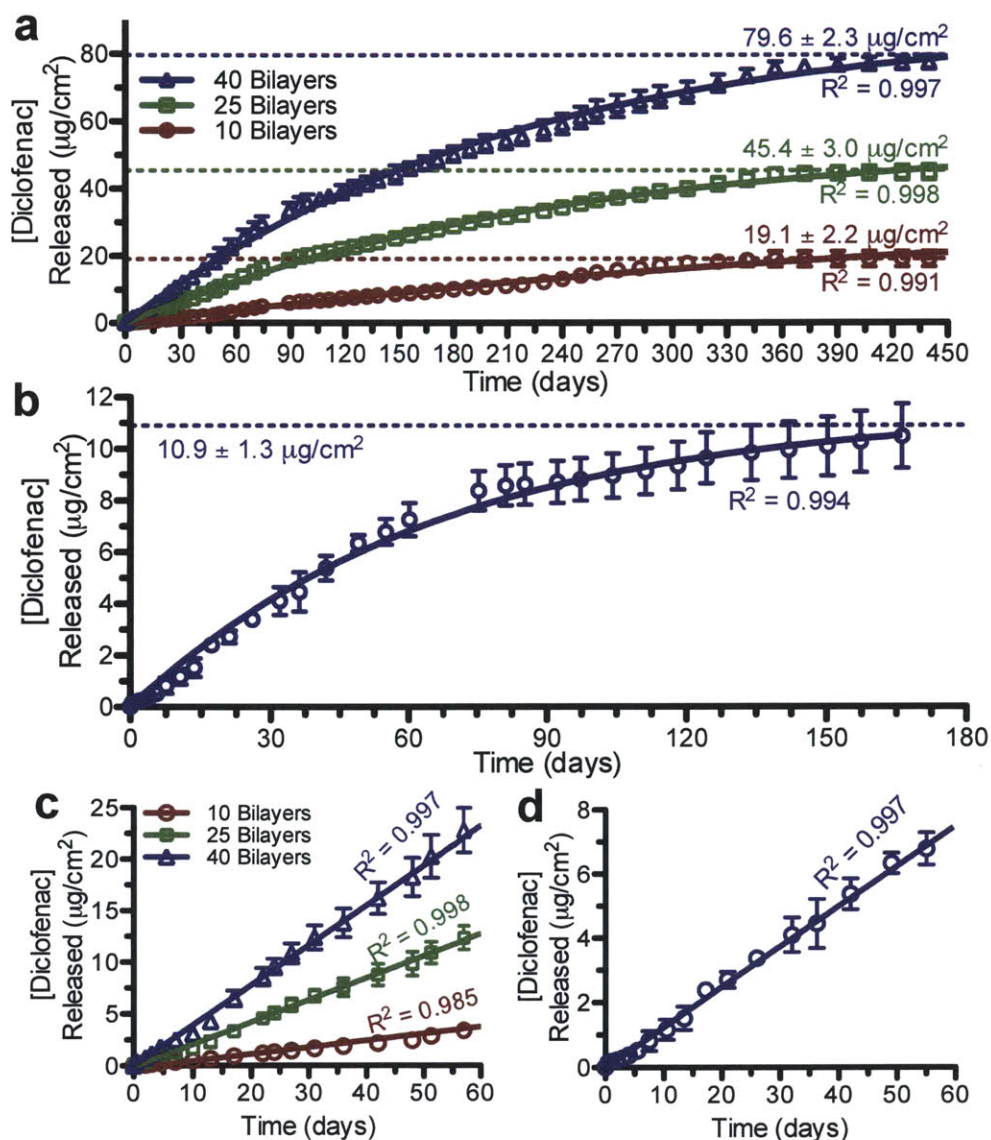
Figure 5-4. Diclofenac release profiles from (PLL/PGA-TriEG-Diclof)$_n$ films (A,C) and (Chitosan/PGA-TriEG-Diclof)$_{40}$ films (B,D). Fullscale (A,B) and the first 60 days (C,D) are shown. The symbols represent measured data and solid lines represent first order fits (A,B) or linear regressions (C,D).

A highly desirable feature for controlled release systems is zeroth order release kinetics, where the rate of drug release can balance its bioelimination to sustain a therapeutic concentration(10). Linear regression of the drug released from each of our films in the first two months shows constant rates of diclofenac elution from both PLL-based (Figure 5-4C) and chitosan-based (Figure 5-4D) systems. An initial burst release of drug is commonly observed in controlled release systems for small molecules due to their low molecular weights(57) and is frequently undesirable as it can be uncontrollable, irreproducible, and toxic due to a rapid elevation in local drug concentration(58). With our strategy of using a polymer-drug conjugate that is electrostatically immobilized into a film, the drug release is mediated by ester hydrolysis and eliminates this potentially deleterious initial burst release.
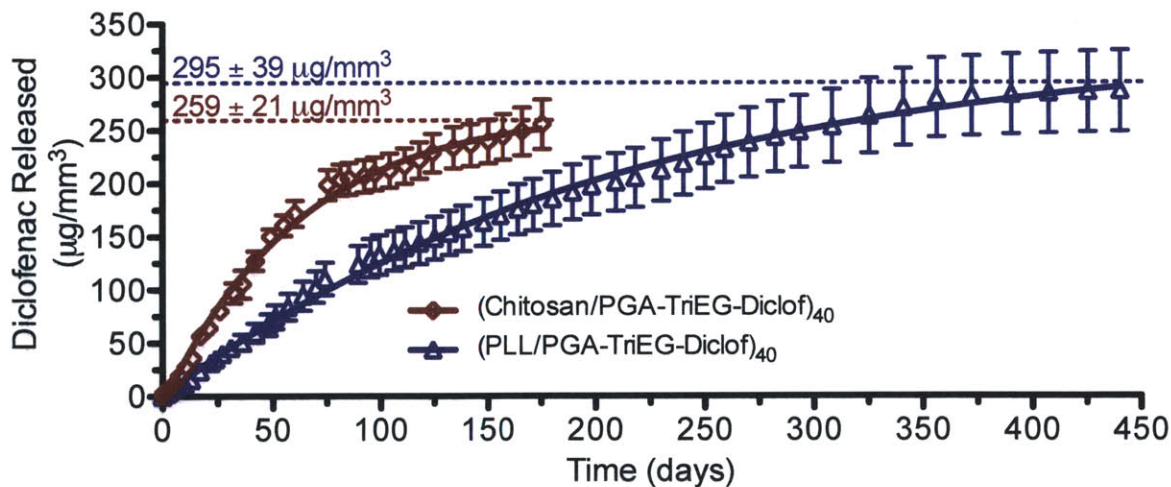
Figure 5-5. Mass of diclofenac per film volume released from (PLL/PGA-TriEG-Diclof)$_{40}$ and (Chitosan/PGA-TriEG-Diclof)$_{40}$ films. Symbols are measured data and solid lines are first order fits.

The differences in diclofenac release rates from PLL-based and chitosan-based films become more evident when their release profiles from 40 bilayer films are presented in terms of the mass of diclofenac released per film volume, as shown in Figure 5-5. Our observations of

faster release rates from chitosan-based films compared to PLL-based films likely reflect the compositional differences within the films, including less water accessibility for the latter, as greater hydrophobicity has been found to slow hydrolysis while increased hydrophilicity accelerates it(59). We suspect the polycation charge density (e.g., PLL and chitosan), ionic strength, and the pH of assembly conditions also cause differences in the effective ionic crosslink density and degree of water swelling within the films, thus impacting hydrolysis rates and influencing the presence of hydrophobic regions (i.e. self assembly of pendant diclofenac into hydrophobic pockets(60)). We gauged the relative water content in these films by comparing their swelling upon hydration in PBS, pH 7.4. The PLL-based films showed relatively moderate swelling ($38 \pm 12\%$), whereas chitosan-based films revealed significantly greater swelling of $116 \pm 14\%$, indicating its greater hydrophilicity. This also corresponds with the more rapid diclofenac elution that we observe from chitosan-based films. Furthermore, the change in pH between the assembly conditions and release conditions for chitosan films may also facilitate increased water accessibility of the ester linkages, as pH-induced morphological changes in LbL films can cause film swelling and rearrangement, and consequently increased water access to moieties previously hidden in hydrophobic pockets(61).

Myriad factors can contribute to the characteristics of controlled release films, and interestingly our system showed significantly higher loading and extended release in comparison to another LbL-film based on a polymer-drug conjugate: (chitosan/hyaluronic acid-paclitaxel)$_n$ films(62). For our PLL-based and chitosan-based films of 40 bilayers (Figure 5-5), diclofenac loading densities were 295 $\mu g/mm^3$ (30 wt%) and 259 $\mu g/mm^3$ (26 wt%). This is also significantly greater in drug loading and release duration of diclofenac than other non-conjugate LbL-based(24, 25), PLGA-based(63), and lipid nanoparticle-based systems(64).

While ester hydrolysis facilitates diclofenac liberation and elution, the polypeptide-based film remains intact. We found that after 10.6 months of incubation and drug release, the (PLL/PGA-TriEG-Diclof)$_{40}$ dry film thickness was 2.9 ± 0.2 μm, a comparable value to its thickness prior to release (2.7 ± 0.5 μm), indicating that any small changes in charge distribution and net charge balance within the LbL films during diclofenac release are insufficient to cause destabilization of the films. We propose that during hydration, the film effectively swells and the pendant drug is believed to uniformly undergo hydrolysis-based release with time. This leaves the poly(L-glutamic acid) backbone intact in the LbL film, thus making the film less sensitive to some of the complexities (e.g., autocatalysis, non-uniformity, pore-formation, cracks and/or structural collapse) that plague certain other drug release systems(14). This behavior also differs from the erosion-based, hydrolytically degradable LbL films used for controlled delivery developed previously that rely on poly(β-amino ester)s with cleavable ester linkages along the polymer backbone. The hydrophobicity of these degradable polycations can be tuned and thus the release kinetics from the film(65). Differential rates of water uptake and consequently hydrolysis-mediated film erosion in such systems allow for diverse release kinetics, but are not as easily adapted to the controlled release of small molecules, which are bound to undergo some rapid diffusion with swelling, as they rely on trapping of molecules within the ionic network rather than covalent conjugation.

While film degradation by polypeptide bond hydrolysis is relatively inconsequential compared to the rate of diclofenac release, its proteolysis can accelerate disassembly. This biodegradability is a coveted feature for implantable materials and its rate is highly dependent on the biological fluid's enzyme composition. Investigations into tuning proteolytic susceptibility have shown that while some human proteases have poor activity against LbL films(66), film

characteristics like covalent crosslinking(67), L- or D-polypeptides(68), and terminal layer charge(69), among others, can enhance or inhibit degradation. In addition, anti-fouling modifications like PEGylation(70), and mixed-charge nanodomains(71) can introduce a protein resistance that reduces enzyme contact with the film. This versatility in LbL assembled films, coupled with the non-enzymatic hydrolytic release mechanism, can easily accommodate a variety of modifications that specifically tune film characteristics to the desired application.

Anti-Inflammatory Activity.

We examined the efficacy of diclofenac derived from our various formulations to identify potentially deleterious effects from the synthesis, film assembly, and release process. By investigating its inhibition of cyclooxygenase-1 (COX) activity *in vitro*, we can gain insight into diclofenac's ability to reduce the downstream effects of inflammation and pain. As shown in Figure 5-6, stock diclofenac yields substantial COX inhibition whereas polymer conjugation (i.e., PGA-TriEG-Diclof) eliminates it. This inactivation is likely due to the masking of diclofenac's carboxylic acid by esterification and the introduction of steric bulkiness from the polymer-linker component, both of which can prevent binding with the COX enzyme(72). To regenerate activity, we hydrolyzed the ester linkages and found that diclofenac recovered from the polymer-drug conjugate also retains its functionality for COX inhibition (Figure 5-6). In our controlled release films, we incorporated PGA-TriEG-Diclof into electrostatically assembled LbL films incubated under physiological conditions of PBS, pH 7.4 at 37°C for multiple months, possibly submitting diclofenac to the degradative effects of prolonged hydration and elevated temperature. Therefore, we tested the undiluted release of diclofenac at 0.5, 3.0, and 6.0 months from (PLL/PGA-TriEG-Diclof)$_{40}$ films and found that the drug, as released, retained substantial

COX inhibition on a similar level to stock diclofenac solutions. We have previously found that therapeutics released from LbL films remain active, even after weeks of incubation, which may stem from the stabilization provided by the milieu of intermolecular interactions with the surrounding matrix. In addition, the degradation pathways for diclofenac mainly involve intramolecular cyclization with its carboxylic acid(73), which may be inhibited by its esterification.
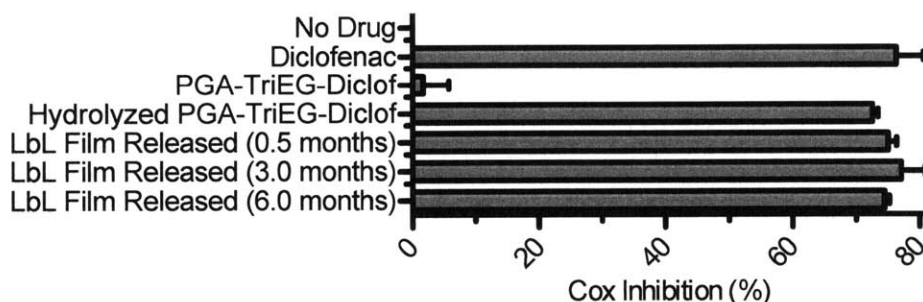
Figure 5-6. COX inhibition activity of diclofenac-based compounds. Diclofenac released from LbL films were examined for COX inhibition activity at the concentration released into PBS, pH 7.4.

The intrinsic potency of the LbL incorporated diclofenac was also examined by measuring the IC_{50} (concentration required for 50% inhibition of COX). As shown in Table 5-2, the diclofenac IC_{50} is comparable between an unfunctionalized diclofenac control, hydrolyzed drug from the PGA-TriEG-Diclof, and drug released from (PLL/PGA-TriEG-Diclof)$_{40}$ films. This confirms that none of the steps—including synthesis of the polymer-drug conjugate, LbL assembly into a film, long-term hydration and incubation at elevated temperature, and ester hydrolysis to regenerate the drug—have a deleterious effect; the efficacy of the drug is maintained throughout the long term release.

Table 5-2. Inhibiting concentrations of various materials necessary to elicit 50% inhibition of COX activity.

Source	IC_{50} (ng/mL)
Unfunctionalized Diclofenac*	24.2 ± 5.7
Hydrolyzed PGA-TriEG-Diclof	26.4 ± 12.4
LbL Film Released Diclof	25.8 ± 4.8

*From ref(74)

5.4 Conclusions

Long-term small molecule treatment from a biodegradable device can have a significantly positive impact on a broad spectrum of chronic or recalcitrant medical issues. We have generated a polymer-drug conjugate capable of relatively slow release based on ester hydrolysis and incorporated it into LbL films, yielding a robust nanoscale film with substantial payload that elutes active drug for more than 14 months. The versatility of this strategy is applicable to a broad range of therapeutics and demonstrates promising approach for the treatment of a multitude of targets.

5.5 References

1. Connolly LE, Edelstein PH, & Ramakrishnan L (2007) Why is long-term therapy required to cure tuberculosis? *Plos Medicine* 4(3):435-442.
2. Konstan MW, Schluchter MD, Xue W, & Davis PB (2007) Clinical use of ibuprofen is associated with slower FEV1 decline in children with cystic fibrosis. *Am. J. Respir. Crit. Care Med.* 176(11):1084-1089.
3. Kroon F, Landewe R, Dougados M, & van der Heijde D (2012) Continuous NSAID use reverts the effects of in ammation on radiographic progression in patients with ankylosing spondylitis. *Ann. Rheum. Dis.* 71(10):1623-1629.
4. Hazirolan D & Pleyer U (2013) Think Global - Act Local: Intravitreal Drug Delivery Systems in Chronic Noninfectious Uveitis. *Ophthalmic Res.* 49(2):59-65.
5. Blackwell D & Clarke T (2013) Percentage of Adult Aged ≥ 18 Years Who Often Had Pain in the Past 3 Months, by Sex and Age Group - National Health Interview Survey, United States 2010-2011. in *Morb. Mortal. Weekly Rep.* (Centers for Disease Control and Prevention), pp 321-342.
6. Institute of Medicine (2011) *Relieving pain in america: a blueprint for transforming prevention, care, education, and research* (The National Academies Press, Washington, D.C.).
7. Zhang W, *et al.* (2010) OARSI recommendations for the management of hip and knee osteoarthritis Part III: changes in evidence following systematic cumulative update of research published through January 2009. *Osteoarthritis Cartilage* 18(4):476-499.
8. Franceschi M, *et al.* (2008) Prevalence, clinical features and avoidability of adverse drug reactions as cause of admission to a Geriatric Unit - A prospective study of 1756 patients. *Drug Saf.* 31(6):545-556.
9. Richette P, *et al.* (2011) Comparison of general practitioners and rheumatologists' prescription patterns for patients with knee osteoarthritis. *BMC Musculoskel. Disord.* 12.
10. Siepmann J, Siegel RA, & Rathbone MJ eds (2012) *Fundamentals and Applications of Controlled Release Drug Delivery* (Springer).
11. Tugwell PS, Wells GA, & Shainhouse JZ (2004) Equivalence study of a topical diclofenac solution (Pennsaid((R))) compared with oral diclofenac in symptomatic treatment of osteoarthritis of the knee: A randomized controlled trial. *J. Rheumatol.* 31(10):2002-2012.
12. Willis JV, Kendall MJ, Flinn RM, Thornhill DP, & Welling PG (1979) The pharmacokinetics of diclofenac sodium following intravenous and oral administration. *Eur. J. Clin. Pharmacol.* 16(6):405-410.
13. Richter A, Anton SF, Koch P, & Dennett SL (2003) The impact of reducing dose frequency on health outcomes. *Clin. Ther.* 25(8):2307-2335.
14. Fredenberg S, Wahlgren M, Reslow M, & Axelsson A (2011) The mechanisms of drug release in poly(lactic-co-glycolic acid)-based drug delivery systems—A review. *Int. J. Pharm.* 415(1–2):34-52.

15. Klose D, Siepmann F, Elkharraz K, Krenzlin S, & Siepmann J (2006) How porosity and size affect the drug release mechanisms from PLGA-based microparticles. *Int. J. Pharm.* 314(2):198-206.

16. Goldberg M, Langer R, & Jia X (2007) Nanostructured materials for applications in drug delivery and tissue engineering. *Journal of Biomaterials Science-Polymer Edition* 18(3):241-268.

17. Uhrich KE, Cannizzaro SM, Langer RS, & Shakesheff KM (1999) Polymeric systems for controlled drug release. *Chem. Rev.* 99(11):3181-3198.

18. del Amo EM & Urtti A (2008) Current and future ophthalmic drug delivery systems. A shift to the posterior segment. *Drug Discov. Today* 13(3-4):135-143.

19. Sprintz M, *et al.* (2011) Nanomedicine: Ushering in a new era of pain management. *European Journal of Pain Supplements* 5(S2):317-322.

20. Hyder MN, Shah NJ, & Hammond PT (2012) Design and Translation of Nanolayer Assembly Processes: Electrochemical Energy to Programmable Pharmacies. *Multilayer Thin Films*, eds Decher G & Schlenoff JB (Wiley-VCH), 2nd Ed.

21. Moskowitz JS, *et al.* (2010) The effectiveness of the controlled release of gentamicin from polyelectrolyte multilayers in the treatment of Staphylococcus aureus infection in a rabbit bone model. *Biomaterials* 31(23):6019-6030.

22. Shukla A, Avadhany SN, Fang JC, & Hammond PT (2010) Tunable Vancomycin Releasing Surfaces for Biomedical Applications. *Small* 6(21):2392-2404.

23. Kim B-S, Park SW, & Hammond PT (2008) Hydrogen-bonding layer-by-layer assembled biodegradable polymeric micelles as drug delivery vehicles from surfaces. *Acs Nano* 2(2):386-392.

24. Smith RC, Riollano M, Leung A, & Hammond PT (2009) Layer-by-Layer Platform Technology for Small-Molecule Delivery. *Angew. Chem. Int. Ed.* 48(47):8974-8977.

25. Shukla A, Fuller RC, & Hammond PT (2011) Design of multi-drug release coatings targeting infection and inflammation. *J. Controlled Release* 155(2):159-166.

26. Bonina FP, *et al.* (2001) In vitro and in vivo evaluation of polyoxyethylene esters as dermal prodrugs of ketoprofen, naproxen and diclofenac. *Eur. J. Pharm. Sci.* 14(2):123-134.

27. Li C, *et al.* (1998) Complete regression of well-established tumors using a novel water-soluble poly(L-glutamic acid) paclitaxel conjugate. *Cancer Res.* 58(11):2404-2409.

28. Ananthapadmanabhan KP, Goddard ED, Turro NJ, & Kuo PL (1985) FLUORESCENCE PROBES FOR CRITICAL MICELLE CONCENTRATION. *Langmuir* 1(3):352-355.

29. Dominguez A, Fernandez A, Gonzalez N, Iglesias E, & Montenegro L (1997) Determination of critical micelle concentration of some surfactants by three techniques. *J. Chem. Educ.* 74(10):1227-1231.

30. Itano K, Choi J, & Rubner MF (2005) Mechanism of the pH-Induced Discontinuous Swelling/Deswelling Transitions of Poly(allylamine hydrochloride)-Containing Polyelectrolyte Multilayer Films. *Macromolecules* 38(8):3450-3460.

31. Chluba J, et al. (2001) Peptide Hormone Covalently Bound to Polyelectrolytes and Embedded into Multilayer Architectures Conserving Full Biological Activity. *Biomacromolecules* 2(3):800-805.

32. Schultz P, et al. (2005) Polyelectrolyte multilayers functionalized by a synthetic analogue of an anti-inflammatory peptide, a-MSH, for coating a tracheal prosthesis. *Biomaterials* 26(15):2621-2630.

33. Ochs CJ, Such GK, Yan Y, van Koeverden MP, & Caruso F (2010) Biodegradable Click Capsules with Engineered Drug-Loaded Multilayers. *Acs Nano* 4(3):1653-1663.

34. Fini A, Fazio G, & Feroci G (1995) Solubility and solubilization properties of non-steroidal anti-inflammatory drugs. *Int. J. Pharm.* 126(1-2):95-102.

35. Hao AJ, et al. (2006) Degradation kinetics of fluorouracil-acetic-acid-dextran conjugate in aqueous solution. *Drug Dev. Ind. Pharm.* 32(6):757-763.

36. Larsen C & Johansen M (1985) Macromolecular prodrugs. 1. Kinetics and mechanism of hydrolysis of O-benzoyl dextran conjugates in aqueous buffer and in human-plasma. *Int. J. Pharm.* 27(2-3):205-218.

37. Larsen C (1989) Macromolecular prodrugs. 12. Kinetics of release of naproxen from various polysaccharide ester prodrugs in neutral and alkaline-solution. *Int. J. Pharm.* 51(3):233-240.

38. Wu C, Xie J, Branford-White C, Quan J, & Zhu L (2011) In Vitro Controlled Release of Polymeric Drug-Saccharide Conjugates with Ketoprofen, Ibuprofen, and Naproxen Pendants. *J. Appl. Polym. Sci.* 121(3):1654-1660.

39. Rajewski LG, Stinnett AA, Stella VJ, & Topp EM (1992) Enzymatic and nonenzymatic hydrolysis of a polymeric prodrug- hydrocortisone esters of hyaluronic acid. *Int. J. Pharm.* 82(3):205-213.

40. McCoy CP, Morrow RJ, Edwards CR, Jones DS, & Gorman SP (2007) Neighboring group-controlled hydrolysis: Towards "designer" drug release biomaterials. *Bioconj. Chem.* 18(1):209-215.

41. Kondo S, Murase K, & Kuzuya M (1994) Mechanochemical solid-state polymerization. 7. The nature of hydrolysis of novel polymeric prodrugs prepared by mechanochemical copolymerization. *Chem. Pharm. Bull. (Tokyo)* 42(12):2412-2417.

42. Jo YS, Gantz J, Hubbell JA, & Lutolf MP (2009) Tailoring hydrogel degradation and drug release via neighboring amino acid controlled ester hydrolysis. *Soft Matter* 5(2):440-446.

43. Heller J, Helwing RF, Baker RW, & Tuttle ME (1983) Controlled release of water-soluble macromolecules from bioerodible hydrogels. *Biomaterials* 4(4):262-266.

44. Schoenmakers RG, van de Wetering P, Elbert DL, & Hubbell JA (2004) The effect of the linker on the hydrolysis rate of drug-linked ester bonds. *J. Controlled Release* 95(2):291-300.

45. Kataoka K, Harada A, & Nagasaki Y (2001) Block copolymer micelles for drug delivery: design, characterization and biological significance. *Adv. Drug Del. Rev.* 47(1):113-131.

46. Deo P, Deo N, Somasundaran P, Jockusch S, & Turro NJ (2005) Conformational changes of pyrene-labeled polyelectrolytes with pH: Effect of hydrophobic modifications. *J. Phys. Chem. B* 109(44):20714-20718.

47. Lee AS, Gast AP, Bütün V, & Armes SP (1999) Characterizing the Structure of pH Dependent Polyelectrolyte Block Copolymer Micelles. *Macromolecules* 32(13):4302-4310.

48. Decher G (1997) Fuzzy Nanoassemblies: Toward Layered Polymeric Multicomposites. *Science* 277(5330):1232-1237.

49. Porcel C, *et al.* (2006) From exponential to linear growth in polyelectrolyte multilayers. *Langmuir* 22(9):4376-4383.

50. Dos A, Schimming V, Tosoni S, & Limbach H-H (2008) Acid-Base Interactions and Secondary Structures of Poly-L-Lysine Probed by (15)N and (13)C Solid State NMR and Ab initio Model Calculations. *J. Phys. Chem. B* 112(49):15604-15615.

51. Myer YP (1969) The pH-Induced Helix-Coil Transition of Poly-L-lysine and Poly-L-glutamic Acid and the 238-mμ Dichroic Band. *Macromolecules* 2(6):624-628.

52. Lavalle P, *et al.* (2002) Comparison of the structure of polyelectrolyte multilayer films exhibiting a linear and an exponential growth regime: An in situ atomic force microscopy study. *Macromolecules* 35(11):4458-4465.

53. Picart C, *et al.* (2002) Molecular basis for the explanation of the exponential growth of polyelectrolyte multilayers. *Proc. Natl. Acad. Sci. U. S. A.* 99(20):12531-12535.

54. Song ZJ, *et al.* (2009) Layer-by-Layer Buildup of Poly(L-glutamic acid)/Chitosan Film for Biologically Active Coating. *Macromol. Biosci.* 9(3):268-278.

55. Shiratori SS & Rubner MF (2000) pH-dependent thickness behavior of sequentially adsorbed layers of weak polyelectrolytes. *Macromolecules* 33(11):4213-4219.

56. Wang QZ, *et al.* (2006) Protonation constants of chitosan with different molecular weight and degree of deacetylation. *Carbohydr. Polym.* 65(2):194-201.

57. Huang X & Brazel CS (2001) On the importance and mechanisms of burst release in matrix-controlled drug delivery systems. *J. Controlled Release* 73(2-3):121-136.

58. Allison SD (2008) Analysis of initial burst in PLGA microparticles. *Expert Opinion on Drug Delivery* 5(6):615-628.

59. Pitt CG, Cha Y, Shah SS, & Zhu KJ (1992) Blend of PVA and PGLA - Control of the permeability and degradability of hydrogels by blending. *J. Controlled Release* 19(1-3):189-199.

60. Fini A, Fazio G, Rabasco AM, & Hervas MJF (1994) SELF-ASSOCIATION PROPERTIES OF DICLOFENAC. *Farmaco* 49(2):141-146.

61. Li Y & Kwon GS (2000) Methotrexate esters of poly(ethylene oxide)-block-poly(2-hydroxyethyl-L-aspartamide). Part I: Effects of the level of methotrexate

conjugation on the stability of micelles and on drug release. *Pharm. Res.* 17(5):607-611.

62. Thierry B, *et al.* (2005) Delivery platform for hydrophobic drugs: Prodrug approach combined with self-assembled multilayers. *J. Am. Chem. Soc.* 127(6):1626-1627.

63. Tuncay M, *et al.* (2000) Diclofenac sodium incorporated PLGA (50 : 50) microspheres: formulation considerations and in vitro/in vivo evaluation. *Int. J. Pharm.* 195(1-2):179-188.

64. Liu DF, *et al.* (2010) Solid lipid nanoparticles for transdermal delivery of diclofenac sodium: preparation, characterization and in vitro studies. *J. Microencaps.* 27(8):726-734.

65. Zhang JT, Fredin NJ, Janz JF, Sun B, & Lynn DM (2006) Structure/property relationships in erodible multilayered films: Influence of polycation structure on erosion profiles and the release of anionic polyelectrolytes. *Langmuir* 22(1):239-245.

66. Craig M, Bordes R, & Holmberg K (2012) Polypeptide multilayer self-assembly and enzymatic degradation on tailored gold surfaces studied by QCM-D. *Soft Matter* 8(17):4788-4794.

67. Picart C, *et al.* (2005) Controlled degradability of polysaccharide multilayer films in vitro and in vivo. *Adv. Funct. Mater.* 15(11):1771-1780.

68. Jessel N, *et al.* (2003) Bioactive coatings based on a polyelectrolyte multilayer architecture functionalized by embedded proteins. *Adv. Mater.* 15(9):692-695.

69. Serizawa T, Yamaguchi M, & Akashi M (2002) Enzymatic Hydrolysis of a Layer-by-Layer Assembly Prepared from Chitosan and Dextran Sulfate. *Macromolecules* 35(23):8656-8658.

70. Heuberger R, Sukhorukov G, Vörös J, Textor M, & Möhwald H (2005) Biofunctional Polyelectrolyte Multilayers and Microcapsules: Control of Non-Specific and Bio-Specific Protein Adsorption. *Adv. Funct. Mater.* 15(3):357-366.

71. Wong SY, *et al.* (2012) Drastically Lowered Protein Adsorption on Microbicidal Hydrophobic/Hydrophilic Polyelectrolyte Multilayers. *Biomacromolecules* 13(3):719-726.

72. Sidhu RS, Lee JY, Yuan C, & Smith WL (2010) Comparison of Cyclooxygenase-1 Crystal Structures: Cross-Talk between Monomers Comprising Cyclooxygenase-1 Homodimers. *Biochemistry (Mosc).* 49(33):7069-7079.

73. Galmier MJ, *et al.* (2005) Identification of degradation products of diclofenac by electrospray ion trap mass spectrometry. *J. Pharm. Biomed. Anal.* 38(4):790-796.

74. Kato M, Nishida S, Kitasato H, Sakata N, & Kawai S (2001) Cyclooxygenase-1 and cyclooxygenase-2 selectivity of non-steroidal anti-inflammatory drugs: investigation using human peripheral monocytes. *J. Pharm. Pharmacol.* 53(12):1679-1685.

Chapter 6
Clotting Mimicry from Robust Hemostatic Bandages Based on Self-Assembling Peptides

A version of this chapter is in preparation for publication.

Authors:
Bryan B. Hsu[1,3,4], William Conway[2], Monica Perez[5], Shuguang Zhang[6], and Paula T. Hammond[2,3,4]

Departments of [1]Chemistry and [2]Chemical Engineering, Massachusetts Institute of Technology, Cambridge, MA 02139
[3]Koch Institute for Integrative Cancer Research, Massachusetts Institute of Technology, Cambridge, MA 02139
[4]Institute for Soldier Nanotechnologies, Cambridge, MA 02139
[5]Department of Chemical Engineering, Georgia Institute of Technology, Atlanta, GA 30332
[6]Center for Bits & Atoms, Massachusetts Institute of Technology, Cambridge, MA 02139

6.1   Introduction

Blood loss is one of the greatest causes of mortality during military conflict, as more than 85% of deaths from potentially survivable wounds are due to exsanguinating hemorrhage(1). In addition, a substantial fraction of deaths from civilian trauma are also due to uncontrolled bleeding(2). In the history of medically documented US military engagements ranging from the Civil War to Operations Iraqi Freedom and Enduring Freedom, the most significant mechanism of injury has shifted from ballistics (e.g., gunshots) to explosives (e.g., improvised explosive devices, mortars, rocket-propelled grenades and landmines), increasing the potential for large traumatic wounds affecting multiple areas of the body(3). To minimize blood loss, improve survivability, and prevent hemorrhage shock, it is critical to establish hemostasis immediately(4). Current hemostatic devices use various types of materials ranging from chitosan to inorganics like kaolin or smectite and while these systems have addressed some of the issues on the battlefield(5, 6), serious challenges remain for addressing acute cases of uncontrolled bleeding. Ideally, it would be desirable to have a system that rapidly coagulates blood even after long term storage, that is simple to apply, degradable or resorbable to avoid the need for removal, and one that avoids undesirable side effects (e.g., burns or thrombosis)(5).

Biomaterials based on self-assembling peptides have shown interesting properties for biomedical applications(7). Early examination of one such type of peptide with the self-complementary ionic tetramer repeat motif of $(RADA)_4$, also identified as RADA16-I, revealed their ability to rapidly form β-sheets with oriented hydrophobic and hydrophilic faces that naturally aggregate into highly entangled nano-fibrillar hydrogels(8). These supramolecular assemblies were found to be robust against various pH and ionic strength conditions(9, 10) and reformed rapidly within minutes after disruption by sonication(8). A diverse set of therapeutic

134

biomedical applications have since been discovered(11) including three-dimensional cell culture(12-14), axonal regeneration(15), middle-ear mucosal regeneration(16), and controlled drug delivery(17-19). Most prominently, RADA16-I peptides were discovered to generate hemostasis *in vivo*(20-22) within seconds, in addition to other similar self-assembling peptides(23, 24). This suggests that the mechanical and web-like properties of the entangled networks may be the key feature in plugging blood vessel damage(24). These combinations of features including coagulative action, biocompatibility, and biodegradability make RADA16-I a very promising topical hemostatic agent(25). Current formulations utilize the peptide in solution as a viscous gel to be applied from syringes for application by medical professionals, but if these hemostatic peptides could be adapted to readily stored, solid state, thin films that could be revived into entangled nanofibers upon exposure to blood, it would be possible to generate a portable and more broadly applicable hemostatic agent for use by untrained personnel ranging from the military to civilians. Additionally, films deposited on to absorbent bandaging materials provide a convenient means to applying the peptide in a concentrated dry form, which would help overcome some challenges presented by severely bleeding wounds that can dilute materials before reaching the site of injury, or extreme environmental conditions (e.g., wind and precipitation) that can make application of powders or solutions challenging. To create a highly effective hemostatic bandage for potentially life-threatening trauma, formulating RADA16-I into a rapid-release film on a field dressing would allow it to be applied from a lightweight, easily stored, uncomplicated, and immediately functional bandage, each of which are highly desirable features(26). Key to the combination of these peptides with a bandage substrate is the strategy of coating, as this will dictate the loading and robustness in the film, which are necessary considerations to ensure maximal beneficial effect.

The layer-by-layer (LbL) assembly technique has shown abundant applications in delivery of therapeutics ranging from small molecules to proteins and nucleic acids(27). We have thus far demonstrated the ability to incorporate high aspect ratio materials including carbon nanotubes and graphene sheets, as well as supramolecular aggregates like micelles(28). In the case of controlled drug delivery, elution with spatiotemporal precision can significantly improve therapeutic outcome and we have demonstrated a range of release kinetics including instantaneous, multi-day and multi-week release(29) (*see Chapter 2*), sequential release(30) (*see Chapter 3*), and sustained release for more than 14 months(31) (*see Chapter 5*) by exploiting a variety of different types and arrangements of intermolecular interactions.

We aimed to create an advanced dressing capable of rapid hemostasis by coating common bandaging material (e.g., gauze and gelatin sponges) with RADA16-I based thin films. First, we studied the interaction of these nanofibers with whole blood for insight into its coagulation mechanism. Then we developed dip-LbL and spray-LbL assembled films utilizing facile, pH-sensitive, intermolecular interactions between the RADA16-I nanofibers and natural polyanionic polysaccharides to facilitate rapid film dissolution upon immersion in physiological pH. We found the *in vitro* activity of these nanofibers was retained after release from LbL films and further discovered that nanofiber based clots formed when these films were mixed with whole blood. Furthermore, films remained robust despite week-long exposure to extreme temeratures (-80°C to 60°C) and were still able to form nanofiber clots, even after extended (2 month) exposure to 60°C.

6.2 Materials and Methods

Unless otherwise noted, all materials were obtained from Sigma Aldrich and used without further purification. Hyaluronic acid (HA, M_W = 2 MDa and 500 kDa) was obtained from Lifecore Biomedical, chondroitin sulfate sodium salt (CS, M_W = 85 kDa) from TCI International, and dextran sulfate sodium salt (DS, M_W = 500 kDa) from Calbiochem. Glutaraldehyde (Grade I 25%) and collegenase (Type I) were purchased from Sigma Aldrich. Human whole blood (EDTA anti-coagulated) was obtained from Hemacare and washed and pooled 10% rabbit red blood cells (RBCs) were obtained from Lampire Biological Laboratories. Solutions of 1% (10 mg/mL) RADA16-I were a generous donation from 3DMatrix. Fluorescently labeled RADA16-I (RADA16-I^{FAM}) was functionalized by 5-carboxyfluorescein at the N-terminus through a -Gly-Gly- linker and synthesized by the MIT Biopolymers Laboratory. Gelatin sponges were a generous donation from Ferrosan.

LbL Film Assembly

Substrates of silicon wafers or glass microscope slides were pre-cleaned with methanol, acetone, and water prior to plasma irradiation (Harrick PDC-32G) for at least 1 min and immersion in RADA16-I solution (1 mg/mL in 10 mM HCl for dip-LbL and 0.1 mg/mL in 10 mM HCl for spray-LbL) for at least 15 min before additional film assembly. Cotton gauze was prepared by ~30 sec of plasma irradiation and the immersed in 0.1 mg/mL in 10 mM HCl prior to spray-LbL assembly. Gelatin sponges were used as received without additional preparation.

Dip LbL films of (RADA16-I/polyanion)$_n$ were assembled onto silicon (prepared as described above) by sequential immersion into 1 mg/mL RADA16-I in 10 mM HCl (30 min), rinsing in 10 mM HCl (10 s, 20 s, 30 s), immersion into 1 mg/mL polyanion (30 min), and

rinsing in 10 mM HCl (10 s, 20 s, 30 s), which constituted one bilayer and was repeated for *n*-bilayers.

Spray LbL films of (RADA16-I/polyanion)$_n$ were assembled onto glass, cotton gauze, and gelatin (prepared as described above). For the latter two, house vacuum was applied behind the substrates to facilitate more thorough film coatings. Solutions were aerosolized at 15 PSI at 0.25 mL/sec flow rates using an automated film assembly instrument (Svaya). Bilayer films were constructed by spraying substrates in the following sequence: 0.1 mg/mL RADA16-I in 10 mM HCl (2 sec), waiting period (5 sec), wash with 10 mM HCl (3 sec), air-drying (8 sec), 0.1 mg/mL polyanion in 10 mM HCl (2 sec), waiting period (5 sec), wash with 10 mM HCl (3 sec), and air-drying (8 sec). This constituted one bilayer and was repeated for *n*-bilayers. For gelatin sponges, the use of air-drying generated a bridged film conformation, while its replacement with a waiting period generated conformal coatings.

Film characterization

Thicknesses of films deposited onto flat substrates (silicon or glass) were determined by measuring the step-height difference between the film and a razor-scored region (Dektak 150 Profilometer).

Release profiles of films deposited onto silicon, glass, and gauze were quantified by immersion in 500 μL of PBS, pH 7.4 at 37°C and periodic replacement with fresh aliquots of PBS pre-warmed to 37°C. The collected aliquots were analyzed for their RADA16-I content using a bicinchoninic acid (BCA) assay (Thermo Scientific) according to the manufacturer's instructions with incubation of the reagent and sample for 30 min at 60°C to enhance sensitivity. Under these conditions we saw no background signal from the polyanions used in this study.

This BCA assay was capable of distinguishing RADA16-I released from all substrates, except the gelatin sponges, which released protein that obscured measurement. For quantification of the RADA16-I released from these samples, films were assembled with a RADA16-I solution containing a 1:20 fraction of RADA16-I^{FAM} and peptide release was studied by incubating in 1 mL of PBS or FBS at 37°C and periodically sampling 300 μL for analysis and replacing it with fresh pre-warmed solution. The collected aliquots were measured for fluorescence (λ_{ex} = 480 nm; λ_{em} = 525 nm) and RADA16-I was quantified by comparison to a standard curve.

Total RADA16-I loadings on glass, silicon and gauze were determined by complete dissolution of the films in 225 μL of 0.1 M NaOH at 37°C for ~2 hours, after which the solution was quenched with 225 μL of 0.1 M HCl and the addition of 50 μL of 10X PBS (for a final 1X concentration) to stabilize the pH. The RADA16-I content was measured by a BCA assay, similarly to as described earlier. Because the gelatin sponges introduced difficulties in completely eluting RADA16-I from the films, the substrate was digested using collagenase prior to fluorescence quantification. To the 1 mL of PBS or FBS containing film deposited onto gelatin sponges, 100 μL of 10 mg/mL collagenase and 50 mM CaCl$_2$ in PBS was added prior to incubation at 37°C for ~4 hours and then fluorescence quantification.

Nanofiber activity in vitro

The ability for RADA16-I to form a nanofiber-based clot *in vitro* was determined using a similar assay previously described(24). Volumes of 95 μL of PBS solutions containing RADA16-I diluted from stock or released from films were added to V-shaped 96-well microtiter plates followed by 10 μL of 10% rabbit RBCs. The wells were sealed with an optically clear

adhesive film, agitated at ~900 rpm for 15 min prior to incubating at 4°C for at least 4 hours and then examination.

Clotting characterization

Fibrin clots were generated by adding 25 µL of 0.2 M $CaCl_2$ to 475 µL of anti-coagulated whole blood and gently rocked at room temperature for 30 min. To study the nanofiber interaction with blood, 1 µL of 1% RADA16-I was mixed with 9 µL of anti-coagulated whole blood and incubated at room temperature for ~5 min. Anti-coagulated whole blood was studied without additional treatment and RADA16-I was studied at 0.1% in PBS, pH 7.4. For examination of blood's interaction with (RADA16-I/polyanion)$_{200}$ films, 5 µL of anti-coagulated whole blood was deposited on top of film-coated gauze and incubated at room temperature for ~5 min, exposed to a humidifier to prevent drying out. All samples were chemically fixed, dehydrated, and critical point dried as described below.

Scanning Electron Microscopy

Biological samples were prepared on a 0.03 µm polyethersulfone membrane filter (Sterlitech) by fixation with 2.5% glutaraldehyde (diluted from 25%) in PBS for 4 hours at room temperature, then serially dehydrated with 10 mL of H_2O (twice), 25% ethanol, 50% ethanol, 75% ethanol, 80% ethanol, 90% ethanol, and 100% ethanol (twice). Samples in ethanol were then critical point dried using CO_2 (Sorvall Critical Point Drying System). These dried biological samples and other samples already in dry form were sputter coated with ~8 nm of Au/Pd prior to examination using a field-emission SEM (JEOL 6700F). Dry LbL films were studied in LEI

mode (10 kV and 8 mm working distance) while biological samples were studied in SEI mode

(5.0 kV and ~6 mm working distance).

6.3   Results and Discussion

Nanofiber Clotting Mechanism

The ability for self-assembling peptides to rapidly coagulate blood has been hypothesized to occur through nanofiber entanglements entrapping blood components(24). To elucidate this effect and its possible implications on RADA16-I for thin film assembly and biomedical application, we studied the morphological characteristics of the solution-phase nanofibers by scanning electron microscopy (SEM). For SEM examination of these solution-phase structures, the materials in solution were chemically fixed using glutaraldehyde, then serially dehydrated in ethanol, and critical point dried with CO_2 after which they were sputter-coated with ~8 nm of Au/Pd. We found that RADA16-I in PBS, pH 7.4 (Figure 6-1A) forms a dense network of highly entangled nanofibers that is morphologically consistent with previous observations by SEM(32, 33) and atomic force microscopy(8). A closer look at higher magnification reveals the individual nanofibers to be highly interpenetrated with nanoscale pores (Figure 6-1A, *inset*) that are consistent with its macroscopic formation of a hydrogel(8). Separate characterization of EDTA anti-coagulated whole blood reveals the presence of red blood cells (RBCs) and platelets with fibrin clot formation inhibited (Figure 6-1B). To examine the mechanisms of hemostasis of RADA16-I in a wound, we recapitulated this scenario *ex vivo* by combining RADA16-I with anti-coagulated whole blood, and found that the interwoven nanofibers visibly entrapped blood components (Figure 6-1C). Interestingly, this nanofiber-based clot appears to have morphological similarities with a fibrin clot, in which the blood components are physically trapped by polymerized fibrin stalks during the natural coagulation process (Figure 6-1D). Although this effect has been hinted to as the mechanism behind nanofiber hemostatic activity with histology(21) and AFM(22) characterizations providing circumstantial evidence, our insight

provided by SEM clearly demonstrates this effect where physical entanglement of blood components with RADA16-I forms a nanofiber-based clot.
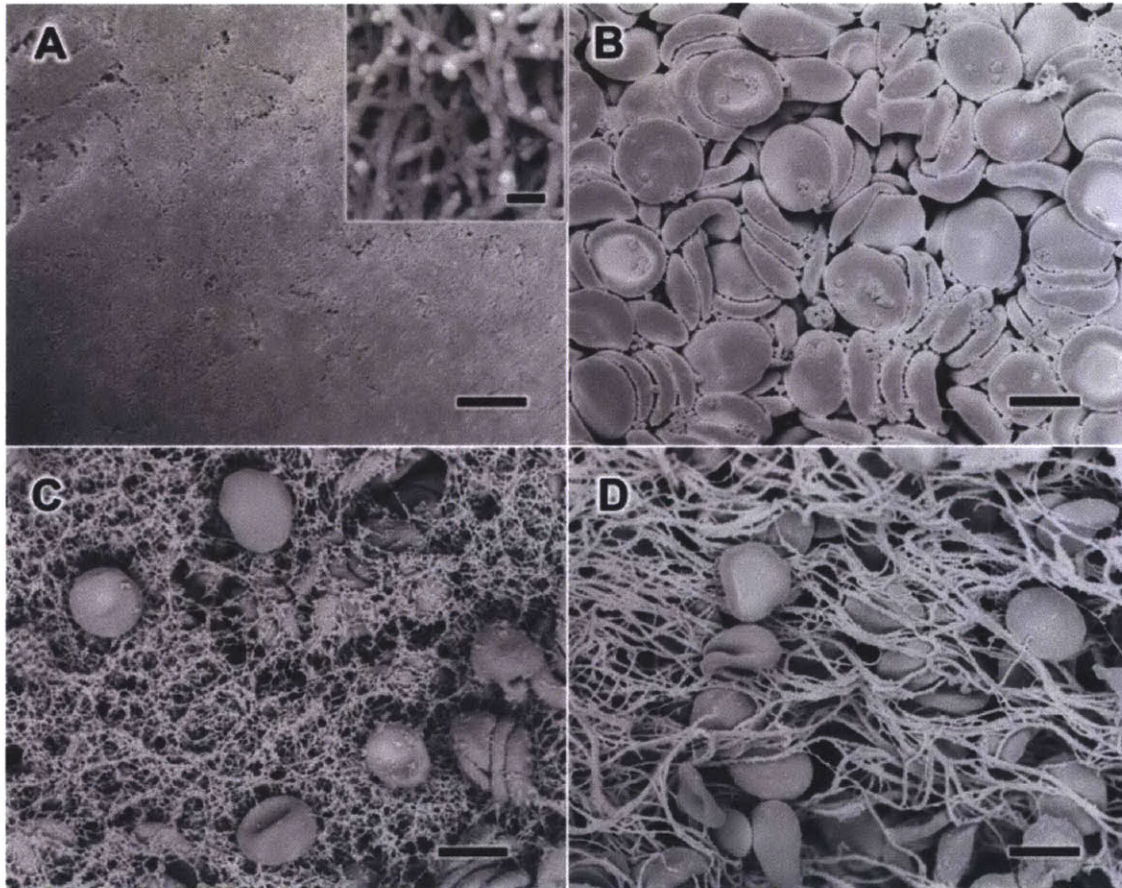
Figure 6-1. Scanning electron microscopy (SEM) of the morphology of RADA16-I (A), anti-coagulated whole blood (B), a mixture of RADA16-I and anti-coagulated whole blood (C), and coagulated whole blood (D). Scale bars represent 5 μm (A-D) and 100 nm (A, *inset*).

Numerous topical approaches can facilitate hemostasis by activating or enhancing the body's natural coagulation mechanisms to form a fibrin clot more quickly. Hemostatic dressings based on organics like chitosan and fibrin, or inorganics like kaolin and smectite are capable of facilitating fibrin clot formation but each suffers from some drawbacks including limited effectiveness, difficult to apply formulations (e.g., viscous gel or powder), exothermic reactions

on contact with blood, and non-biodegradability that requires debridement after use(5). Hemostasis generated by nanofiber clots based on the RADA16-I self-assembling peptide has been shown to rapidly stop bleeding(20) and because of the biodegradability, biocompatibility, low cost, and thermal stability it is an interesting strategy to hemostasis. Having a self-assembling peptide capable of generating nanofiber-based clots presents an interesting aspect for topical hemostasis. By forming a mechanical plug it is critical for these nanofibers to directly reach the site of injury and by coating them onto common bandaging materials, it becomes easier to direct their application in a concentrated dry film-based formulation.

Multilayer Film Assembly

We developed a thin-film coating using the all-aqueous layer-by-layer (LbL) assembly approach that has shown the versatility to coat a variety of materials with tunable loading and release properties. In developing a bilayer (RADA16-I/polyanion)$_n$ film architecture, we examined biocompatible and naturally derived polyanions like hyaluronic acid (HA, 2 MDa and 500 kDa), chondroitin sulfate (CS), and dextran sulfate (DS), as shown in Figure 6-2. These films were assembled by dip-LbL under acidic water conditions (pH ~2) to facilitate ionic and hydrogen bonding interactions between the polysaccharides and RADA16-I (Figure 6-2), whose aspartic acid and arginine side chains are neutral and cationic, respectively, at this pH(9). After deposition and dehydration, the film's subsequent exposure to physiological conditions (PBS, pH 7.4) significantly changes the nature of the pH-sensitive intermolecular interactions established at low pH and the increased negative charge density due to deprotonation of the acid groups initiates film disassembly and nanofiber release.
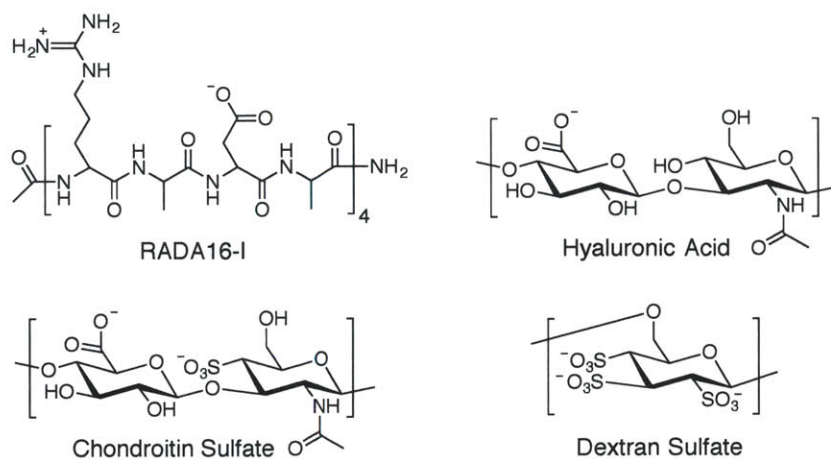
Figure 6-2. Chemical structures of components used in LbL film assembly
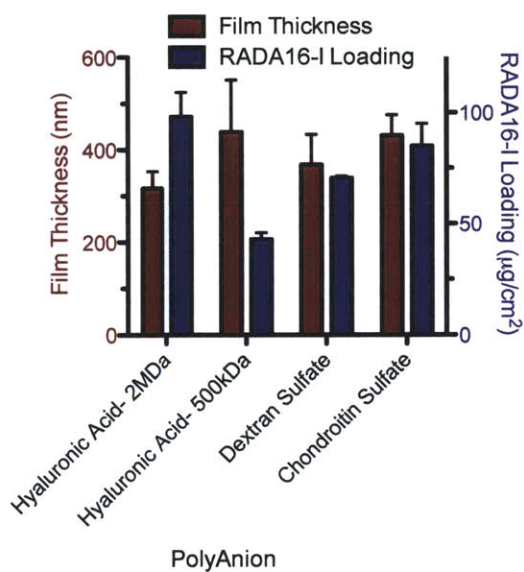
Figure 6-3. Characteristics of different dip-LbL assembled (RADA16-I/polyanion)$_{40}$ films deposited onto silicon.
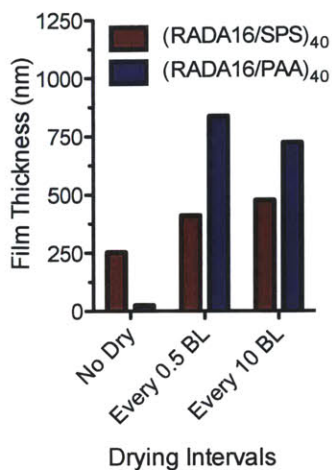
Figure 6-4. Film growth characteristics of dip-LbL assembled (RADA16-I/SPS)$_{40}$ and (RADA16-I/PAA)$_{40}$ films with intermittent dry steps.

We screened through these possible film components, using the dip-LbL technique and compared their resultant properties. Out of the four polyanions examined, DS and HA (2MDa) yielded films with the best RADA16-I loadings and comparable thicknesses (Figure 6-3), which can result from a number of factors including charge density(34, 35), secondary interactions(35-37), and molecular weight(38). We examined their growth curves by the dip LbL process and found it was imperative to include a "dry step" in which the film was periodically dried (either by compressed air or by evaporation). Without this, the films did not optimally assemble (Figure 6-4). The introduction of drying has been shown to not deleteriously affect LbL film growth(39), and can sometimes promote multilayer assembly when it may otherwise be difficult(40, 41)— increasing the amount of material deposited per layer through film reorganization of more hydrophobic components near the surface(42, 43). We found that drying, in conjunction with incubation steps of 30 min, significantly improved the film assembly. Based on linear regression of the growth curves for DS and HS based films, 16.9 and 10.9 nm was deposited per bilayer,

respectively (Figure 6-5A), consistent with an approximate monolayer of the nanofibers, which have diameters ~5-10 nm.
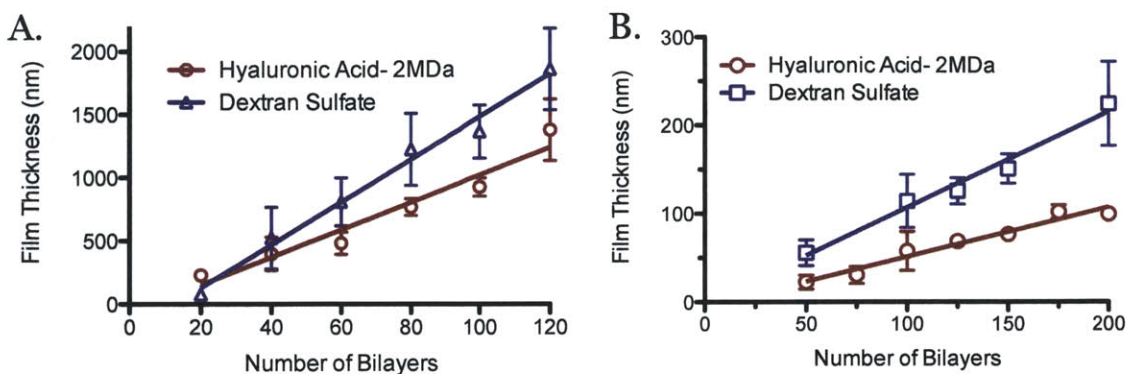
Figure 6-5. Film growth characteristics of (RADA16-I/hyaluronic acid) and (RADA16-I/dextran sulfate) films assembled by dip LbL (A) and spray LbL (B).

In addition to using dip-LbL, we examined spray-LbL assembly in which the substrate is exposed to aerosolized solutions rather than being immersed in these solutions. This technique is more amenable for coating porous and absorbent materials with film assembly finished in a fraction of the time that would typically be required for dip LbL(44, 45). Examinations of these same architectures constructed by spray-LbL onto solid materials (glass slides) yielded much thinner films with 1.09 and 0.56 nm per bilayer for the DS and HA-based films, respectively (Figure 6-5B). This sub-monolayer deposition of nanofibers and polyelectrolyte per bilayer is likely due to a combination of the 10-fold lower concentrations of RADA16-I and polyanion used during assembly and the significantly shorter deposition times associated with spray-LbL assembly, which exploits kinetic trapping for adsorption(45) rather than approaching equilibrium as is the case for dip-LbL assembly. By aerosolizing these materials in a predefined sequence, films can be rapidly assembled within hours onto a variety of possible substrates with uniquely tunable properties(44) and scalable fabrication for continuous high throughput

manufacturing(46). In both cases of dip- and spray-LbL, we found linear growth behavior, which is typically indicative of minimal interdiffusion occurring during film assembly. With the growth characteristics being quite similar, we continued our examination of spray-LbL films because of its greater translational potential.

Film Characteristics

The spray LbL assembled films showed interesting surface morphologies, which differed between DS and HA polyanions. On flat surfaces, (RADA16-I/DS)200 films have a rough appearance (Figure 6-6A) with the distinct outlines of randomly overlapping nanofibers that are more clearly distinguishable at higher magnification (Figure 6-6A, inset). For (RADA16-I/HA)200 similarly deposited onto glass (Figure 6-6B), the films have a much smoother texture with higher magnification also showing the outlines of nanofibers, though less obvious (Figure 6-6B, inset). The less apparent nanofiber structures may be a characteristic of a denser and/or thicker adsorbed HA layer that fills the voids between layered nanofibers; a lower charge density yielding loopier and denser chain conformations due to decreased charge repulsion between chain segments may generate thicker monolayers. When depositing these films onto cotton gauze, (Figures 6-6C-D) and onto gelatin sponges in bridged (Figure 6-6E-F) and conformal (Figure 6-6G-H) coatings, the film morphologies were clearly transferred as evidenced by the distinctly different surface textures as compared to plain (uncoated) substrates (Figure 6-7). We discovered that during assembly of these films onto the gelatin sponges, the air-drying we used after each layer caused films to bridge across the pores due to the drying out of nanofibers before they have the opportunity to directly interact completely with the surface of the gelatin. This forms a thin film across the pores, onto which subsequent layers are deposited. By avoiding this

air-drying, we were able to conformally coat the intricate geometry of the gelatin surface. This effect is similar to what we have observed before with electrospun mats(44).
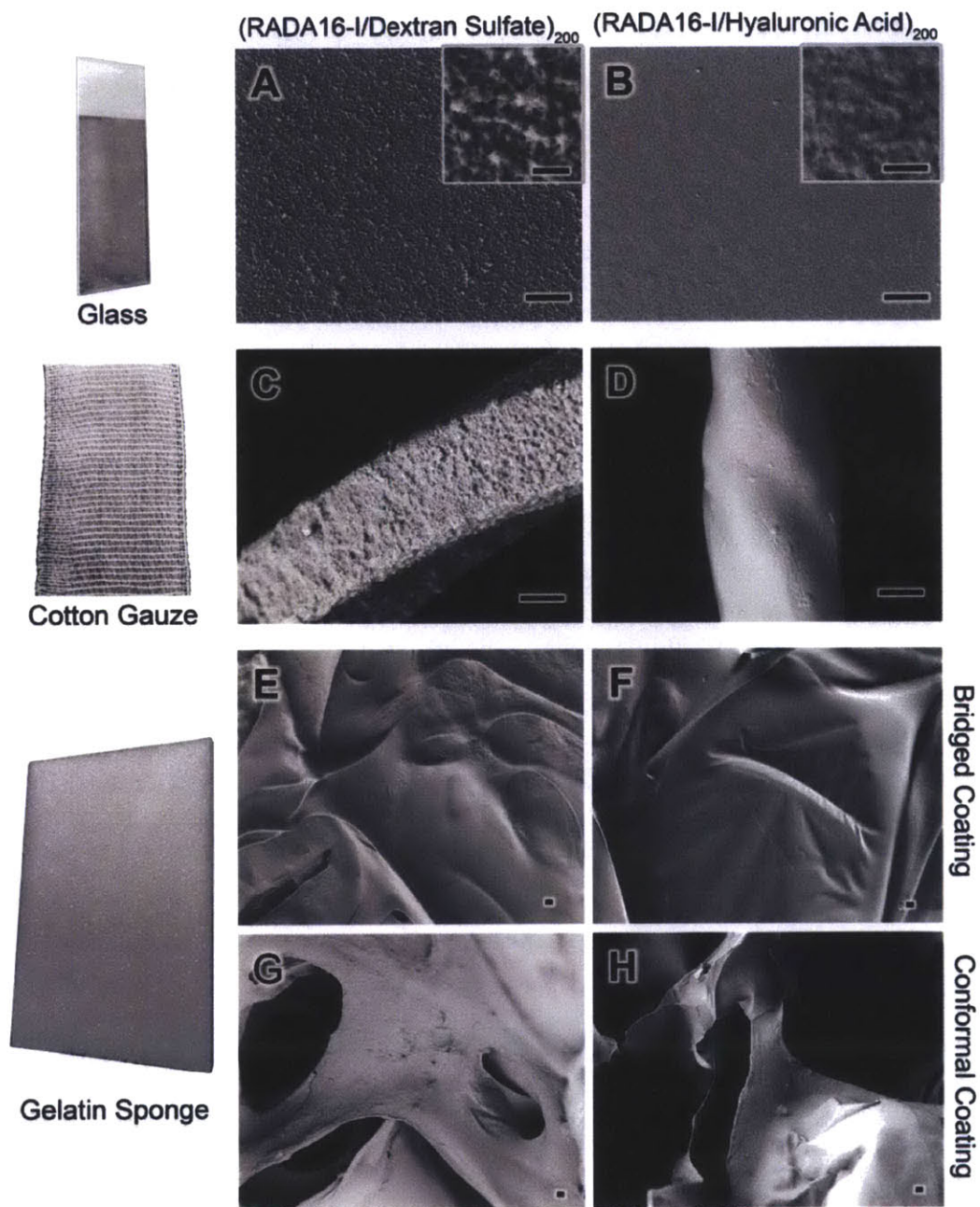

Figure 6-6. SEM images of surface morphologies for spray-LbL assembled (RADA16-I/DS)$_{200}$ films (A,C,E,G) and (RADA16-I/HA)$_{200}$ films (B,D,F,H). These films were characterized on glass (A-B), cotton gauze (C-D), and gelatin sponges in bridged (E-F) and conformal (G-H) coatings. Scale bars represent 5 μm (A-H) and 500 nm (A-B, *insets*).
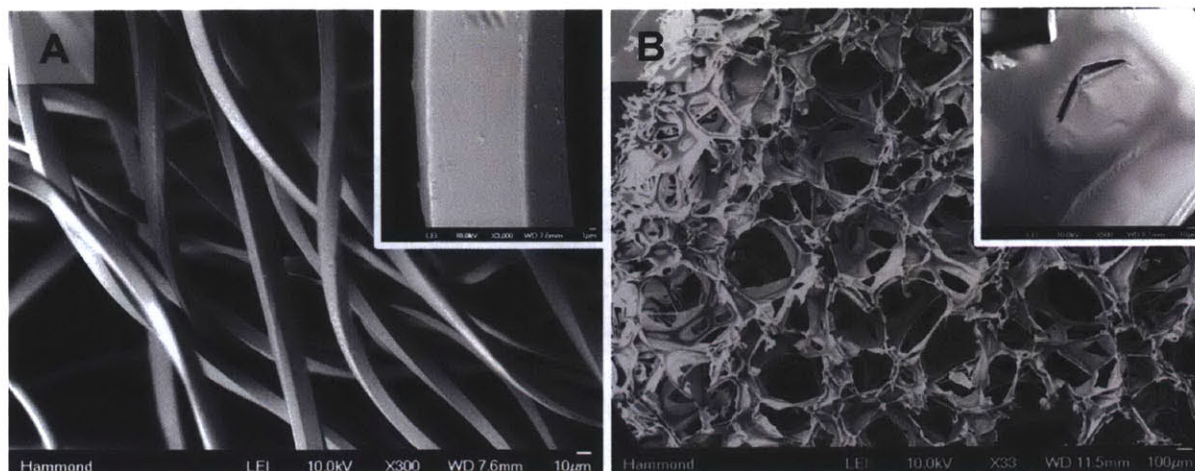
Figure 6-7. SEM images of uncoated gauze (A) and gelatin sponge (B) substrates and a higher magnification examination of their surface morphologies (*insets*). Scale bars represent 10 μm (A-B) and 1 μm (*insets*).

Under the acidic pH conditions we used to facilitate film assembly, it has been shown that nanofibers ably form(9). When aiming to generate rapid hemostasis on-contact, it is imperative that the film be immediately capable of forming a nanofiber-based clot, and examinations of the dry films (Figure 6-6) suggest that the RADA16-I is indeed incorporated in fibrillar form. For additional insight into RADA16-I's supramolecular structure within the film, we studied the morphology of (RADA16-I/DS)$_{200}$ films on gauze after partial hydration provided by exposure to a humidifier followed by chemical crosslinking with glutaraldehyde, serial dehydration, and critical point drying to preserve the structure. SEM examination reveals that this film is fractured and swollen (Figure 6-8A), which can be expected as RADA16-I typically forms a hydrogel in solution. Higher magnification of the interior of the film shows that it is composed of highly entangled and interwoven nanofibers that are clearly discernable (Figure 6-8B) indicating that RADA16-I is indeed incorporated into the film as nanofibers. With the supramolecular structure being a critical component to generating hemostasis, its film incorporation as already-assembled nanofibers potentially improves the film's response time.

150
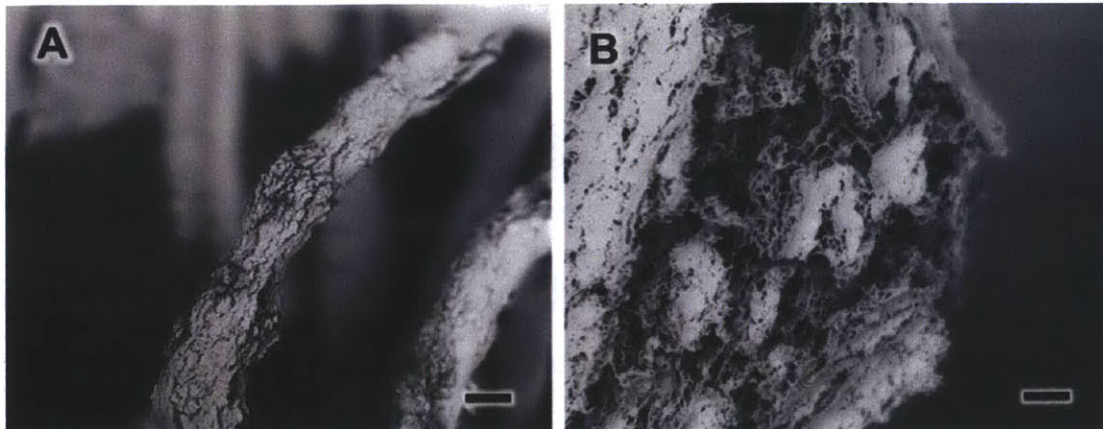
Figure 6-8. SEM images of (RADA16-I/DS)$_{200}$ films immediately after hydration (A) and at higher resolution (B). Scale bars represent 10 μm (A) and 1 μm (B).

To confirm that LbL assembly with a polyanion could generate superior coatings over other basic deposition approaches, we also examined the surface morphologies of gauze coated by a spray-LbL architecture of (RADA16-I/nothing)$_{200}$, where "nothing" was the aqueous solution without polyanion (Figure 6-9A and 6-9B) and by immersion in a 0.1 mg/mL solution of RADA16 (the same concentration used for spray-LbL) (Figures 6-9C and 6-9D). Examination of their surfaces revealed little deposition of RADA16-I with some small regions coated, but large swaths of areas bare. Quantification of RADA16-I showed relatively low loadings 5.0 ± 1.3 μg/cm^2 and 4.0 ± 1.0 μg/cm^2 for these two films, respectively.
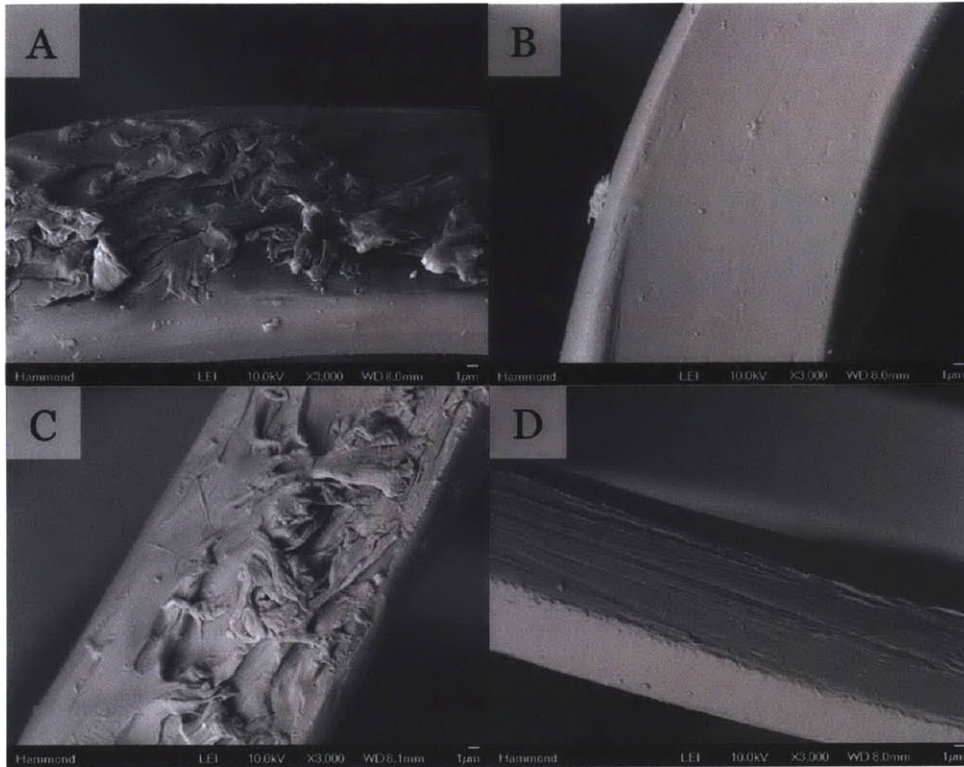
Figure 6-9. SEM images of two representative regions with coating (A,C) and without coating (B,D) of gauze after immersion in a RADA16-I solution (A,B) or spray-LbL coated with (RADA16-I/nothing)$_{200}$ films (C,D). Scale bars represent 1 μm.

Nanofiber Release and Functionality

For insight into how these films based on the hemostatic self-assembling peptide would respond to full hydration, we studied the RADA16-I release behavior into the physiological conditions of PBS, pH 7.4 at 37°C and quantified their overall loadings in spray-LbL films deposited onto glass, gauze, and gelatin sponges. For (RADA16-I/DS)$_{200}$ films (Figure 6-10A) and (RADA16-I/HA)$_{200}$ films (Figure 6-10B) on glass and gauze, the peptides release rapidly within the first half-day with substantial amounts of peptide loaded into the film (Figure 6-10C); similar release profiles to our observations with dip-LbL films as well (Figure 6-11). Comparatively, when these films are deposited onto gelatin sponges, both DS-based films (Figure 6-10D) and HA-based films (Figure 6-10E) show a more sustained release with

152

substantial RADA16-I loadings (Figure 6-10F). We suspected there may be stronger intrinsic interaction between the films and the gelatin substrate through additional intermolecular interactions (e.g., hydrogen bonding) and when compounded with the absorptive nature of the biodegradable foam, may allow for greater entanglement and more intrinsic association between the film and the substrate. By assembling these films under acidic conditions (pH~2), the pH-sensitive hydrogen-bonding and electrostatic interactions that were established during assembly are disrupted in a PBS, pH 7.4 solution and hence the charge imbalance facilitates film disassembly. Ideally, the release would be immediate, but our observation suggests some additional factors are able to slow RADA16-I release, which may be due to the high degree of entanglement of the nanofibers when dried in a film, as well as some remaining weak intermolecular interactions. As we found with other hydrogen-bonded films, immersion in blood facilitated film disassembly when PBS did not, which is likely due to proteins displacing the intermolecular interactions of the film(47). With our own films of (RADA16-I/DS)$_{200}$ (Figure 6-10D) and (RADA16-I/HA)$_{200}$ (Figure 6-10E) deposited onto gelatin sponges, we similarly found significantly accelerated release when fetal bovine serum (FBS) was used as opposed to PBS.
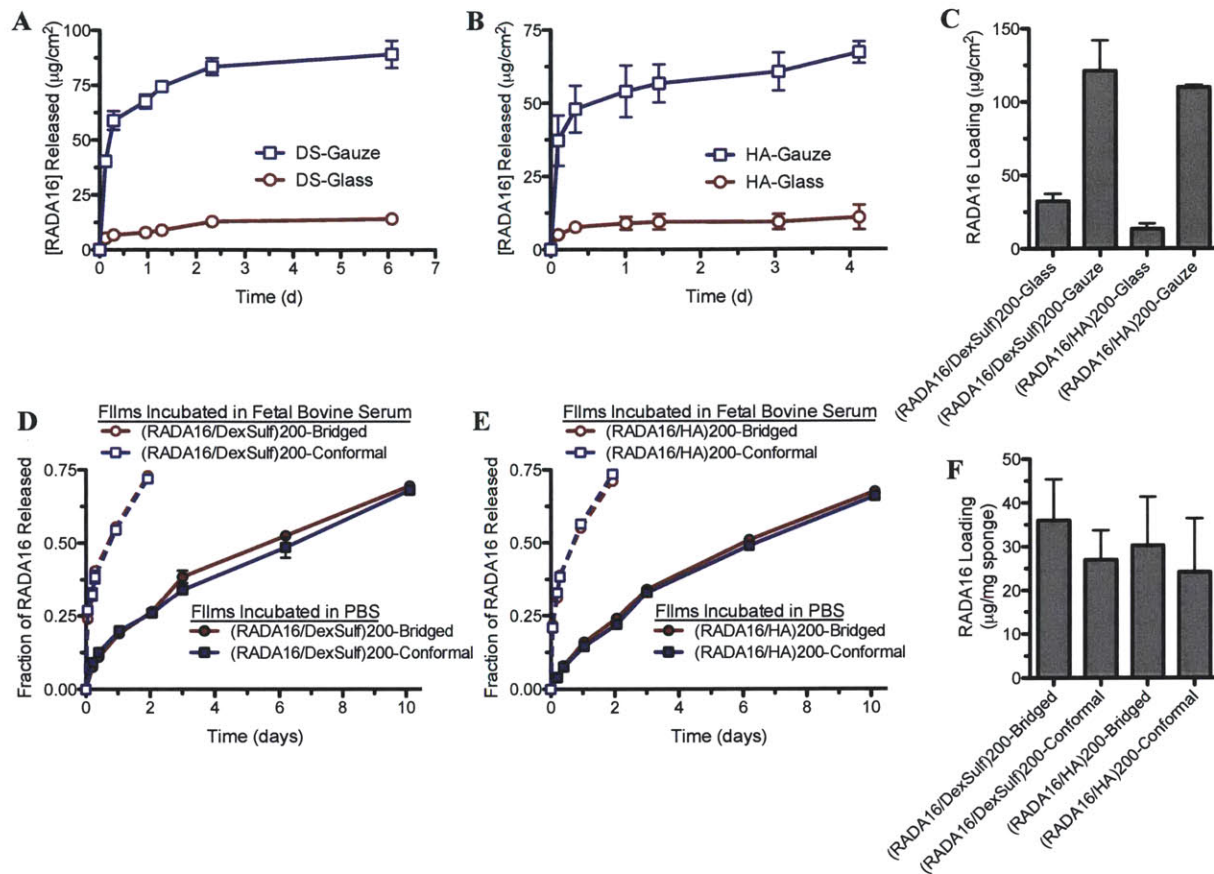
Figure 6-10. Release curves of RADA16-I from in (RADA16-I/Dextran Sulfate)$_{200}$ films (A,D) and (RADA16-I/Hyaluronic Acid)$_{200}$ films (B,E) deposited onto glass and gauze (A,B) and gelatin sponges (D,E), as well as the total peptide loadings for these films on glass and gauze (C), and on the gelatin sponge (F).
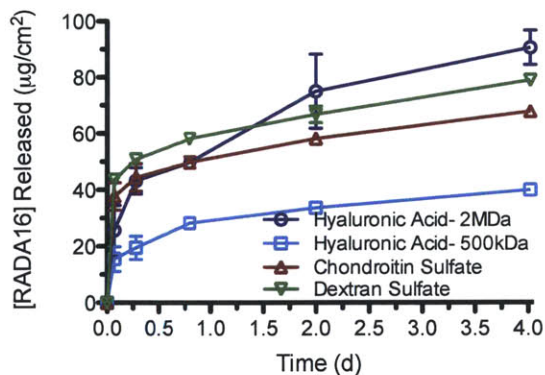
Figure 6-11. Release profiles of dip-LbL assembled (RADA16-I/polyanion)$_{40}$ films incubated in PBS, pH 7.4 at 37°C.

Although the release of peptide into solution is likely beneficial to hemostasis, its response when in direct physical contact with blood at the site of injury is the most critical determinant to its success. For example, a nanofiber clot not only generates a mechanical plug to stop additional bleeding, but also aggregates and concentrates blood components (e.g., platelets and RBCs) to further enhance the coagulative response(48, 49). Therefore to gain greater insight into how these nanofiber-based films would respond to a wound, we studied the morphology of gauze coated with (RADA16-I/DS)$_{200}$ films (Figure 6-12A-D) and (RADA16-I/HA)$_{200}$ films (Figure 6-12E-H), upon contact with anti-coagulated whole human blood. These films showed that nanofiber clotting was capable of occurring both on the gauze fibers (Figure 6-12A,B,E,F) as well as in the films detached from the gauze (Figure 6-12C,D,G,H), and in each of these cases, the morphological appearances resemble what we observed for a simple mixture of RADA16-I with anti-coagulated whole blood (Figure 6-1C). These studies show that RADA16-I remains capable of forming a nanofiber-clot in contact with blood and their formulation with DS and HA in LbL films allows the nanofibers to form an entangled and interpenetrated network that can entrap and aggregate blood components on contact.
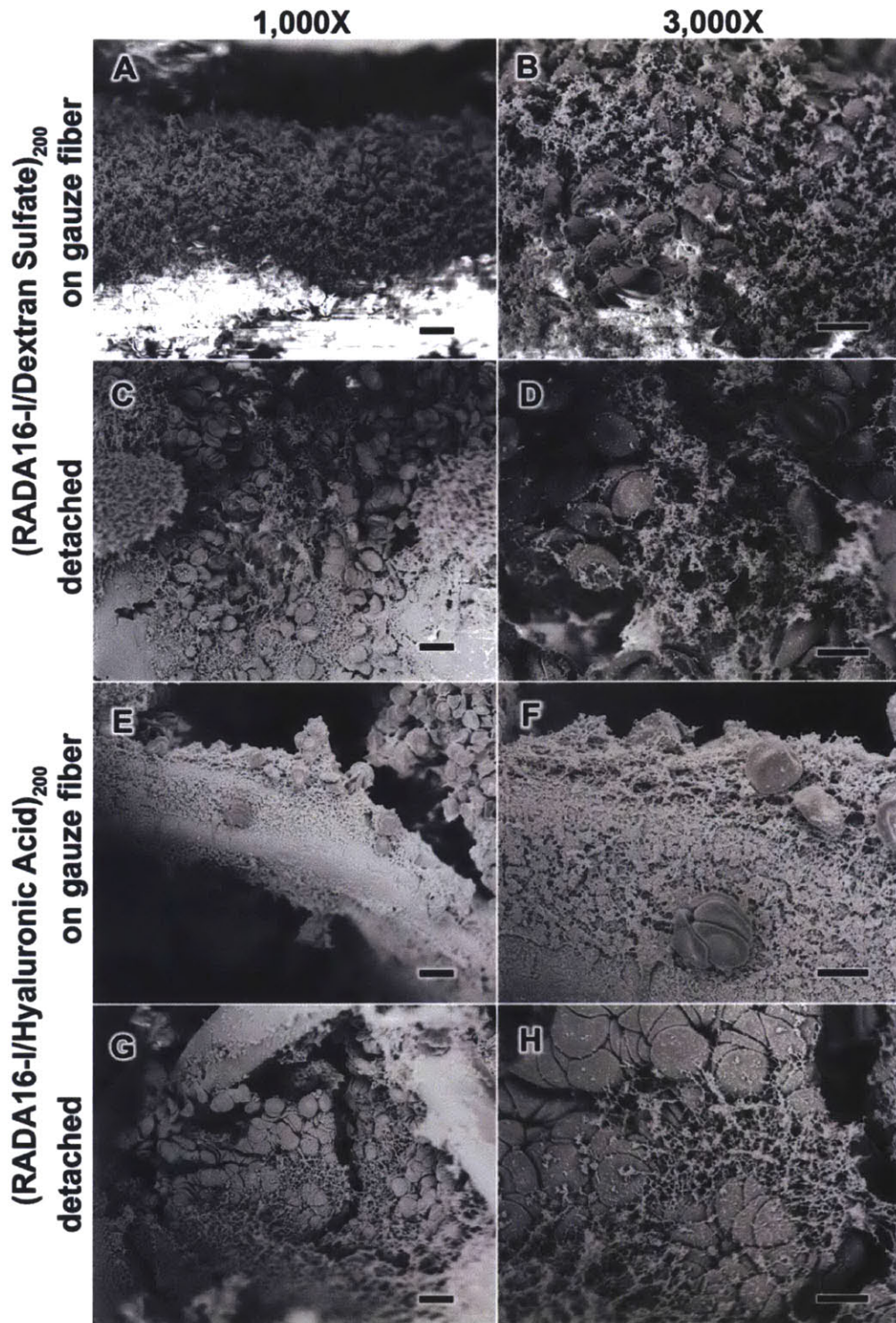
Figure 6-12. SEM images of $(RADA16-I/DS)_{200}$ films (A-D) and $(RADA16/HA)_{200}$ films (E-H) in contact with anti-coagulated whole blood. The interaction of films that remained on the gauze fibers (A,B,E,F) and detached (C,D,G,H) were characterized. Scale bars represent 10 μm (A,C,E,G) and 5 μm (B,D,F,H).

In addition to the microscopic morphological examination of these films with blood, we utilized an *in vitro* test for nanofiber formation of film components released into PBS by adopting a suspension assay that had previously been correlated to *in vivo* hemostatic activity(24). We mixed PBS solutions with rabbit RBCs in a 96-well microtiter plate with V-shaped wells and allowed the RBCs to settle. For solutions containing sufficient concentrations of nanofibers their entanglement with the RBCs keeps them in suspension and thus a view from underneath shows red in the well's entirety (Figure 6-13A). For insufficient concentrations, the RBCs settle to the bottom of the wells to form a small red area in the center when viewed from underneath (Figure 6-13B). We used this approach to examine serial dilutions of RADA16-I alone, in equal concentration mixtures with DS or HA, and for DS or HA alone (Figure 6-13C). These results show that we can indeed titrate the loading of nanofibers to entrap RBCs in solution, and that the polyanions did not have significant impact on this effect, nor could the polyanions entrap RBCs on their own. Examination of the activity of film-components released into solution from gauze and gelatin sponge substrates showed they retained the ability to maintain RBCs in suspension while uncoated substrates had no activity (Figure 6-13D). This in effect supports our observations for blood interacting with films deposited onto gauze (Figure 6-12) and in a more rapid approach indicates these films deposited on other substrates are also capable of releasing into solution and forming nanofiber-based clots.
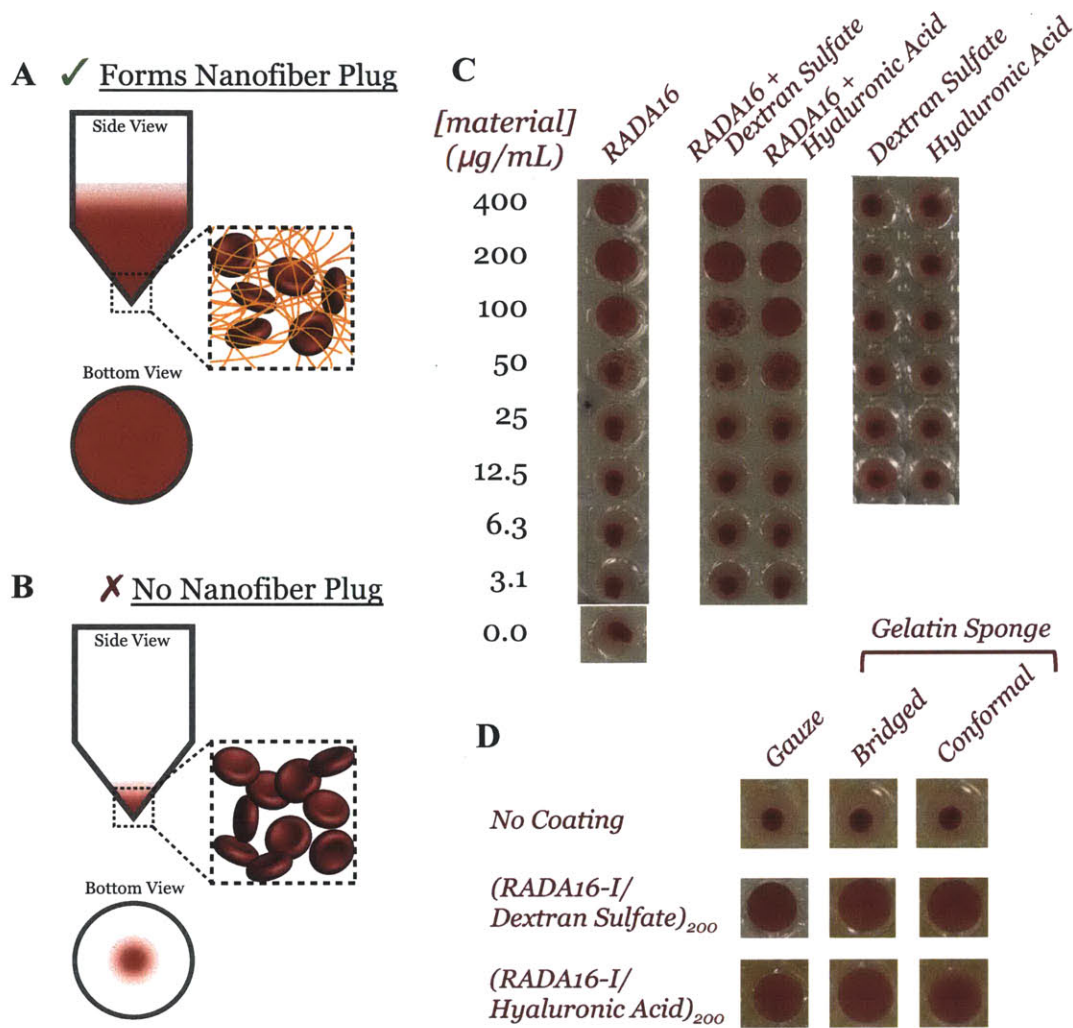
Figure 6-13. *In vitro* determination of nanofiber formation of RADA16-I and its ability to clot with red blood cells. Schematic representation of the assay showing nanofiber clot formation (A) or lack of formation (B) and standard dilutions of various controls (C) and film released into solution from samples (D).

One distinct feature of using these nanofibers as hemostatic agents, in addition to being non-toxic and composed of biodegradable peptides, is their ability to continue to self-assemble despite exposure to harsh environmental conditions such as pH or temperature that would denature and inactivate other biologic hemostats. Exposure of nanofiber solutions to elevated temperatures as high as 80°C was found to disrupt the ionic and hydrogen bonding present in the

supramolecular aggregates, but nanofibers were reformed after returning to room temperature(10). To demonstrate the robustness of these films, we incubated (RADA16-I/DS)$_{200}$ coated gauze at -80, -20, 37, and 60°C for one week in desiccant and found that the nanofibers released into solution retained their activity when mixed with RBCs (Figure 6-14A). Furthermore, films incubated at 60°C for 2 months still released active nanofibers (Figure 6-14A) and closer examination showed that the released peptide could still form the interwoven and entangled nanofibers. With the extremes of world temperatures, the stability of these films at elevated temperatures for extended periods bodes well for the possibility of its use in bandages without the need of the cold-chain that is commonly necessary for preserving the activity of biologics.
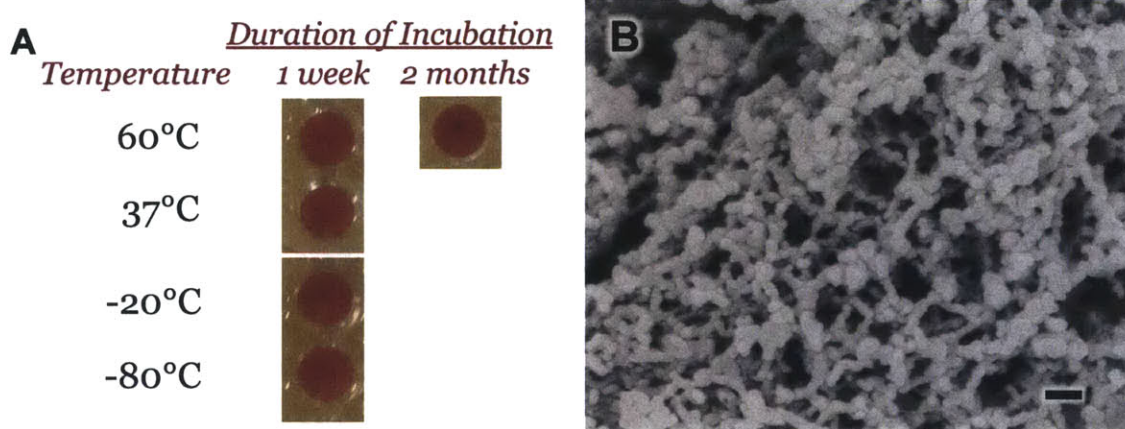
Figure 6-14. Films of (RADA16-I/DS)$_{200}$ deposited on gauze were incubated in desiccant at a range of temperatures for different time periods and then eluted into solution for the study of in vitro activity by clot formation with RBCs (A). The films released into solution after 2 months of incubation at 60°C were also studied by SEM for nanofiber formation (B). Scale bar represents 100 nm.

6.4   Conclusions

Generating rapid hemostasis from a lightweight, flexible, and easily applied device or bandage is highly desirable for improving survival from wounding either from armed conflict, crime, accidents, or disasters. Self-assembling peptides, especially RADA16-I, have demonstrated to be highly effective in generating hemostasis *in vivo* when applied as a solution. Morphological examination of the interaction between these nanofibers and anti-coagulated whole blood shows the formation of a nanofiber-based clot that entraps the blood components in a similar fashion to fibrin-based clots. By incorporation into LbL assembled $(RADA16\text{-}I/DS)_n$ and $(RADA16\text{-}I/HA)_n$ films, we were able to utilize common bandage and wound dressing materials and found nanofiber clots could be generated on contact with blood. These films were also thermally robust against denaturation from a range of temperatures and could release active nanofibers even after 2 months at 60°C. This demonstrates a promising approach to creating a cheap, biodegradable, biocompatible, and robust hemostatic bandage.

6.5 References

1. Kelly JF, *et al.* (2008) Injury severity and causes of death from operation Iraqi freedom and operation enduring freedom: 2003-2004 versus 2006. *Journal of Trauma-Injury Infection and Critical Care* 64(2):S21-S26.

2. Evans JA, *et al.* (2010) Epidemiology of Traumatic Deaths: Comprehensive Population-Based Assessment. *World J. Surg.* 34(1):158-163.

3. Belmont PJ, Schoenfeld AJ, & Goodman G (2010) Epidemiology of combat wounds in Operation Iraqi Freedom and Operation Enduring Freedom: orthopaedic burden of disease. *Journal of surgical orthopaedic advances* 19(1):2-7.

4. Spahn DR, *et al.* (2013) Management of bleeding and coagulopathy following major trauma: an updated European guideline. *Critical Care* 17(2).

5. Gordy SD, Rhee P, & Schreiber MA (2011) Military applications of novel hemostatic devices. *Expert Review of Medical Devices* 8(1):41-47.

6. Pusateri AE, *et al.* (2006) Making sense of the preclinical literature on advanced hemostatic products. *Journal of Trauma-Injury Infection and Critical Care* 60(3):674-682.

7. Zhang SG (2003) Fabrication of novel biomaterials through molecular self-assembly. *Nat. Biotechnol.* 21(10):1171-1178.

8. Yokoi H, Kinoshita T, & Zhang SG (2005) Dynamic reassembly of peptide RADA16 nanofiber scaffold. *Proc. Natl. Acad. Sci. U. S. A.* 102(24):8414-8419.

9. Arosio P, Owczarz M, Wu H, Butté A, & Morbidelli M (End-to-End Self-Assembly of RADA 16-I Nanofibrils in Aqueous Solutions. *Biophys. J.* 102(7):1617-1626.

10. Ye Z, *et al.* (2008) Temperature and pH effects on biophysical and morphological properties of self-assembling peptide RADA16-1. *J. Pept. Sci.* 14(2):152-162.

11. Luo Z & Zhang S (2012) Designer nanomaterials using chiral self-assembling peptide systems and their emerging benefit for society. *Chem. Soc. Rev.* 41(13):4736-4754.

12. Horii A, Wang X, Gelain F, & Zhang S (2007) Biological Designer Self-Assembling Peptide Nanofiber Scaffolds Significantly Enhance Osteoblast Proliferation, Differentiation and 3-D Migration. *Plos One* 2(2).

13. Gelain F, Bottai D, Vescovi A, & Zhang S (2006) Designer Self-Assembling Peptide Nanofiber Scaffolds for Adult Mouse Neural Stem Cell 3-Dimensional Cultures. *Plos One* 1(2).

14. Degano IR, *et al.* (2009) The effect of self-assembling peptide nanofiber scaffolds on mouse embryonic fibroblast implantation and proliferation. *Biomaterials* 30(6):1156-1165.

15. Ellis-Behnke RG, *et al.* (2006) Nano neuro knitting: Peptide nanofiber scaffold for brain repair and axon regeneration with functional return of vision. *Proc. Natl. Acad. Sci. U. S. A.* 103(13):5054-5059.

16. Akiyama N, Yamamoto-Fukuda T, Takahashi H, & Koji T (2013) In situ tissue engineering with synthetic self-assembling peptide nanofiber scaffolds, PuraMatrix, for mucosal regeneration in the rat middle-ear. *International Journal of Nanomedicine* 8:2629-2640.

17. Schneider A, Garlick JA, & Egles C (2008) Self-Assembling Peptide Nanofiber Scaffolds Accelerate Wound Healing. *Plos One* 3(1).

18. Nagai Y, Unsworth LD, Koutsopoulos S, & Zhang S (2006) Slow release of molecules in self-assembling peptide nanofiber scaffold. *J. Controlled Release* 115(1):18-25.

19. Koutsopoulos S, Unsworth LD, Nagaia Y, & Zhang S (2009) Controlled release of functional proteins through designer self-assembling peptide nanofiber hydrogel scaffold. *Proc. Natl. Acad. Sci. U. S. A.* 106(12):4623-4628.

20. Ellis-Behnke RG, *et al.* (2006) Nano hemostat solution: immediate hemostasis at the nanoscale. *Nanomedicine : nanotechnology, biology, and medicine* 2(4):207-215.

21. Song H, Zhang L, & Zhao X (2010) Hemostatic Efficacy of Biological Self-Assembling Peptide Nanofibers in a Rat Kidney Model. *Macromol. Biosci.* 10(1):33-39.

22. Wang T, Zhong X, Wang S, Lv F, & Zhao X (2012) Molecular Mechanisms of RADA16-1 Peptide on Fast Stop Bleeding in Rat Models. *International Journal of Molecular Sciences* 13(11):15279-15290.

23. Ruan L, *et al.* (2009) Designed amphiphilic peptide forms stable nanoweb, slowly releases encapsulated hydrophobic drug, and accelerates animal hemostasis. *Proc. Natl. Acad. Sci. U. S. A.* 106(13):5105-5110.

24. Luo Z, Wang S, & Zhang S (2011) Fabrication of self-assembling D-form peptide nanofiber scaffold d-EAK16 for rapid hemostasis. *Biomaterials* 32(8):2013-2020.

25. Ellis-Behnke R (2011) At the nanoscale: nanohemostat, a new class of hemostatic agent. *Wiley Interdisciplinary Reviews-Nanomedicine and Nanobiotechnology* 3(1):70-78.

26. Anonymous (2004) *Capturing the Full Power of Biomaterials for Military Medicine: Report of a Workshop* (The National Academies Press).

27. Hyder MN, Shah NJ, & Hammond PT (2012) Design and Translation of Nanolayer Assembly Processes: Electrochemical Energy to Programmable Pharmacies. *Multilayer Thin Films*, eds Decher G & Schlenoff JB (Wiley-VCH), 2nd Ed.

28. Kim B-S, Park SW, & Hammond PT (2008) Hydrogen-bonding layer-by-layer assembled biodegradable polymeric micelles as drug delivery vehicles from surfaces. *Acs Nano* 2(2):386-392.

29. Hsu BB, *et al.* (2014) Multilayer films assembled from biocompatible, naturally-derived materials for controlled protein release. *Biomacromolecules* in press.

30. Hsu BB, *et al.* (2014) Ordered and kinetically discrete sequential protein release from biodegradable thin films. *Angew. Chem. Int. Ed.* In Press.

31. Hsu BB, Park M, Hagerman SR, & Hammond PT (2014) Multi-month controlled small molecule release from biodegradable thin films. *Proc. Natl. Acad. Sci. U. S. A.* In Review.

32. Gelain F, Horii A, & Zhang S (2007) Designer self-assembling peptide scaffolds for 3-D tissue cell cultures and regenerative medicine. *Macromol. Biosci.* 7(5):544-551.

33. Ho D, *et al.* (2011) The effects of concentration-dependent morphology of self-assembling RADA16 nanoscaffolds on mixed retinal cultures. *Nanoscale* 3(3):907-910.

34. Shiratori SS & Rubner MF (2000) pH-dependent thickness behavior of sequentially adsorbed layers of weak polyelectrolytes. *Macromolecules* 33(11):4213-4219.

35. Xu L, Ankner JF, & Sukhishvili SA (2011) Steric Effects in Ionic Pairing and Polyelectrolyte Interdiffusion within Multilayered Films: A Neutron Reflectometry Study. *Macromolecules* 44(16):6518-6524.

36. Clark SL & Hammond PT (2000) The Role of Secondary Interactions in Selective Electrostatic Multilayer Deposition. *Langmuir* 16(26):10206-10214.

37. Gilbert JB, Rubner MF, & Cohen RE (2013) Depth-profiling X-ray photoelectron spectroscopy (XPS) analysis of interlayer diffusion in polyelectrolyte multilayers. *Proc. Natl. Acad. Sci. U. S. A.* 110(17):6651-6656.

38. Sui Z, Salloum D, & Schlenoff JB (2003) Effect of Molecular Weight on the Construction of Polyelectrolyte Multilayers: Stripping versus Sticking. *Langmuir* 19(6):2491-2495.

39. Halthur TJ, Claesson PM, & Elofsson UM (2004) Stability of polypeptide multilayers as studied by in situ ellipsometry: Effects of drying and post-buildup changes in temperature and pH. *J. Am. Chem. Soc.* 126(51):17009-17015.

40. Raposo M, Pontes RS, Mattoso LHC, & Oliveira ON (1997) Kinetics of adsorption of poly(o-methoxyaniline) self-assembled films. *Macromolecules* 30(20):6095-6101.

41. Wang L, Wang L, & Su Z (2011) Surface defects in polyelectrolyte multilayers: Effects of drying and deposition cycle. *Soft Matter* 7(10):4851-4855.

42. Decher G, Lvov Y, & Schmitt J (1994) PROOF OF MULTILAYER STRUCTURAL ORGANIZATION IN SELF-ASSEMBLED POLYCATION POLYANION MOLECULAR FILMS. *Thin Solid Films* 244(1-2):772-777.

43. Lvov Y, Ariga K, Onda M, Ichinose I, & Kunitake T (1999) A careful examination of the adsorption step in the alternate layer-by-layer assembly of linear polyanion and polycation. *Colloids and Surfaces a-Physicochemical and Engineering Aspects* 146(1-3):337-346.

44. Krogman KC, Lowery JL, Zacharia NS, Rutledge GC, & Hammond PT (2009) Spraying asymmetry into functional membranes layer-by-layer. *Nature Materials* 8(6):512-518.

45. Krogman KC, Zacharia NS, Schroeder S, & Hammond PT (2007) Automated process for improved uniformity and versatility of layer-by-layer deposition. *Langmuir* 23(6):3137-3141.

46. Krogman KC, Cohen RE, Hammond PT, Rubner MF, & Wang BN (2013) Industrial-scale spray layer-by-layer assembly for production of biomimetic photonic systems. *Bioinspiration & Biomimetics* 8(4).

47. Shukla A, Fang JC, Puranam S, Jensen FR, & Hammond PT (2012) Hemostatic Multilayer Coatings. *Adv. Mater.* 24(4):492-496.

48.   Andrews DA & Low PS (1999) Role of red blood cells in thrombosis. *Curr. Opin. Hematol.* 6(2):76-82.
49.   Monroe D, Hoffman M, & Roberts HR (2002) Platelets and thrombin generation. *Arteriosclerosis Thrombosis and Vascular Biology* 22(9):1381-1389.

Appendix
Curriculum Vitae

BRYAN B. HSU

61 Brookline Ave #415	Doctoral Candidate
Boston, MA 02215	Hammond Lab	MIT
805-807-1367	bbhsu@mit.edu	http://web.mit.edu/hammond/lab/hsu.htm

Education

Massachusetts Institute of Technology 2011 - Present
Ph.D. | Chemistry (Expected Sept 2014) Cambridge, MA
  Thesis Title: "Multilayer thin films with tunable release kinetics for biomedical applications"

Massachusetts Institute of Technology 2007 - 2011
M.S. | Chemistry Cambridge, MA
  Thesis Title: "Investigation of microbicidal activity of surface-immobilized hydrophobic polycations"

University of California, Berkeley 2002 - 2007
B.S. | Chemical Engineering Berkeley, CA
B.S. | Materials Science and Engineering

Research Experience

Graduate Student Researcher (Ph.D.) 2010 – Present
Advisor: Professor Paula T. Hammond
Massachusetts Institute of Technology, Department of Chemical Engineering
  Research Summary | Used the layer-by-layer assembly to develop films with uniquely designed drug release rates for wound healing applications. Material applications include use of (1) hemostat (thrombin) and antibiotic (vancomycin) for their rapid and sustained releases, respectively, (2) polymer-conjugated small molecule prodrugs for long-term (1+ yr) sustained release, (3) sequential, non-overlapping protein release from biodegradable thin films, (4) assembly and release of biologically regenerative self-assembling peptides, (5) development of a spray-assisted LbL film assembly for maximal recovery efficiency, and (6) the fabrication of free-standing, peelable, biodegradable controlled drug release thin films.

Graduate Student Researcher (M.S.) 2007 – 2010
Advisor: Professor Alexander M. Klibanov
Massachusetts Institute of Technology, Department of Chemistry
  Research Summary | Investigated the antibacterial and antiviral mechanism of microbicidal hydrophobic polycations. Also designed and developed a photo-crosslinkable microbicidal polymer that derivatives materials (e.g., cotton textiles) by one step functionalization with light.

Undergraduate Student Researcher 2004 – 2007
Advisor: Professor Gabor A. Somorjai
University of California, Berkeley, Department of Chemistry
  Research Summary | Examined activity and selectivity of heterogeneous catalysts for (1) cyclohexene hydrogenation/dehydrogenation over Pt nanoparticles in order to determine the influence of particle size in controlling selectivity, and (2) hot-electron generation by exothermic catalytic reactions over a thin-film catalytic Schottky diodes.

Summer Research Fellow Summers of 2006 and 2007
Advisor: Dr. Mohsen S. Yeganeh
ExxonMobil Research and Engineering Co., Corporate Strategic Research Laboratory
  Research Summary | Used Sum Frequency Generation (SFG) in total internal reflection geometry for *in situ* characterization of the liquid/solid interface for determination of the molecular orientation of small molecules (e.g. acetonitrile, methanol, etc.) upon interaction with a hydrophobic or hydrophilic surface and the surface-adsorbed reactive intermediates formed during ethylene hydrogenation over micron-sized Pt powders.

Undergraduate Mentorship

William Conway | MIT
August 2013 – Present   (8 mo.)

Sarah Alkilany | MIT
June 2012 – August 2012 (3 mo.)

Kelsey Jamieson | MIT
January 2012 – Present   (1 yr. 3 mo.)

Jovana Veselinovic | MIT
September 2011 – June 2012 (10 mo.)

Samantha R. Hagerman | MIT
September 2011 – Present (2 yr. 7 mo.)

Nicholas O'Neill | University of Notre Dame
June 2011 – August 2011 (3 mo.)

Monica Perez | University of Puerto Rico, Mayaguez
June 2013 – August 2013 (3 mo.)

Peter Tieu | MIT
June 2010 – December 2010 (7 mo.)

Publications

16. **BB Hsu**, SR Hagerman, ME Welch and PT Hammond. "Drug delivery stickers—facile fabrication of degradable, free-standing and adhesive films for controlled drug release". *In Preparation*

15. **BB Hsu**, W Conway, M Perez, S Zhang, and PT Hammond. "Clotting mimicry from robust and biodegradable self-assembling peptide hemostat bandages". *In Preparation*

14. **BB Hsu***, SR Hagerman*, and PT Hammond. "Rapid and efficient sprayed multilayer film assemblies for controlled drug delivery". (*) denotes equal contribution. *In Preparation*

13. **BB Hsu**, SR Hagerman, K Jamieson, E Holler, JY Ljubimova, and PT Hammond. "Multifunctional self-assembled films for rapid hemostat and sustained anti-infective delivery". *Submitted*

12. **BB Hsu**, M Park, SR Hagerman, PT Hammond. "Multi-month controlled small molecule release from biodegradable thin films". *Proc Natl Acad Sci USA.* (2014). *In Press*

11. **BB Hsu**, K Jamieson, SR Hagerman, E Holler, JY Ljubimova, and PT Hammond. "Ordered and kinetically discrete sequential protein release from biodegradable thin films". *Angew Chem Int Ed.* (2014). *In Press*

10. **BB Hsu**, SR Hagerman, K Jamieson, J Veselinovic, N O'Neill, E Holler, JY Ljubimova, PT Hammond. "Multilayer films assembled from biocompatible, naturally-derived materials for controlled protein release". *Biomacromol. (2014). In Press*

9. A Ghosh, **BB Hsu**, SM Dougal, M Afeworki, PA Stevens, MS Yeganeh. "Effects of gas feed ratios and sequence on ethylene hydrogenation on powder Pt catalyst studied by sum frequency generation and mass spectrometry". *ACS Catalysis.* (2014). *In Press*

8. TP Schaer, S Stewart, **BB Hsu**, AM Klibanov. "Hydrophobic polycationic coatings that inhibit biofilms and support bone healing during infection". *Biomaterials.* 33:1245-1254 (2012).

7. **BB Hsu**, SY Wong, PT Hammond, JZ Chen, and AM Klibanov. "Mechanism of influenza virus inactivation by immobilized hydrophobic polycations". *Proc Natl Acad Sci USA.* 108:61-66 (2011).

6. **BB Hsu**, and AM Klibanov. "Light-activated covalent coating of cotton with bactericidal hydrophobic polycations". *Biomacromol.* 12:6-9 (2011).

5. **BB Hsu**, J Ouyang, SY Wong, PT Hammond, and AM Klibanov. "On structural damage incurred by bacteria upon exposure to hydrophobic polycationic polymers". *Biotechnol Lett.* 33:411-416 (2011).

4. AM Larson, **BB Hsu**, D Rautaray, J Haldar, JZ Chen, and AM Klibanov. "Hydrophobic polycationic coatings disinfect poliovirus and rotavirus solutions". *Biotechnol Bioeng.* 108: 720-723 (2011).

3. A Onnis-Hayden, **BB Hsu**, AM Klibanov, and A Gu. "An antimicrobial polycationic sand filter for water disinfection". *Water Sci Technol.* 63: 1997-2003 (2011).

2. RM Rioux, **BB Hsu**, ME Grass, H Song, and GA Somorjai. "Influence of particle size on reaction selectivity in cyclohexene hydrogenation and dehydrogenation over silica-supported monodisperse Pt particles". *Catal Lett.* 126:10-19 (2008).

1. JY Park, JR Renzas, **BB Hsu**, and GA Somorjai. "Interfacial and chemical properties of Pt/TiO2, Pd/TiO2, Pt/GaN catalytic nanodiodes influencing hot electron flow". *J Phys Chem C.* 111:15331-15336 (2007).

Book Chapters

2. **BB Hsu**. "Multilayer thin films as bioactive wound dressings". *Wound Healing Biomaterials Volume 2: Functional Biomaterials.* Magnus Ågren and Laura Overend (Eds.). Woodhead Publishing. *In Preparation.*

1. NJ Shah, **BB Hsu**, EC Dreaden, and PT Hammond. "Engineering Layer-by-Layer Thin Films for Multiscale and Multidrug Delivery Applications". *Layer-by-Layer Films for Biomedical Applications.* Wiley-VCH. *In Press.*

Patents

2. **BB Hsu**, and PT Hammond. "Compositions and methods for controlled long-term small molecule release." Filed Dec 2, 2013

1. MS Pederson, S Gouin, AM Klibanov, **BB Hsu**. "Method and substrate with quat coating." WO2012065610 A1. May 24, 2012

Presentations

11. **BB Hsu**, MH Park, SR Hagerman, and PT Hammond. "Sustained long-term delivery of small molecules for pain relief". *Layer-by-Layer Assemblies Conference: Science and Technology.* Hoboken, NJ, June 2014 (Oral)

10. **BB Hsu**, MH Park, SR Hagerman, and PT Hammond. "Sustained long-term delivery of small molecules for pain relief". *Materials Research Society Meeting.* Boston, MA, December 2013 (Oral)

9. **BB Hsu**, and PT Hammond. "Multilayer Films Addressing Bleeding and Infection". *Society for Biomaterials Meeting.* Boston, MA, April, 2013 (Oral)

8. **BB Hsu**, J Veselinovic, N O'Neill, E Holler, JY Ljubimova, and P.T. Hammond, "Protein Releasing Layer-By-Layer Films Using a Naturally Derived PolyAnion, Poly(β-L-Malic Acid)" *American Chemical Society National Meeting.* Philadelphia, PA, August 2012 (Poster)

7. **BB Hsu**, FR Jensen, and PT Hammond. "Rapid Hemostat and Sustained Antibiotic Release from Multilayer Films for Wound Dressings" *IUPAC Macro World Polymer Congress.* Virginia Tech University in Blacksburg, VA, June, 2012 (Oral)

6. **BB Hsu**, FR Jensen, and PT Hammond. "Dual Release Multilayer Films for Immediate Hemostasis and Sustained Antibiotic Treatment". *Biomedical Engineering Society Meeting.* Atlanta, GA, October, 2012 (Oral)

5. **BB Hsu**, JZ Chen, and AM Klibanov. "Mechanistic Insights into the inactivation of influenza viruses by antimicrobial hydrophobic polycationic coatings". *American Chemical Society, Fall National Meeting.* August 2010. Boston, MA. (Poster)

4. **BB Hsu**, SY Wong, AM Larson, D Rautaray, JZ Chen, PT Hammond, and AM Klibanov. "Bactericidal and virucidal coatings". *ISN Army-Industry Collaboration Conference.* June 2010. Cambridge, MA. (Poster)

3. **BB Hsu**, JZ Chen, and AM Klibanov "Resent insight into the mechanism of antiviral action of microbicidal coatings". *ISN-Army Labs Research Innovation Symposium.* June 2009. Cambridge, MA. (Oral)

2. **BB Hsu**, S Dougal, P Stevens, and MS Yeganeh. "*In Situ* characterization of ethylene hydrogenation on Pt powder using mass spectrometry- sum frequency generation technique". *American Physical Society, APS March Meeting.* March, 2008. New Orleans, Louisiana. (Oral)

1. **BB Hsu**, V Lachat, GA Somorjai, and MS Yeganeh. "Hydrophobic dependence of molecules at the liquid/solid interface as studied with infrared-visible sum frequency generation spectroscopy" *American Physical Society, APS March Meeting.* March, 2007. Denver, Colorado. (Oral)